JOURNAL OF THE INDIAN ASSOCIATION OF SEDIMENTOLOGISTS

VOLUME 28 **NUMBER 1** **JAN. - JUNE 2009**

CONTENTS

Jour. Indian Association of Sedimentologists, Vol. 28, No. 1 (2009), pp.1-7

Inference on Polymodal Phi-Size Distribution Component Fractions of Clastic Rocks using corrected 3D Size Moments of Thin-section 2D Circle Radii or 1D Semi-Intercepts

BASANTA K. SAHU
Emeritus Professor, Dept. Earth Sciences, IIT, Bombay, Mumbai - 400076
Email: bksahu@iitb.ac.in

Abstract: Thin/polished section size analysis is essential for highly indurated (sedimentary) rocks ,(such as sandstones and siltstones but can be extended to include conglomerates as well), and for very hard ores that cannot be easily disaggregated for size analysis by other methods, such as sieving, settling velocity, loose grain counting etc .It is very precise, of the order of ¼ microns, and is required for estimating assay values of ore minerals in the ore samples and for inferences on mechanisms of transport/deposition processes during sedimentation of clastics as well as for recognition of possible depositional environments of these sedimentary rocks. Although introduced in early 1925 by Wicksell, no realistic sedimentological applications are made as yet, because the crucial transformations of corrected weight frequency moments about origin (zero millimeters) of the grain size distributions in 3D space (sphere radii, in mm) are not yet available in literature in terms of bimodal/polymodal phi-normal components comprising commonly occurring suspension- , saltation- and various (like rolling,sliding,gravity induced) bed-load modes in the sedimentary rocks (sandstones and conglomerates). This problem is now solved using the corrected weight frequency moments about origin (zero mm) in the 3D space (sphere radii in mm) (see, Sahu, 1974 a,b,c for theory of correction to yield 3D moments and of transformation of number to weight frequency) for bimodal phi-normal size components in the samples and extend it to trimodal phi-normal (or, if required to polymodal phi-normal) components. The bimodal solution includes unimodal phi-normal size component (100% in one component, say bedload. or saltation or suspension loads/deposits) as originally solved in Sahu (1965a). These new results, presented here, would be of much value to interpret the mechanisms of transportation/deposition of each of these modal components and in estimating their relative component weight fractions as well as for simultaneous multi-group (or two-group) linear discrimination among several possible clastic sedimentary depositional environments (see, Sahu, 1983, 1962 and 1964). In addition, practical helps for correct sampling process for sedimentary rocks on basis of sedimentation units and for directions of cutting these rock samples for optimal fabric interpretations and optimal numbers of circle radii/ half-intercepts required in the thin sections to yield the same precision in the 3D space are also discussed.

Keywords: Polymodal Phi-size Distribution, Clastic Rocks, Size moments, Thin section, Semi-intercepts.

INTRODUCTION

Thin/polished section method is the only recourse for grain size analysis of indurated (sedimentary) rocks and ores which are not easily disaggregated for size analysis by other methods such as, sieving or settling velocity methods (see, Sahu,1987).Thin section grain sizes are measured as equivalent circle radii(x in 2D) or as half-intercepts(t in 1D) but it may be clearly understood that half-intercepts in 1D exist only if the corresponding circle radii in 2D is cut by the section and available for measurement,(i.e., data of half-intercepts are conditional on the existence of 2D circle and 1D data CANNOT be transformed directly to 3D data(sphere radii,r in 3D) (as has been suggested and utilized in their papers on Stereology by a few western-school authors) unless conditional probability is multiplied by the correct/ proper marginal probability (see, Sahu,1974b) and an intermediate stage of computing the harmonic mean of circle radii(x) from corrected half-intercept(t) distribution is absolutely necessary(see,Sahu,1974b)). The added advantages of thin/polished section size analysis are: simultaneous measurement of mineralogy, shape, sphericity, roundness of these grains/pores as well as of bulk properties like porosity, packing, cement type and its intensity, diagenesis etc. The advantage of excellent measurement precision of abouts ¼ micron on thin sections, is marred by certain difficulties such as: (i) frequency is recorded as numbers whereas sedimentologists usually need volume/weight frequency since numbers are impossible to count for fine sizes such as silts and clays , (ii) observed size distributions of circle radii/half-intercepts are highly biased towards smaller sizes as the section cannot pass through centres of all the grains cut by it (i.e ,x is less than r; t is less than x) and must be corrected probabilistically to yield the true sphere radii distribution on weight frequency basis, (iii) the probabilistically corrected sphere radii (in mm) distribution has to be transformed to equivalent phi-size moments and phi-size parameters in order to make appropriate sedimentological inference, where,

phi is defined as the negative logarithm to the base 2 of the grain diameter in mm, (iv) optimal sample sizes (number of circle radii/half-intercepts) to be counted on thin section are often very large (14 times) to yield the same precision as that in the 3D space (see, Sahu,1977), and finally, (v) the method is rather unsuitable and very difficult to use for very fine clays/colloids or for very coarse gravels and conglomerates. Most of these defects have already been solved by the author in his earlier papers(see, Sahu, 1974a,b,c, 1977, 1976a,b, 1985, 1965a,b for unimodal phi-normal distributions). However, it is well-known that clastic sediments often contain two or three phi-normal size components related to several types of bedload, saltation and suspension loads and are seldom unimodal phi-normal distribution (except for many beach sands which are unimodal bed loads).Therefore, it is crucial to transform the corrected sphere radii distribution moments (from thin/polished section size data) to generate the required phi-size component fractions, phi-size means and phi-size variances of each of these phi-normal modes on weight frequency basis, so that proper inferences can be made on mechanisms of sediment transportation/deposition and also on depositional environment of the analyzed samples.

New mathematical equations are presented now consisting of transformation of weight frequency moments of sphere radii about the origin (zero mm) in 3D space to obtain phi-component weight fraction (k;1-k), phi means (μ_1 & μ_2) and phi variances (σ^2_1 and σ^2_2) of each of the two phi-normal size component(i.e., assuming bimodal phi-normal distributions of each mode in the sample), where mode one refer to bedload mode and mode two refer to saltation-load mode. This method can be extended to include a third phi-normal mode by analysis of a separate bimodal system comprising suspension and saltation loads , and then, integrating the above two bimodal analyses to give a trimodal phi-normal components as the saltation mode is common to both bimodal analyses.

The above proposed method can also be easily extended in the same way to include polymodal size distributions, if required (especially for tillites, fanglomerates, submarine slides, debris flows, other coarse turbidities, etc.). However, it may be noted that the probability of bedload and suspension load forming a bimodal system (without the saltation load), does not form a cogenetic bimodal phi-normal sample because of the contrasting ranges of velocities required of the transporting agent for this purpose.

GEOLOGICAL CONSIDERATIONS

Clastic sediments are transported by some agents such as gravity, glacier, river, wind, ocean waves and currents, turbidity currents under different mechanisms such as various types of bedloads, saltaion load and suspension load and are deposited at places when the velocity of transportation becomes much less than the settling velocity of the concerned clastic grain (depositional environment). Therefore, clastic sediments often exhibit bimodal or trimodal size distributions and rarely show unimodal phi-normal size distribution (beach sands, aeolian flats, loess etc.). Since the natural sizes of clastic grains vary very widely in the arithmetic scale (mm.) from boulders (10^{18}, mm) to fine clays/ colloids($10^{-21.5}$ mm), having a range of 39.5 orders of magnitude, a logarithmic scale is absolutely required and generally used to analyse these size distributions. So, Krumbein's phi-scale, where phi is defined as the negative logarithm to base two of the particle diameter in mm, has found standard use among the sedimentologists world-over but it is inverse/resverse of the arithmetic sizes and range from minus 18 phi (boulders) to plus 21.5 phi (fine clays/colloids). Bimodal phi-normal components may be present in the deposited sediments as saltation cum bedload deposits (river levees and channels, aeolian dunes, deltas, shallow marine/laccustrine, distal turbidites etc.) or as rolling grain bedload cum sliding grain bedload deposits (alluvial fans, glacio-fluvial, debris flows, river channels, submarine channels, proximal turbidites, etc.). Trimodal phi-size deposits are less frequent but are characteristic of proximal turbidites, glacial tills, delta distributary channels, alluvial fan channels, debris flows etc. Thus, grain size distributions, if properly utilized, can give very useful sedimentological inferences as to the mechanisms of transportation/deposition of the different size fractions as well as regarding the nature of depositional environment .In order to achieve useful results, samples must be collected and analysed with proper reference to sedimentation units which represent the thickness deposited under similar fluctuations of the velocity conditions (Otto, 1938). Thin sections must be cut with reference to the sedimentation unit and with reference to primary fabric within the sedimentation unit. If the sediment is homogeneous and isotropic then any random section would yield equivalent result. But most sediments are known to have preferred fabrics (such as monoclinic under unidirectional flow, orthotropic under bidirectional orthogonal flow, rarely triclinic fabric also). Hence, thin sections must be cut along a-c plane, b-c plane and a-b plane for monoclinic fabric and three mutually perpendicular sections, one along bedding plane, and two sections perpendicular to bedding plane for orthotropic fabrics and homogeneous and isotropic fabrics etc. In a turbidite sample showing graded bedding, thin section must be cut perpendicular to the bedding plane in order to include all the size components in the graded bed (sedimentation unit).

Thin section size analysis is ideal and suitable for sandstones, siltstones and coarse claystones and gives a precision of the order of ¼ micron that is impossible to achieve in the other commonly used methods such as sieving, settling, loose grain analysis. However, the precision of 1/4 micron cannot be translated from 2D/

1D sizes measured on section plane to the corrected sizes in 3D space, and 14 times circle radii (2D) or (14 x 14=) 196 times half-intercepts (t in 1D) are required to be measured to reach equivalent precision (Sahu, 1977). Hence, if one circle radius within the sample zone has probabilistic correction using Krumbein model; we require 13 circle radii to be cut and measured for probabilistic correction using Wicksell model on number frequency basis and both these models would yield same precision of sphere radii in 3D space (see, Sahu, 1977). Thus, 50 sphere radii(r in 3D) are equivalent to taking measurements of 700 circle radii(x in 2D), or 9800 half-intercepts (t in 1D) on the section plane on number frequency basis.

REVIEW OF MATHEMATICAL AND PROBABLITY PROBLEMS

Size analysis of single sedimentation units (Otto, 1938) are known to be sedimentologically meaningful as regards inferences on mechanisms of transportation and deposition of clastic grains present in the sample as well as of depositional environments (Sahu, 1962, 1964, 1983). Hence, thin sections of sediment samples must be cut parallel to the bedding planes of the sedimentation unit if no preferred primary shape fabric is existing (Sahu,1974a,b,c), otherwise cut sections parallel to a-c planes in monoclinic fabric, perpendicular to size grading in graded beds ,or in three mutually perpendicular directions (one perpendicular(a-c), another perpendicular(b-c) and third parallel(a-b) to bedding within the sedimentation unit in order to reconstruct the size distribution in 3D space and 3D fabrics. Let the observed size distribution on the thin section plane be designated as q(x), x being circle radii in mm, and this distribution is highly biased towards finer sizes as section plane does not intersect all the grains at their centres to give maximum (true) grain size of the particle intersected. Two types of probabilistic corrections have been advanced : (i) probability of intersection is directly proportional sphere radii(r in mm) and is(r/r(max)) = (r/R) where r(max) is taken as R, which is correct if grain centre lies outside section plane but incorrect for the grains whose centres lie on section plane(Wicksell,1925 model), and (ii) probability of intersection of grains is independent of sphere radii (r in mm) ,hence grains of different sizes have same probability of intersection (Krumbein,1935 model), which seems to be incorrect but gives better results than Wicksell‘s model in practice. This paradox has been resolved using author‘s (Sahu,1974, a,b,c or Sahu model where probability of intersection of grain lying within the unit cell of thickness 2R where the grain centre lies between plus and minus r(maximum in mm.)= R, perpendicular to section plane depends on two factors: (a) size(radius) factor (probability of intersection (r/r(max)); r(max) = R in some equations, and also (b) the unmeasurable perpendicular distance factor(z/r(max)) of grain centre from the section plane which is integrated out being a nuisance variable. Under the assumption that grain centers in the unit cell are having uniform(POISSON) distribution as to their perpendicular distance (z) from thin section plane. The weighted average of the two probabilities from Wicksell and Krumbein models, with a weighting factor of (α/(α + 1)) for Krumbein and of 1/(α+1) for Wicksell model probabilities is the correct solution(see, Sahu model,Sahu,1974a,b). Although, circle radii of grains lying on the section plane do not need any probabilistic corrections, we are unable to distinguish between the grains whose centres lie on the section and those which do not, therefore, probabilistic corrections are to be involuntarily made for all the measured circle radii distribution. The relative weight factors of Krumbein and Wicksell probability models can be estimated by a few iterations till convergence of initial α value of α(o), which is the ratio of maximum value of sphere radius (approximated as maximum size of observed circle radius) divided by the Krumbein model - corrected(estimated average sphere radii) average value of circle radii (Sahu,1974a). Probability of intersection ,p(int,r), of a sphere of radius r by the thin section plane is given by integrating out distance z under uniform distribution within the unit cell is given by p(int,r) = ½ + ½ (r/ R= ½ + ½ (r/($_{r(av)}$) . (1/ R/($_{r(av)}$))= ½ + ½ (r/ r(av)) . (1/α), where α = R/($_{r(av)}$) and R is the maximum sphere radius,(r(max), in the sample. More details of mathematical theories for thin section size studies are given in the publications (Sahu, 1974a,b,c;19 76a,b,1977).

Let n(r,i) be the ith arithmetic number frequency moments about origin of sphere radii in mm, and n(x,i) be the ith arithmetic number frequency moments about origin of the observed (biased to much smaller radii) circle radii(x in mm), (with n(x, -1) being the harmonic mean of circle radii). As given in Sahu (1974a) the solution, for i more than 1, is given as Equation 1 below:

$$n(r,i)=(\alpha/(\alpha+1))\{\int_0^{\pi/2} \mathrm{Sin}\,\theta\, d\theta)^{i+1}\}^{-1} n(n,i) + (1/(\alpha+1))\{\int_{\pi/2}^{I} \mathrm{Sin}\,\theta\, d\theta)\}^{-1} n(x,i-1) \times ((\pi/2)\, n(x,-1)); \quad (1)$$

These equations can be easily solved to get all the higher positive moments from i= 1 ,2,3,4,5,6, onwards. For example, the first four number frequency sphere radii moments are as follows:

$$n(r,1)=(1/(\alpha+1))\{\alpha(4/\pi)\, n(x,1) + (\pi/2)\, n(x,-1)\}, \quad (2)$$

$$n(r,2)=(1/(\alpha+1))\{\alpha(3/2)\, n(x,2) + (4/\pi)\, n(x,1)\,.(\pi/2)\, n(x,-1)\}, \quad (3)$$

$$n(r,3)=(1/(\alpha+1))\{\alpha(16/3\,\pi)\, n(x,3) (3/2)\, n(x,2)\,.(\pi/2)\, n(x,-1)\}, \quad (4)$$

$$n(r,4)=(1/(\alpha+1))\{\alpha(15/8)\, n(x,4) + (16/3\,\pi)\, n(x,3)\,.(\pi/2)\, n(x,-1). \quad (5)$$

The inverse of correction factors given under integral sign of some power of sinθ for various integer values of i in Eqn(1) are listed below for convenience as follows:

It is usual practice in sedimentology to utilize weight (volume) frequency, as silt- and clay-sized grains are uncountable in the samples, rather than number frequency which isa impossible to obtain/count for very fine silt or clay sized particles. So, we must convert the corrected number frequency moments, n(r,i), given by Eqn.(1), to corresponding (corrected) weight frequency moments w(r,i) for i= 1,2,3, etc. (Sahu, 1974 a,b) as:

$$w(r,i)=n(r,(3+i))/(n(r,3)) \quad (6)$$

Thus, we conclude that on basis of equivalent precision in the 3D space (Sahu, 1977) Krumbein model is dominant (13/14= 93%) over Wicksell model (1/14 = 7%) on number basis. Although both these models are partly incorrect, they are jointly necessary in combination to obtain the true sphere radii distributions (Sahu1974a,b,c). The total number of grains present in the unit cell covered by thin section size measurements (in 3D space per unit volume as cubic mm) is given by N(o)(Sahu,1974a):

$$N(o) = (1- Q) / (4 \pi/3). n(r,3),$$

where Q is the porosity volume-fraction in the sample that is thin-sectioned, and, also the

average grain sphericity ($\overline{\psi}$) in 3D is given by (Sahu,1974c):

$$=(36)^{1/3} (3/4 \pi)^{1/3}(n(r,2)/n(r,3)) \{(1–Q)/(s) \},$$

where, s is the specific surface (surface area per unit bulk volume of rock), (see,Sahu,1974c for details). The porosity volume fraction Q can be obtained by point counts on a square grid superposed on the thin/polished section.

Equations(6) for i greater than zero would be required to generate modal weight fraction (k(i)) phi means and phi variances of each of the modes(suspension, saltation and bedload) which are considered to be individually ph-normal in their distributions (Sahu,1962,1964). In most sandstones and siltstones bimodal phi-normal distributions are frequent comprising saltation and rolling-grain bedload transportation/deposition. We develop new linearized moment equations to estimate all the five independent

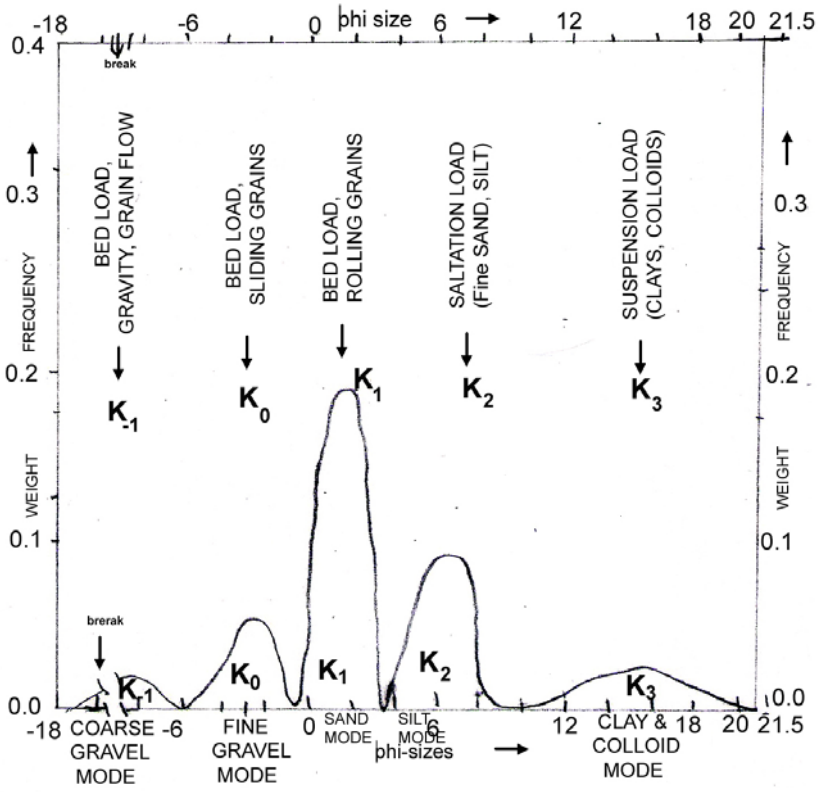

Fig. 1. Conceptual polymodal phi-normal size components of deposited clastic sediments with their mechanisms (modes) of transport and deposition. Usually only 2 or 3 contiguous modes may be present in the sample.

parameters of the sample in 3D space using w(r,i) values of Eqn.6 ,for the i values necessary, as inputs. The bimodal solution reduces readily to unimodal phi-normal solution (Sahu, 1965a,b) if we put k(i) = 1.0; and can be easily extended to trimodal phi-normal component modes(including sliding-grain bedload), if required and desired (see, Fig. 1). If graphical statistics based cumulative weight frequency curves for sphere radii distribution is necessary, then the readers may follow methods of Gram-Charlier/ Edgeworth expansions as given in Sahu (1967, 1968).

THEORY OF ESTIMATION OF BIMODAL/ POLYMODAL PHI PARAMETER

The weight frequency moments of sphere radii w(r,i) for all intergers, i greater than 0, are inputs (where r is available as arithmetic mm scale) and these are to be transformed to bimodal/polymodal phi-normal components (suspension ,saltation, several types of bedload) with parameters as the ith. component fraction,k(i), phi-mean and phi-variance of each mode, but since k(i) sum to 1.0,only (i-1) component fractions are independent. Thus, bimodal distributions have 5 (one proportion,two phi-means, and two phi-variances) and trimodal distribution have 8 (two proportions, three phi-means and three phi-variances) parameters to estimate. The moment equations are in arithmetic scale and hence are highly nonlinear exponential equations and have to be linearized by taking natural logarithmic (ln) transform on both right-(RHS) and left-handsides(LHS). Fortunately, we need only three w(r,i) equations to solve bimodal parameter estimation problem because arithmetic and phi moments are related by log-normal distribution model. We denote rolling-grain bedload mode as mode 1 and saltation mode as mode 2 with the knowledge that phi mean and phi variance of saltation mode would be much greater relative to corresponding phi mean and phi variance of rolling-grain bedload mode .Also, phi mean and phi variance of saltation mode deposits would be much less than the corresponding phi mean and phi variance for suspension mode. Similar relations exist for other bedload modes (gravity,sliding and rolling grains) (see,Figure 1) (Sahu, ms. in preparation). It may be noted that only the (corrected) moments in mm. are available in the higher dimensional space (3D) and hence can be used in estimation of parameters in the higher dimensional space. But the detailed size distribution is not available in higher dimensional space and thence any other statistical estimation method such as maximum likelihood etc. cannot be utilized.

If k(1) = 1 (unimodal phi normal component), then the linearized solution taking natural logarithm transform, ln transform, to both sides is given in Sahu(1965a):

$$\ln w(r,1) = -(\ln 2)\mu_1 + (1/2)(\ln 2)^2(\sigma_1)^2 \quad (7)$$

$$\ln w(r,2) = -2(\ln 2)\mu_1 + 2(\ln 2)^2(\sigma_1)^2 \quad (8)$$

Solving these two equations simultaneously, we obtain (Sahu,1965a):

$$\ln(w(r2)/w(r,1)^2) = (\ln 2)^2(\sigma_1)^2 \quad (9)$$

$$\text{or,}((\sigma_1)^2) = \ln(w(r,2)/w(r,1)^2)/(\ln 2)^2 \quad (9A)$$

$$(\ln 2)\mu_1 = (1/2)\ln(w(r,2)/(w(r,1)^4) \quad (10)$$

$$\text{or,}\mu_1 = (1/2)\ln(w(r,2)/(wr,1)^4)/(\ln 2) \quad (10A)$$

Substituting the values of phimean(10A) and phivariance (9A) into third moment equation(i=3) of Eqn.1 and the fourth moment equation(i = 4) of Eqn.1 give phi-skewness and phi-kurtosis, respectively (see, Sahu, 1965a), which would be zeros if the size distribution for sphere radii on weight frequency is truly unimodal and phinormal and hence, the above solution is acceptable. Eqns. 10A and 9A give the phimean and phi variance of rolling-grain bedload mode in the sample.

For bimodal phinormal distribution, we have five independent parameters, on component fraction k(1) for rolling-grain bedload mode (which is greater than zero but less than unity) with phimean μ_1 and phivariance $(\sigma_1)^2$: μ_2 and $(\sigma_2)^2$ for saltation load mode with k(2) = 1- k(1). The mth moment,linearized by ln transform, is given by:

$$\ln(w(r,m)) = \ln(k(1)) - m(\ln 2)\mu_1 + (1/2)m^2(\ln 2)^2(\sigma_1)^2 + \ln(1-k(1)) - m(\ln 2)\mu_2 + (1/2)m^2(\ln 2)^2(\sigma_2)^2 \quad (11)$$

If k(1) =1, then saltation load is zero and its parameters need not be estimated and we obtain bedload phi-size parameters (mean and variance) ,respectively, as μ (1) and $(\sigma_1)^2$, using equations (10A), and (9A), respectively. If k(1) lies strictly between zero and unity , then saltation fraction is also existing and need to be estimated for its phi mean μ_2 and $(\sigma_2)^2$ as well as k(1) or 1-k(1). Equating one part of left-hand-side (LHS) of Eqn11 multiplied by k(1) and to the second term or saltaion component of the right-hand-side (RHS) of Eqn 11 , we obtain:

$$\ln(w(r,m)) = \ln(1-k(1))/k(1)) - m(\ln 2)\mu_2 + (1/2)m^2(\ln 2)^2(\sigma_2)^2 \quad (12)$$

In Eq(12), there are three parameters, so we should have three linearized moment equations to solve these three unknowns.

Differencing Eqn(12) for m=1 from Eqn(12) for m=2, we get,

$$\ln((w(r,2)/w(r,1)) = -(\ln 2)\mu_2 + (3/2)m^2(\ln 2)^2(\sigma_2)^2 \quad (13)$$

Similarly, differencing Eqn.12 for m =2 from Eqn. 12 for m=3, we get

$$\ln((w(r,3)/(w(r,2))=-(\ln 2)\mu_2+(5/2)(\ln 2)^2.(\sigma_2)^2. \quad (14)$$

Subtracting Eqn 13 from Eqn 14 , we obtain

$$(\ln 2)^2.(\sigma_2)^2=\ln\{(w(r,3).w(r,1))/(w(r,2)^2)\} \quad (15)$$

$$\text{or},(\sigma_2^2)=[\ln((w(r,3).w(r,1))/w(r,2)^2)]/(\ln 2)^2 \quad (15A)$$

Similarly, multiplying Eqn 13 by 5 and Eqn 14 by 3 and then subtracting the first from second product, we get,

$$(\ln 2)\mu_2=\ln\{((w(r,1)^5.w(r,3)^3)^{1/2}/(w(r,2)^4\} \quad (16)$$

$$\text{or},\mu_2=\ln\{((w(r,1)^5.w(r,3)^3)^{1/2}/(w(r,2)^4\}/(\ln 2). \quad (16A)$$

Substituting, Eqns 16 and 15 into Eqn 12 having a value of m=1, we get,

$$\ln\{(1-k(1))/k(1))\}=\ln[\{w(r,1)^3.w(r,3)\}/w(r,2)^3] \quad (17)$$

$$\text{or},k(1)=w(r,2)^3/\{(w(r,2)^3+w(r,1)^3.w(r,3)\}. \quad (17A)$$

We can easily get the saltation mode phi-normal weight fraction , k(2) = (1 – k(1)) ; where k(1) + k(2) = 1.0. Therefore, k(1) is the modal weight fraction of the rolling-grain bedload mode in the sample.

Equations 15A and 16A give the saltation mode phi-normal parameters; phi variance and phi mean, respectively.

Trimodal phi-normal components (sliding-grain bedload component k(0) and phi parameters of bedload can be estimated by using the bimodal equations developed above for another bimodal distribution with rolling-grain bedload as k(1), μ_1 and $(\sigma_1)^2$ and slisiding-grain bedload phi parameters as μ_0 and $(\sigma_0)^2$, with the restriction that all three component fractions, k's add to 1.0, we then integrate these results of all these three modes for sedimentological inferences.

It may be noted that because of velocity of transportation/deposition processes never overlap in nature from very high values for gravels and extremely low values for fine clays, we cannot expect any cogenetic bimodal phi-normal deposit having gravels and clays (with no sands and silts) and therefore, any bimodal gravel having a lot of clays must have formed by subsequent(later) infiltration of clays into the open pores of these gravels and these components are not cogenetic, and hence cannot be interpreted as deposited by a single process (or a single sedimentation unit).

CONCLUSIONS

Thin/polished section size analysis of most ores and (sedimentary) rocks is essential as induration often defies disaggregation of grains, so that sieving, settling and loose grain size analysis could be performed. This method is very precise(abouts ¼ micron) but require complicated and several mathematical transformations and probabilistic corrections are required in order to use it for estimating assay values of ores precisely on weight basis or for inferring mechanisms of transportation/deposition of different size fractions and depositional environments of clastic sediments (Sahu,1964,1983,1974a,b,c).

Although the mathematical and probabilistic correction methods were introduced as early as 1925(Wicksell), no realistic sedimentological applications of thin section size analysis have been made as yet, except for empirical comparison of samples.

The reason for lack of progress is mainly because available weight frequency of sphere radii (3D space) are in arithmetic(mm) scale(see, Sahu,1974 a,b,c) but sedimentologists require size parameters in phi scale for bimodal/trimodal size components (bedload, saltation or suspension loads) commonly found in the deposited sediments. Therefore, we give new results to transform weight frequency moments of sphere radii (corrected using Sahu 1974a,b,c model) from observed thin section size distributions to yield weight fraction, phi mean and phi variance of each mode present in the sediment. These results would give powerful and precise information for enhancing inferences on mechanisms and environments of deposition (see, Sahu, 1962, 1964, 1983). More details on physics and m,athematics of transportation and deposition of clastics are given elsewhere (Sahu, ms. In preparation).

Thin section of homogeneous and isotropic rocks can be cut in any direction to yield good results and serial sections at intervals of 2 r(maximum) = 2R ,would provide independent information to cover the entire sample. But deposited sediments usually possess monoclinic primary fabrics under unidirectional flow or orthotropic primary fabrics in mutually perpendicular flows. So, thin sections or serial sections should be cut in accordance with the primary fabric in order the results to be meaningful. Thin section size distribution can reflect only the size distribution within the unit cell of thickness 2 r(maximum) in the sample containing the thin section plane(see,Sahu,1974a).For graded beds or turbidites, thin sections must be cut perpendicular to the bedding plane.

Optimal sample sizes on number basis (Sahu, 1976a,b;1977) has been studied and it was shown that 100 sphere radii precision on 3D space would require 1400 circle radii or (14 x 14 =) 19600 half-intercepts to measured on the section plane. This seems rather forbidding but computer/image-analyses methods of thin/polished section size studies are now common, hence thin section size analysis is now practicable and very useful for making sedimentological inferences on mechanisms and environments of deposition of clastic sediments.

References

Krumbein,W.C., (1935). Thin-section mechanical analysis of indurated sediments. Jour.Geol.,43, 482-496.

Otto,G.H., (1938). The sedimentation unit and its use in field sampling. Jour. Geol., 46, 569-582.

Sahu, B.K., (1962). Environments of deposition from size analysis of clastic sediments., Ph.D., Univ. Wis. (Madison), 99p.

Sahu, B.K., (1964). Depositional mechanisms from size analysis of clastic sediments. J. Sedim.Petrol., 34, 73-83.

Sahu, B.K.,(1965a).Transformation of arithmetic and phi size distribution moments. J.Sedim.Petrol., 35, 969-972.

Sahu, B.K.,(1965b).Transformation of weight and number frequency for phi-normal size distribution.J.Sedim.Petrol.35, 973-975.

Sahu, B.K.,(1967). Generation of cumulative frequencies from corrected phi size moments from random thin-section size analysis data. Sedimentology, 8, 329-335.

Sahu, B.K.,(1968). Thin-section size analysis and the moment problem.Sedimentology,10, 147-151.

Sahu, B.K., (1974a). Probabilistic solution to thin section size measures. Ind.J.Earth Sci, 1(1), 22-36.

Sahu, B.K., (1974b). Probabilistic solution to thin section size studies expressing size as intercepts and frequency as number or as measure. Ind. J. earth Sci., 1(2), 168-176.

Sahu, B.K., (1974c). Determination of average grain sphericity in granular porous media. J.Sedim.Petrol., 44(2), 578-582.

Sahu, B.K., (1976a). Size interpretation in higher space from size measurements in lower space. Intl. Sem. Stereology, Kosice, Checkoslovakia, 88-95.

Sahu, B.K.,(1976b), Mathematical theory of counting 2D grains by line and ribbon methods. Sed. Geol.,16, 177-192.

Sahu, B.K., (1977). Optimal sample size for thin section size studies. Sed. Geol., 19, 185-196.

Sahu, B.K.,(1983). Multigroup discrimination of depositional environments using size distribution statistics.Ind.J.Earth Sci.,10, 20-29.

Sahu, B.K., (1985). Prediction of size and shape statistics in 3D space from thin section studies of natural quartz grains. 4th European Symposium Stereology,Goteburg,Sweden,Extended Abs.(94) 4p.

Sahu, B.K., (1987). Statistical applications in sedimentological analysis of Purana Basins. Mem.Geol.Soc.Ind., No.6, 287-293.

Sahu,B.K., (2009). Physics and mathematics of transportation and depositional processes for clastic sediments.(In preparation).

Wicksell,S.D.(1925). The corpuscule problem. Biometrika, 17, 84-99.

Jour. Indian Association of Sedimentologists, Vol. 28, No. 1 (2009), pp. 9-16

Potential Evaluation of Thin Bedded Sand Shale Sequences in Deep Water Settings

ANIL KUMAR TYAGI and RABI BASTIA*,
Reliance Industries Limited, Madhumita Das, Utkal University, India
*E-mail: rabi.bastia@ril.com

Abstract: Reservoir property estimation of a clean & medium to coarse grained sand is relatively simpler job. However, it gets complicated in the overbank area, where thickness of the sand and shale alternations decreases below the logging tool resolution. These thin laminations require special treatment while identifying and evaluating their properties.

Geologically thin beds are defined as the most readily recognized layers of a sedimentary body, and are considered to be the basic building blocks of these bodies. Beds are bounded by depositional surfaces termed bedding surfaces.

The mains problem in estimating the hydrocarbon pore volume from well logs is that it does not measure directly the reservoir properties, i.e., the net sand thickness, sand porosity, and sand water saturation. Instead, the logs measure petrophysical properties of the rock such as bulk density and resistivity, from which the reservoir properties are inferred. Second, the petrophysical log measurements represent averages over some collection of beds that are too thin to be measured individually. To infer reservoir properties from these measurements, it is necessary to understand how the properties of an extended reservoir volume are related to the properties of the individual bed types within that volume. The third reason is that some petrophysical properties are anisotropic — their values depend not only on the composition of the measured volume, but on a choice of orientation within that volume. Anisotropy further complicates the inference of reservoir properties from measured petrophysical properties.

There are various techniques available in the industries for the net pay estimation. These are counting laminations using the Image logs, Lam count study on cores, Thomas Stiber Technique using conventional logs etc. The real challenge lies in the hydrocarbon saturation estimation, where resistivity is highly affected due to conductive shales in-between the resistive sands. Some experts like to assign the same hydrocarbon saturation and porosities to thin beds as that of the thick beds. Some prefer to classify the facies based on the resistivity micro Image logs and than carry out de-convolution does derive the properties of the beds using Inverse modeling Technique. Both has some advantages / dis-advantages, but the problem gets complicated once the drilling mud is changed over to Oil Base Mud(OBM), as the facies classification is no more a easy job. Tri-axial resistivity tools provide an alternative to the thin bed analysis as it does not depend on the vertical resolution of individual beds. The technique use the resistivity anisotropy approach coupled with the modified Thomas-Stiber technique for the estimation of porosity and saturation.

Keywords: Thin beds, Deep water setting, Reservoir property, Overbank area.

INTRODUCTION

The log interpretation problem in laminated shaly sand formations is not only due to log resolution, but also because of conventional resistivity measurements are dominated by low resistivity layers. This means that the majority of the response is due to the conductive shales, while the sand layers containing either hydrocarbon or water will have little effect as the current bypass them..

The Fig. 1 shows conventional resistivity in a laminated shaly-sand formation The sand resistivity (R_{sd}) is 20ohm-m and the shale resistivity (R_{sh}) is 1 ohm-m. As the laminar shale increases the resistivity decreases drastically. This leads to very large uncertainties in the apparent sand resistivity, even at relatively small volumes of shale.

The reason for this effect is that conventional resistivity measurements are made horizontally into the formation, and follow the parallel resistor model:
Hence:

$$\frac{1}{R_t} = \frac{1}{R_{ss}}(1 - Vsh_{lam}) + \frac{1}{R_{sh}}(Vsh_{lam}) \quad \text{.....(Eq.1)}$$

Where:

R_t = formation resistivity (also referred to as R_h)
R_{ss} = sandstone layer resistivity
R_{sh} = shale layer resistivity
Vsh_{lam} = Volume of laminar shale

The current takes the path of least resistance through the more conductive shale layers of the formation and hence bypass the more resistive sand

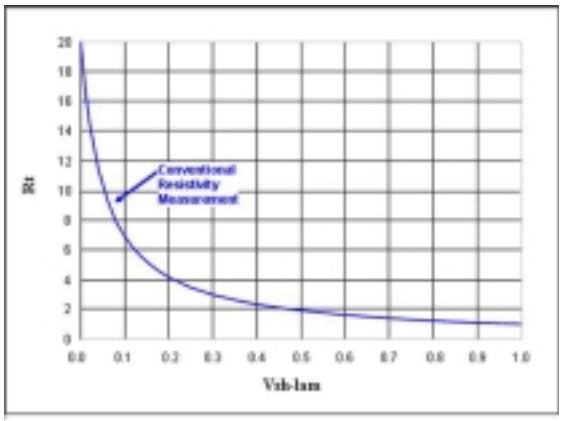

Fig. 1. Theoretical response of a horizontal resistivity measurement in a flat, laminated shaly sand formation, where R_{sd} = 20 ohm-m, and R_{sh} = 1 ohm-m.

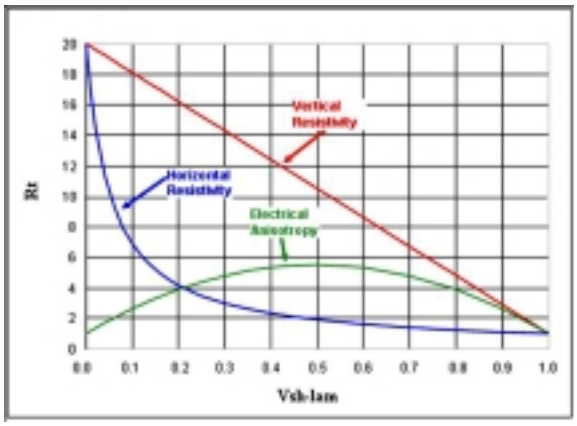

Fig. 2. The theoretical responses of horizontal and vertical resistivity measurements in a flat, laminated shaly sand formation, where R_{sd} = 20 ohm-m, and R_{sh} = 1 ohm-m.

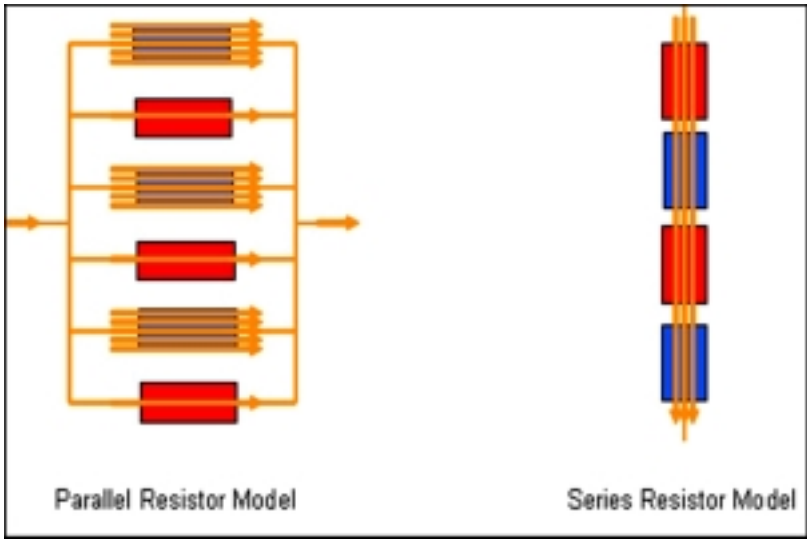

Fig. 3. Representation of the theoretical difference between horizontal and vertical resistivity measurements in flat laminated shaly sand formations.

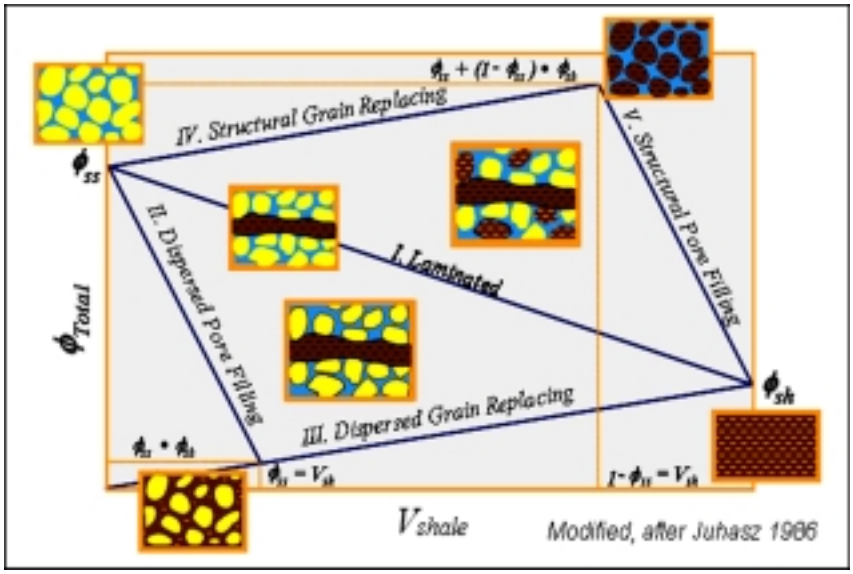

Fig. 4. Thomas Stieber Shale Distribution Model.

layers. The greater is the contrast between the layers the more acute is the problem.

The new generation 3D induction tools measures both the horizontal and vertical resistivities of the layered formation. The advantage of making a vertical resistivity measurement is that the current is forced through all layers of the formation, and is therefore affected by both horizontal and vertical components. Fig. 2 compares the conventional horizontal measurement with the vertical measurement in the same formation, where the sand layers have a resistivity of 20 ohm-m and the shale layers have a resistivity of 1 ohm-m.

While the horizontal measurement was described above as following the parallel resistor model, the vertical measurement follows the series resistor model. Therefore;

$$R_v = R_{ss}\ (1-V_{shlam}) + R_{sh}\ V_{shlam} \qquad \text{(Eq.2)}$$

Where:

R_{ss} = sandstone layer resistivity
R_{sh} = shale layer resistivity
Vsh_{lam} = volume of laminar shale

The theoretical difference between horizontal and vertical resistivity measurements in flat laminated shaly-sand formations is graphically represented by the two models in Fig. 3.

The parallel and series equations above are generally written in terms of conductivity:

$$C_h = C_{ss}(1 - Vsh_{lam}) + C_{sh} \cdot Vsh_{lam} \qquad \text{(Eq.3)}$$

$$C_v = \frac{1 - Vsh_{lam}}{C_{ss}} + \frac{Vsh_{lam}}{C_{sh}} \qquad \text{(Eq.4)}$$

Where:

C_h = horizontal conductivity
C_v = vertical conductivity
Vshlam = volume of laminar shale
C_{ss} = conductivity of the laminar sandstone
C_{sh} = conductivity of shale

Equation 3 & 4 are solved for three unknowns, Vsh_{lam}, C_{sh} and C_{ss} using measured values of C_h and C_v. Using C_{sh} from nearby thick shale beds, which is common practice in conventional shaly sand interpretation, the equations can be solved two remaining unknowns. Thus:

$$C_{ss} = C_v \frac{C_{sh} - C_h}{C_{sh} - C_v} \quad \text{and} \quad Vsh_{lam} = \frac{C_h - C_{ss}}{C_{sh} - C_{ss}} \qquad \text{(Eq.5)}$$

This is a simple version of the model, used here to illustrate the general theory. In reality, anisotropy is present not just in the overall formation, but also on a micro-scale in the shales themselves. Therefore we need to introduce two shale conductivity terms, Csh_h and Csh_v, which are the horizontal and vertical conductivities of shale. This means that the above equations may be modifies as below;

where,

$$C_{ss} = \frac{1}{2}\{C_{isd} + Csh_h \pm \sqrt{(Csh_h + C_{isd})^2 \cdot (1 + \triangle C)}\} \qquad \text{(Eq.6)}$$

$$\triangle C = 4\, C_{isd} \frac{Csh_h - Csh_v}{(C_{isd} - Csh_h)^2}$$

And

$$C_{isd} = C_v \cdot \frac{Csh_h - C_h}{Csh_v - C_v}$$

C_{isd} is the isotropic sand conductivity. If the shale is isotropic (Csh_h=Csh_v) then C_{isd} would equal the sand conductivity, C_{ss}.

$$Vsh_{lam} = \frac{C_h - C_{ss}}{C_{sh_h} - C_{ss}}$$

In this way, the shale lamination effects are removed from the overall measurements and only the sand properties remain. Thus, the water saturation of the sands can be found using the appropriate 'dispersed' shaly sand water saturation model. Laminated Shaly-Sand Analysis allows for an amount of dispersed shale to be present in the sand layers, and for this reason the Waxman-Smits equation is used. If no such dispersed shale is present the Archie equation is used.

THE THOMAS-STIEBER SHALE DISTRIBUTION MODEL

In laminated shaly-sand analysis the tensor resistivity model described above is used in conjunction with the Thomas-Stieber shale distribution model to provide additional information regarding the nature of the laminar shale. In known laminar sections, these two methodologies should closely agree and provide a model stability that neither methodology has independently.

The Thomas-Stieber 'volumetric' shale distribution model is based on the petrophysical assumption that if the maximum clean sand porosity, PHIT_MAX, and shale porosity, PHIT_SH, can be determined then the distribution of the shale in the formation can be derived from the total porosity to V_{sh} relationship (Fig. 4). This distribution divides the shale content into three shale

components (i) shale grains which replace porosity in the sand (dispersed shale), (ii) shale grains which replace sand grains of equal size (structural shale) and (iii) shale layers which replace both sand grains plus sand porosity (laminar shale). This relationship was derived from a material balance relationship published by Thomas and Stieber (1975).

The only input data for this model is total shale volume and total porosity. This is a 'shale' model, not a 'clay' model. Shale, by definition in this model, is a 'clay rich rock', generally composed of 40% to 60% clay and other silt size or smaller mineral grains. In this model, there is only one shale, and it is the same shale that may have three different distributions. Given that there are only two data inputs (total shale volume and total porosity) and two user defined parameters (clean sand porosity and shale porosity), the deterministic model is limited to either a laminar-dispersed shale or a laminar-structural shale solution.

In this approach, the volume of laminar shale is determined twice, first from the tensor equations and second by using the Thomas Stieber model. If the formation is laminated then both of these results should be the same. The Thomas Stieber model is simple with only two basic inputs, while the tensor model is more complex, relying on correct user input values for horizontal and vertical shale resistivity which are not always easily determined. The convergence of the two models in laminated intervals can be used by the analyst as a check that the shale resistivity values are valid.

However, it must be noted that there are fundamental differences between the definitions of laminated shale in the two models. In the Thomas Stieber model, shale which is both grain and porosity replacing is described as laminar. This means that a laminated formation which has been disturbed by bioturbation or slumping will still appear as laminated, even though the reservoir properties may not be good. On the other hand, for shale to be classed as laminar in the tensor model, the laminations must be laterally extensive, over the depth of investigation of the measurements. If the laminations are laterally extensive then the two volumes of laminar shale will agree. If the laminations have been disturbed in some way, the Thomas Stieber laminar shale volume will remain high, while the tensor version will be low. If the opposite occurs, and the Thomas Stieber laminar shale volume is low while the tensor volume is high, we can assume that there is an additional factor causing electrical anisotropy, such as thin highly resistive layers.

LAMINATED SHALY-SAND ANALYSIS WORKFLOW

Laminated Shaly-Sand Analysis (LSSA) is the implementation of a petrophysical model that is internally consistent both petrophysically and mathematically. It is based on the Thomas-Stieber volumetric shale distribution model and the tensor resistivity model.

It must be stressed that LSSA is not a three or more component 'multi-lithology' model, nor are multicomponent induction resistivity tools well suited for high resistivity or multi-lithology geological environments. The introduction of a high resistivity component, particularly thin limestone or dolomite stringers, will introduce significant electrical anisotropy that is not associated with the identification and petrophysical analysis of hydrocarbon bearing sandstones. The Thomas-Stieber model is based on an unconsolidated clastic (granular) relationship where shale either replaces grains, fills pore space, or replaces sand (grains + pore space). Carbonates and highly altered, cemented sandstones cannot be defined in the Thomas-Stieber porosity model.

The results from LSSA must be treated differently to conventional petrophysical results for shaly sand formations. Using conventional techniques for determining net pay, cut-offs for V_{sh}, S_w and porosity or permeability are used, and if an interval is considered too shaly then it is not counted as pay, even though thin layers of hydrocarbon bearing sand may be present.

In LSSA no V_{sh} cut-off is used. Instead only the sand layers in the formation are considered and those which pass the porosity or permeability and Sw cut-offs are counted as net pay. Therefore in a laminated shaly sand formation, which is 10m thick and contains 50% laminar shale, and 50% porous HC bearing sand layers, the net pay would be 5m. The typical workflow for LSSA is given below (Fig. 6).

The different steps followed during the LSSA workflow are summarized below;

1. Calculate V_{sh} using one or more of the conventional techniques available.
2. Calculate total and effective porosities using one of the conventional techniques available.
3. Use the Thomas-Stieber model to define the shale distribution (laminar and either dispersed or structural) from V_{sh} and total porosity.
4. Use the tensor resistivity model to determine the resistivity of the sand layers and the volume of laminar shale.
5. Ensure that the volumes of laminar shale from the Thomas-Stieber and Tensor models agree, If not then change parameters for the vertical and horizontal shale resistivities for the tensor model and the sand and shale porosities for the Thomas-Stieber model until a petrophysically sound solution is derived. (Shale porosity is changed at the porosity stage, while sand porosity is changed in the Thomas-Stieber cross-plot).
6. Calculate the total and effective porosity for the sand layers.
7. Determine the fluid saturations in the sand layers from the sand porosity and sand resistivity.

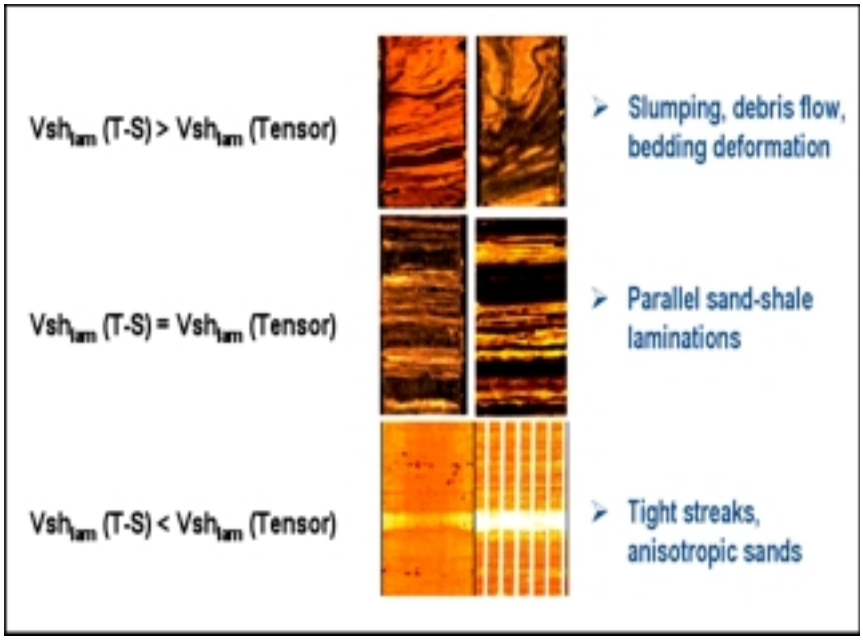

Fig. 5. Comparison of the volume of laminar shale from Thomas-Stieber and Tensor models indifferent formations.

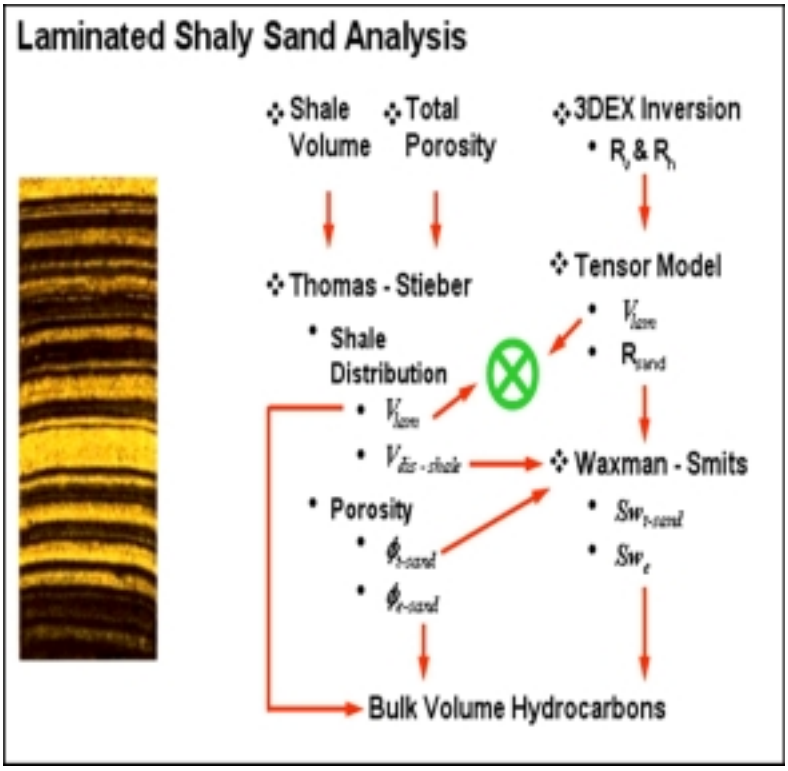

Fig. 6. Generalized LSSA workflow.

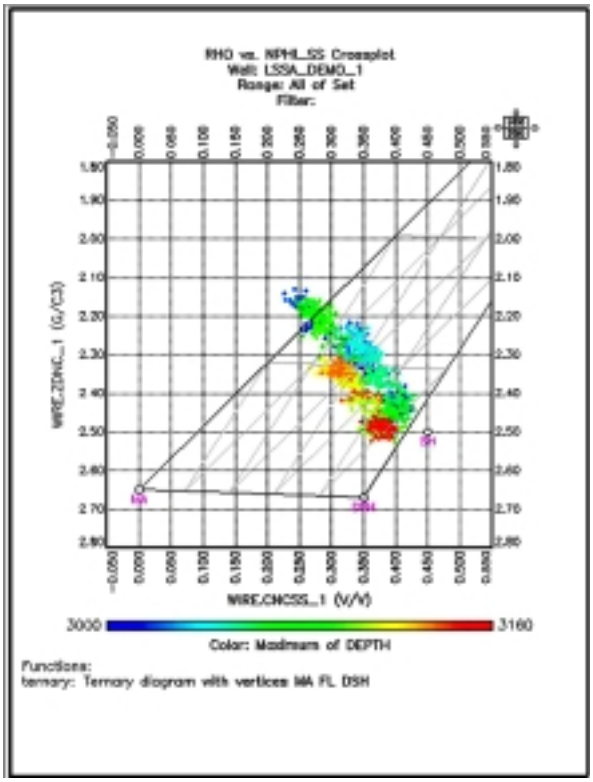

Fig. 7. Neutron Density (ND) cross-plot .

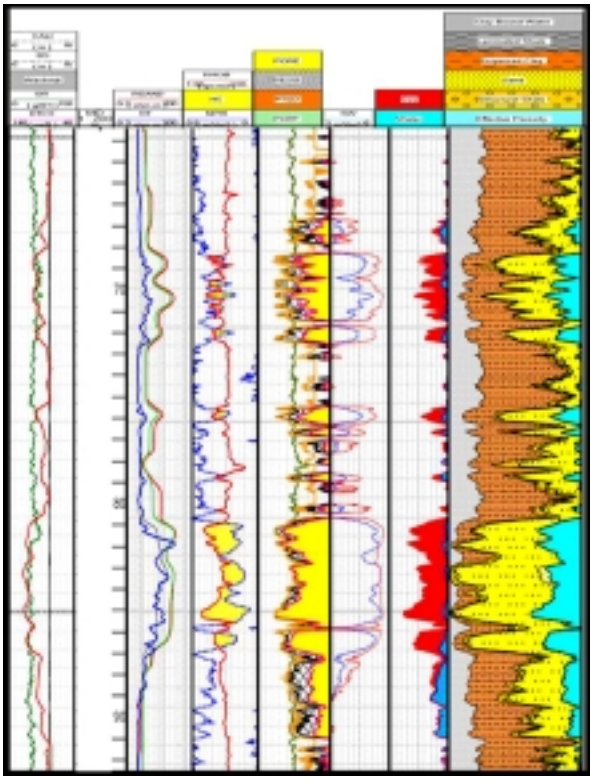

Fig. 9. LSSA processing results calibrated with core data.

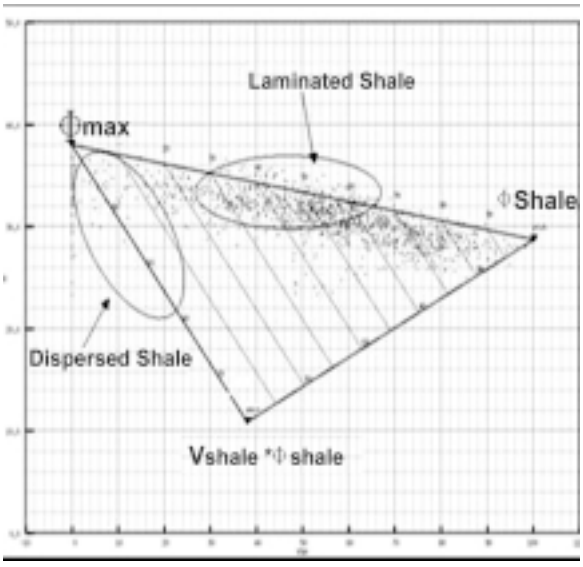

Fig. 8. Thomas Stieber cross-plot. with shale triangle.

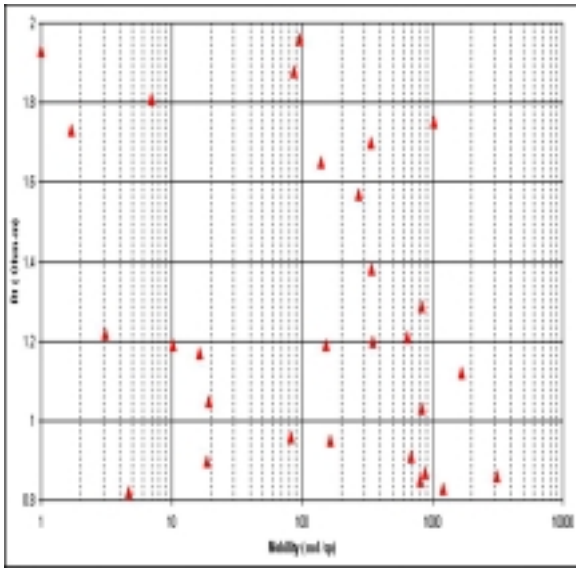

Fig. 10. Plot showing the MDT mobility vs the formation Resistivity showing formation producing gas with 1-2 ohm-m resistivity.

8. Calculate formation and sand permeability from one of the conventional techniques available.

9. Calculate the net sand counts, net pay counts and net to gross ratio, based on user input cutoff criteria.

The results at each stage need to be verified before moving on to the next stage. First Shale volume is to be calculated and verified before proceeding to the porosity estimation. At this stage both Vsh and Porosity will be calculated and the analyst can check that both of these agree before moving on to calculate the Thomas-Stieber shale distributions.

The parameter selection for the different zones can be picked up using the different cross plots like;

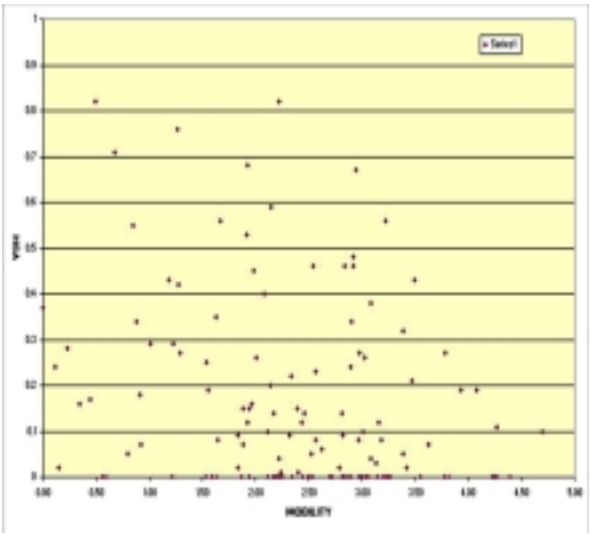

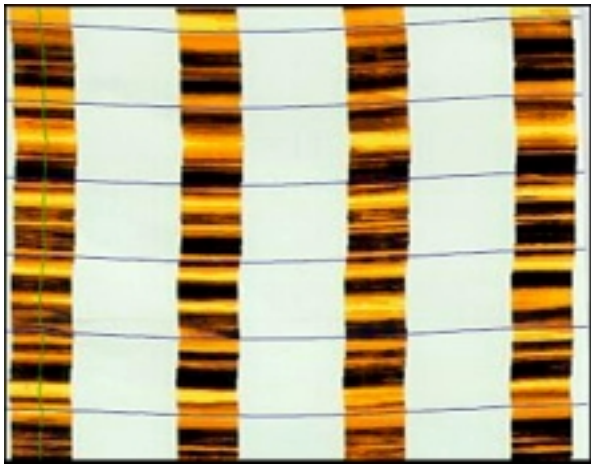

Fig. 11. Plot showing the MDT mobility vs Vshale computed from the processing indication Vshale cutoff as high as 85%.

- Neutron Density cross-plot
- Thomas Stieber cross-plot

The cross-plots also helps in identifying the need for zonation. For this reason the data points are colored based on depth, so if there is a variation in parameters with depth it can easily be seen. In The Neutron Density cross-plot, Fig. 7, is used to pick wet shale points for different zones, if any. When the well is zoned, the cross-plot is viewed zone by zone at a time. The shale point (S_h) is picked for each zone. The example in Fig. 7 shows that there are two zones (green and blue in the upper zone and orange, yellow and red in the lower zone). The Thomas Stieber crossplot, as shown in Fig. 8, is used to pick the maximum porosity in the sandstones, PHIT_MAX.

In the first track there is the GR alongwith the caliper data.

Track 2 is the depth track.

Track 3 shows the R_t (horizontal resistivity and R_{ss} resistivity curves computed using the R_v and R_h resistivities.

Track 4 shows the original neutron and density curves with shading in yellow showing the presence of gas.

Track 5 shows the total and effective porosities.

Track 6 represents the water saturation estimated using LSSA with the core derived water saturation.

Tracks 7 represent the volumetric estimation of the pore volume.

Track 8 shows breakdown of dry volumes for shales and sand, with a single shale bound water volume (CBW) shown on the left alongwith the porosity and volume of the hydrocarbon.

NET PAY ESTIMATION

In LSSA no V_{sh} cut-off is used. Instead only the sand layers in the formation are considered and those which pass the porosity or permeability and Sw cut-offs are counted as net pay. Fig. 10 indicates that resistivity as low as 1-2 ohm can produce the hydrocarbon, which is low due the sand shale intercalations.

Similarly Fig.11 shows the formation tester mobility vs. Rt (conventional) over the reservoir interval. It is apparent that there are many points where Rt is as low as 1 ohm-m but have very good mobility ranging from 10 – 1000 md. This further confirms that these sand shale laminations have very high permeability and potential to flow.

Vsh is very critical parameter for net pay calculation. Fig. 11 represents a cross plot of mobility vs. Vsh. It is clear that there are few high mobility points where Vsh is as high as 85%. Therefore, Vsh cutoff has to be high in case of laminated sand shale reservoir, may be as high as 85%. It will not be advisable to take it more than 85%, as 10- 15 % of quartz can be found in shales also, which if taken will overestimate the net pay.

CONCLUSIONS

There has been a lot of debate about the sustainability of the hydrocarbon production from thin beds. However, there are many examples across the world, where continuous production is going on for many years. One good example is continuous Oil & Gas Production from the tin bedded reservoir of Catshill Field, Deepwater Trinidad for last 47 years. Sustained

production suggests that sands are continuous and have large lateral extant. Sand mapping suggest the extant to several thousands of feet.

The thin bed analysis carried out using the above techniques are very useful in delineating the potential of reservoirs and we can conclude that

Resistivity anisotropy provides better results as it takes care of the beds thinner than the resolution of Image tools

Cutoffs are very sensitive parameters in any volumetric computation, may be different for different techniques

Identifying the thin zones on Image logs and than applying proper petrophysical parameters for resistivity anisotropy approach provides the best results.

Integration of data should be encouraged to minimize the uncertainty within the petrophysical processing and while integrating with seismic.

References

Bastia, R. et. al., (2005). Reservoir characterization and modeling of thin beds in a deep water gas field, offshore India, Petro-Tech, paper 223.

Bastia, R., (2004). Depositional Model and Reservoir Architecture of Tertiary Deep Water Sedimentation, Krishna-Godavari Offshore Basin, India, *Journal, GSI,* 64, 11-20.

Crain, E. R., Hume, D. W , (2000). Productivity estimation in the Milk River laminated shaly sand, South East Alberta and Southwest Saskatchewan, CWLS.

Griffin, T. and Shafer, J.L.(2001). Maximizing the Impact of Routine Core Analysis on Special Core and Log Analysis: Unconsolidated Sandstones, International Symposium of the Society of Core Analysts, Edinburgh, Scotland, September 17-19, paper 2001-07.

Jensen, L., Menke, J. Y, (2006). Some statistical issues in selecting porosity cutoffs for estimating net pay: Petrophysics, 47(4).

Jones, S. C., (1988). Two-point Determinations of Permeability and PV vs. Net Confining Stress, SPE Formation Evaluation, 3(1), 235-241.

Lasswell, P. M., (2006). Core analysis for electrical properties: Petrophysics, 47(3).

Miller, T., and Shafer, J.L., (2003). Calculating In Situ Stresses in Overpressured Settings, International Symposium of the Society of Core Analysts, Pau, France, September 21-24, paper SCA2003-62.

Ronald, A., Haley, R. (2005) Letters to editor /discussion on Improved log analysis in shaly sandstone-based on Sw and hydrocarbon pore volume routine measurements on preser4ved cores cut in oil-base mud by Woodhouse, R and Warner, H. R: Petrophysics, June issue.

Saxena, K., Tyagi Anil, T. Klimentos, C. Morriss, A.Mathew (Schlumberger) (2006). Evaluating Deepwater Thin-Bedded Reservoirs with the Rt Scanner, Petromin, Kaullampur.

Spears, W. R. (2006) Litho-facies based corrections to density-neutron crossplot total porosity in a high porosity gas and oil bearing turbidite sandstone reservoir, Erha field, OPL, deepwater Nigeria, 47th Annual Logging Symposium: SPWLA, June 4-7, paper O.

Thomas, E.C., Stieber, S. J., (1975). The distribution of shale in sandstone and its effect upon porosity, 16th Annual Logging Symposium: SPWLA, June 4 –7.

Tyagi Anil et al., (2008). Triaxial Induction- A New Angle For Old Measurement, Oil Field Review, Summer 2008, Pages 64-87.

Tyagi Anil et al., 2008, Understanding the architecture of Deepwater reservoirs: Application of Borehole images and core in Krishna-Godavary Basin, Eastern Offshore India" AAPG, GEO India, New Delhi

Tyagi Anil et.al. (2008). Evaluating hydrocarbon potential of thin- bedded reservoirs, Petromin, Technology, July 2008, Page 26-35.

Tyagi Anil et.at., (2008) Hyderabad, Identification and evaluation of the thin bedded reservoir potential in the east coast deep water basins of India, Society of Petroleum Geophysicist.

Tyagi Anil, Rupdip Guha, (2007). New Delhi, Formation Dips Computation Using Tri-Axial Induction Tool: An Alternate To Image Logs, Petrotech.

Woodhouse, R., Warner, H. R. Jr. (2004). Improved log analysis in shaly sandstone-based on Sw and hydrocarbon pore volume routine measurements on preser4ved cores cut in oil-base mud: Petrophysics, 45(3).

Jour. Indian Association of Sedimentologists, Vol. 28, No. 1 (2009), pp. 17-30

Textural Characteristics and Heavy Mineral Distribution in the Sediments of Kathjodi-Debi River, Mahanadi Delta, East Coast of India

D. Rajasekhara Reddy[1], T. Karuna Karudu[1] and D. Deva Varma[2]
[1]Delta Studies Institute, Andhra University, Visakhapatnam- 530 017
[2]Department of Geology, Andhra University, Visakhapatnam – 530 003
Email: drsreddy53@gmail.com

Abstract: The paper deals with the textural characters, and the distribution of total and individual heavy minerals in the Kathjodi-Debi river (distributary of the Mahanadi River) sediments, from the apex of the delta to downstream. The grain size of the sediments shows polymodal nature near the apex and changes from bimodal in the upstream to unimodal in the downstream. The sediments show gradual reduction in the grain size from upstream to downstream. They show moderate to very poorly sorted, platy to very leptokurtic and very negative to very positively skewed nature. The percentage of heavies is increasing from upstream to downstream. The average percentage of heavies in the upstream and downstream of Kathjodi-Debi River is 3.25 and 3.55 respectively. Heavies are concentrated more in finer fractions (+230 ASTM) than in the coarser fraction, and increases gradually from +60 to +230 ASTM. The average percentages of heavies in +60, +120 and +230 ASTM fractions are 1.73, 9.68, 18.65, respectively. Magnetite, opaques (other than magnetite), garnets, sillimanite and hypersthene are the predominant heavy minerals, while amphiboles, zircon, monazite, rutile, staurolite, epidote and biotite are the less abundant heavy minerals. The heavy mineral assemblage indicates that the delta sediments of the river are mainly derived from the khondalites and charnockites of Eastern Ghat Group of rocks, occurring in the hinterland.

Keywords: Sediment texture, Heavy minerals, Kathjodi-Debi River, Mahanadi Delta.

INTRODUCTION

The Kathjodi-Debi River is a major and currently the most active distributary of Mahanadi River, located in Orissa State and joins the Bay of Bengal along the east coast of India. The Kathjodi River flows southeastwards. The river splits into branches viz., the Serua, Debi, Biluakhai and Kandala, and encloses the Channel Islands. These branches eventually join the Debi River, before entering into the Bay of Bengal. The river system is anastomosing in nature. The Kathjodi-Debi River flows about 109 km from apex of the delta, before draining into the Bay of Bengal. The width of the river varies from about 0.3 to 3.2 km and the mouth has a width of about 2.5 km.

The Mahanadi River originates in the Sihawa mountain range, situated southeast of Raipur and flows for about 851 km before entering the Bay of Bengal. The Mahanadi River covers an area of 1, 41,589 sq.km, which is nearly 4.3% of total geographical area of the Country. Its basin lies in the states of Madhya Pradesh (75,136 sq km), Orissa (65,580 sq km), Bihar (635 sq km) and Maharashtra (238 sq km). The Mahanadi River drains igneous, metamorphic and sedimentary rocks of Archaean to Recent age viz., Precambrian granites and gneisses, Estern Ghat Group of rocks (khondalites and charnockites), meta-sediments of the Iron Ore Group, Puranas of sediments of Chhatisgarh basin, Gondwana sediments and laterites (Mahalik 2000).

PREVIOUS WORK AND OBJECTIVE OF THE STUDY

Earlier workers have studied the heavy mineral occurrences along the coast of Orissa (Patro et al., 1989; Acharya, et al., 1998; Gajapathi Rao, et al., 2001; Prabhakara Rao, et al., 2005, Jagannadha Rao, et al., 2008). Tewari and Trivedi (2001) studied heavy mineral assemblages, provenance of the Gondwana rocks of peninsular India. Hota and Maejima (2009) have studied heavy minerals of the Barakar Formation in the Talchir Gondwana Basin, Orissa. Details related to geology, resources and biodiversity of the Mahanadi Delta are given in the book, edited by Mahalik (2000). No systematic sedimentological and heavy mineral studies of the Mahanadi delta have been carried out hither to, except a few isolated studies. Texture, mineralogy and geochemistry of the sediments of only the Mahanadi River distributary channel have been studied by Satyanarayana (1973). Satyanarayana and Poornachandra Rao (1980), and Pattnaik (2000) have studied the heavy mineral assemblage in modern sediments of the Lower Mahanadi delta. Ghosh and De (1984) have reported the presence of opaque

(magnetite), zircon, garnet, sillimanite, rutile, pyroxene, biotite and tourmaline based on three samples collected from the Debi River bed near Barada village, berm near Gundalba village and ancient lagoon within the ancient beach environment, south of Konark village. An overview of the textural characteristics of various sub-environments of the Mahanadi delta was presented by Rajasekhara Reddy et al., (2008a). Rajasekhara Reddy et al., (2008b) studied textural characteristics of the sediments of the southwestern part of the Mahanadi Delta, i.e., Kuakhai River system consisting of three distribuataries, viz., the Kushbhadra, Bhargabi and Daya. The present paper is the continuation of this work and deals with the results of detailed studies, carried out on the textural characters and heavy mineral distribution of the Kathjodi-Debi River that is at present the active distributary of Mahanadi delta.

METHODS OF STUDY

Seventyone surface sediment samples were collected from twentytwo stations located from apex to estuary along the Kathjodi-Debi River from different sub-environments, viz., channel bar, point bar, flood plain, etc. The sample station location map is presented in Fig.1.

The surface sediment samples were subjected to size analysis by sieving and pipetting. Pipette analysis of clay samples was carried out following the procedures of Krumbein and Pettijohn (1938), Folk (1968) and Galehouse (1971). The sieve and pipette analysis data were subjected to graphical plottings, and standard statistical parameters, viz., mean, standard deviation, skewness, and kurtosis were computed employing the formulae of Folk and Ward (1957).

Nineteen surface sediment samples were subjected to heavy mineral analysis. The following procedure was adopted for heavy mineral analysis. The sediments were thoroughly washed through an ASTM 230 mesh sieve with water to remove clay and silt material. The washed samples (+230 ASTM fraction) were treated with dilute hydrochloric acid to remove carbonate shell fragments. Small amount of stannous chloride was added to accelerate the removal of iron coating. Then the samples were dried and sieved into three ASTM size fractions, viz., +60 (+0.25 mm), -60 to +120 (-0.25 to +0.125 mm) and -120 to +230 (-0.125 to +0.063 mm). Heavy minerals from the above sand size fractions were separated using bromoform (sp.gr. 2.89) following the procedure outlined by Krumbein and Pettijohn (1938). After separation, the heavy and light fractions were weighed and their weight percentages were calculated. From the heavies, magnetite fraction of heavy minerals was separated by a hand magnet and its weight percentage is computed. Non-magnetite fraction of heavies was mounted on a glass slide with Canada balsam. About 300-400 grains in each slide were identified and counted, using the line method (Galehouse, 1969) and the concentration of each heavy mineral (number %) is computed.

RESULTS AND DISCUSSION

The results of the grain size analyses, consisting of sand, silt, and clay percentages, and grain size parameters, are presented in Table. 1. The range and average values of grain size parameters such as mean size, standard deviation, skewness and kurtosis of the Kathjodi-Debi River sediments are presented in Table. 2.

From upstream to downstream, the **mean sizes** of the channel sediments of the Kathjodi-Debi River vary from 0.4721 Ø to 6.0931 Ø (av. 2.9817 Ø). The grain size of the sediments decreases from upstream to downstream. The downstream decrease in the mean grain size is due to progressive wearing down of the sediments and decrease of transporting capacity of the river. The **sorting** ranges from moderate to very poorly sorted and the average sorting (1.1736) is poor. The **kurtosis** ranges from platy to very leptokurtic. The average kurtosis (1.1034) shows mesokurtic. The **skewness** ranges from very negative to very positively skewed and the average skewness (0.0829) shows symmetrical nature.

The Point bar sediments of the study area are coarse to fine sands with a range of 0.1720 Ø – 2.6370 Ø (av. 1.3789 Ø); well to poorly sorted with a range of 0.3734 – 1.0079 (av. 0.7275); negative to very positively skewed with a range of –0.2668-0.3354 (av. -0.0454); and meso to very leptokurtic nature with a range of 0.9650 - 1.3736 (av. 1.2185). When compared to SW part of the Mahanadi Delta, i.e., Kuakhai River system, the sediments of the study area are coarser (Rajasekhara Reddy et.al., 2008).

The flood plain sediments are characterized by high amounts of silt with mean size varying from 1.5229 to 5.2756 Ø (av. 4.1865 Ø). In general, the flood plain sediments are poorly sorted with the standard deviation values ranging from 0.5762 to 1.7895 (av.1.2521). These sediments are positive to very positively skewed with skewness varying from 0.1785 to 0.3880 (av. 0.2986) and show meso to leptokurtic nature with kurtosis values varying from 0.9650 to 1.3736; av. 1.2185).

Frequency Distribution Curves

Frequency distribution curves are used to describe the nature of sediments. The frequency distribution curves (fig. 2) of the sediments near the apex of the delta show polymodal nature. The first peak shows very coarse sand (-0.5Ø), second conspicuous peak shows medium sand (1.5Ø) and the third peak shows fine sand (3Ø). Most of the sediments are medium sands. The frequency distribution curves of upstream of the Kathjodi-Debi River (fig. 3) shows bimodal nature; their frequency curves show that the first peak is situated around very coarse sand (-0.5 Ø), while the second

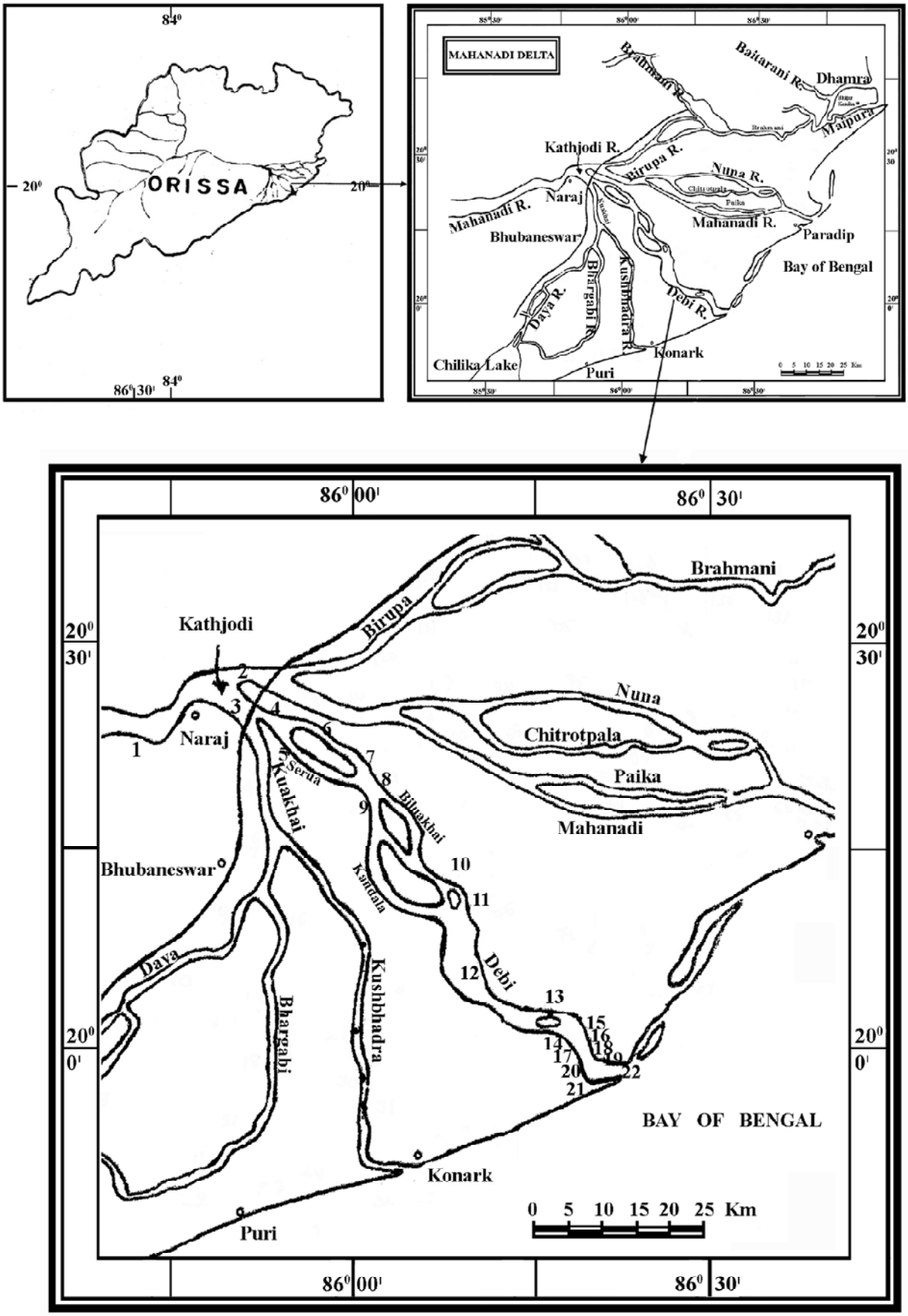

Fig.1. Sample station location map.

Table.1. Grain size parameters of Kathjodi-Devi River sediments.

S.No.	Sample	Sand (%)	Silt (%)	Clay (%)	Mean size	Standard Deviation	Skewness	Kurtosis	Remarks
1	1-MR/CS/1	100	-	-	1.3988	0.6767	0.3275	1.4441	Sand, MS, MSd, PSk, LK
2	1-MR/SR/2	100	-	-	2.2163	0.7915	-0.1167	0.8625	Sand, FS, MSd, NSk, PK
3	2-AMD/CS1/3	100	-	-	1.3283	1.1429	-0.0629	1.1988	Sand, MS, PS, NSk, LK
4	2-AMD/CS2/4	100	-	-	1.1309	1.3495	-0.0375	1.2359	Sand, MS, PS, NSk, LK
5	2-AMD/CS3/5	100	-	-	0.8357	1.1142	-0.2563	0.9032	Sand, CS, PS, NSk, MK
6	2-AMD/A/6	100	-	-	0.7585	1.3798	-0.0933	0.7897	Sand, CS, PS, NSy, PK
7	2-AMD/B/7	100	-	-	1.9997	1.0271	-0.2501	1.1054	Sand, MS, PS, NSk, MK
8	2-AMD/C/8	100	-	-	1.6235	1.0292	-0.1306	1.0865	Sand, MS, PS, NSk, MK
9	3-Kj.R/CS/9	100	-	-	1.1862	0.7476	-0.1785	1.6940	Sand, MS, MSd, NSk, VLK
10	3-Kj.R/PB/10	100	-	-	1.5733	0.7643	-0.0705	1.4233	Sand, MS, MSd, NSy, LK
11	3-Kj.R/PB/2/11	2.40	81.70	15.90	6.0239	1.8426	0.4289	1.0889	silt , Z, PS, VPSk, MK
12	3-Kj.R/PB/3/12	100	-	-	0.8608	1.0130	-0.1423	1.2535	Sand, CS, PS, NSk, LK
13	3-Kj.R/RD/13	100	-	-	2.1255	0.6995	0.0140	0.9436	Sand, FS, MSd, NSy, MK
14	4-Kj.R/CS/14	100	-	-	2.0728	1.0266	-0.4103	1.1269	Sand, FS, PS, VNSk, LK
15	4-Kj.R/PB/15	100	-	-	0.4863	1.0079	-0.0530	0.9022	Sand, CS, PS, NSy, MK
16	4-Kj.R/SB/16	100	-	-	0.2784	0.8174	-0.0023	0.8940	Sand, CS, MSd, NSy, PK
17	5-SR/CS/17	100	-	-	2.1209	0.6464	-0.1628	0.9281	Sand, FS, MSd, NSk, MK
18	5-SR/PB/18	100	-	-	2.6075	0.3877	-0.0305	1.1073	Sand, FS, WS, NSy, MK
19	5-SR/NL/19	24.00	72.10	3.90	4.7087	1.2256	0.3249	1.3613	Sandy silt, Z, PS, VPSk, LK
20	5-SR/FP/20	33.30	61.80	4.90	4.6613	1.3212	0.3817	1.2004	Sandy silt, Z, PS, VPSk, LK
21	6-Kj.R/CS/21	100	-	-	0.8339	0.9508	-0.2992	1.2761	Sand, CS, MSd, NSk, LK
22	6-Kj.R/PB/22	100	-	-	0.5645	0.8749	-0.1454	0.9986	Sand, CS, MSd, NSk, MK
23	6-Kj.R/FP/23	11.50	83.30	5.20	5.1141	1.2682	0.3344	1.2844	Silt, Z, CS, VPSk, LK
24	7-KJR/CS/24	100	-	-	0.4721	0.8557	-0.1591	1.0570	Sand, CS, MSd, NSk, MK
25	7-Kj.R/CB/25	100	-	-	0.2902	0.7743	-0.1624	0.9316	Sand, CS, MSd, NSk, MK
26	7-Kj.R/PB/26	100	-	-	0.1720	0.9116	-0.2668	0.8034	Sand, CS, MSd, NSk, PK
27	7-Kj.R/RB/27	15.90	77.50	6.60	5.2183	1.5509	0.2183	1.4654	Sandy silt, Z, PS, PSk, LK
28	7-Kj.R/RB/28	100	-	-	2.4717	0.4489	-0.0672	0.9974	Sand, FS, WS, NSy, MK
29	7-Kj.R/RB/1/29	5.20	87.60	7.20	5.4744	1.3522	0.3685	1.1507	Silt, Z, PS, VPSk, LK
30	7-Kj.R/RB/2/30	100	-	-	0.8843	0.7259	-0.3076	1.2499	Sand, CS, MSd, VNSk, LK
31	7-Kj.R/RB/3/31	3.70	85.60	10.70	5.6864	1.4975	0.3985	1.0484	Silt, Z, PS, VPSk, MK
32	7-Kj.R/RB/4/32	100	-	-	1.4468	0.6795	0.0778	1.1395	Sand, MS, MSd, NSy, LK
33	7-Kj.R/CI/33	100	-	-	2.7020	0.3352	-0.0309	1.4760	Sand, FS, WS, NSy, LK
34	8-BN/CS/34	100	-	-	2.2483	0.5966	0.1280	0.9352	Sand, FS, MSd, PSk, MK
35	8-BN/PB/35	100	-	-	1.5194	0.8330	0.0508	1.0934	Sand, MS, MSd, NSy, MK
36	8-BN/CI/36	31.80	62.80	5.40	4.7130	1.5161	0.2707	1.0096	Sandy silt, Z, PS, PSk, MK
37	8-BN/FP/37	9.10	85.30	5.60	5.2359	1.3641	0.2683	1.3736	Silt, Z, PS, PSk, LK
38	9-Dv.R/CS/38	100	-	-	0.5433	0.9057	-0.1754	1.0385	Sand, CS, MSd, NSk, MK

Table.1. Contd...

S.No.	Sample	Sand (%)	Silt (%)	Clay (%)	Mean size	Standard Deviation	Skewness	Kurtosis	Remarks
39	9-DVR/PB/39	100	-	-	0.8146	0.6080	-0.0171	1.1077	Sand, CS, MSd, NSy, MK
40	9-Dv.R/FP/40	27.30	66.70	6.00	4.7778	1.5318	0.2713	1.2466	Sandy silt, Z, PS, PSk, LK
41	10-DV.R/CS/41	100	-	-	0.7435	1.2374	-0.1856	0.8795	Sand, CS, PS, NSk, PK
42	10-Dv.R/SB/42	100	-	-	1.3028	0.6066	1.2668	0.0165	Sand, MS, MSd, NSy, LK
43	10-Dv.R/RB/43	1.40	91.60	7.00	5.4303	1.2373	0.3994	1.3354	Silt, Z, PS, VPSk, LK
44	10-Dv.R/FP/44	7.60	86.00	6.40	5.2756	1.3290	0.3880	1.2540	Silt, Z, PS, VPSk, LK
45	11-Dv.R/CS/45	10.60	79.90	9.50	5.4676	1.6259	0.3055	1.2765	Silt, Z, PS, VPSk, LK
46	11-Dv.R/PB/46	100	-	-	2.6370	0.3734	-0.0785	1.2908	Sand, FS, WS, NSy, LK
47	11-Dv.R/FP/47	100	-	-	1.5229	0.5762	0.3064	1.2118	Sand, MS, MSd, VPSk, LK
48	12-DV.R/CS/48	100	-	-	1.4664	0.9773	0.1687	1.2381	Sand, MS, MSd, PSk, LK
49	12-Dv.R/PB/49	100	-	-	1.8596	0.8648	-0.1787	0.9865	Sand, MS, MSd, NSk, MK
50	12-Dv.R/FP/50	100	-	-	2.0315	0.8369	0.1785	0.9650	Sand, FS, MSd, PSk, MK
51	12-Dv.R/PR/51	100	-	-	1.8118	0.7293	0.1910	0.9743	Sand, MS, MSd, PSk, MK
52	13-Dv.R/CS1/52	4.30	83.50	12.20	5.7475	1.5894	0.4214	1.0257	Silt, Z, PS, VPSk, MK
53	13-Dv.R/CB/53	100	-	-	1.5900	0.5899	0.3347	1.1445	Sand, MS, MSd, VPSk, LK
54	13-Dv.R/PB/54	100	-	-	1.5544	0.6494	0.3354	1.2234	Sand, MS, MSd, VPSk, LK
55	13-Dv.R/IRB/1/55	100	-	-	2.5890	0.6188	-0.1439	1.3137	Sand, FS, MSd, NSk, LK
56	13-Dv.R/IRB/2/56	100	-	-	2.6216	0.4154	-0.0927	1.2146	Sand, FS,WS, NSy, LK
57	13-Dv.R/IRB/3/57	3.20	90.20	6.60	5.3589	1.2519	0.3968	1.2683	Silt, Z, PS, VPSk, LK
58	13-Dv.R/IRB/4/58	100	-	-	1.7088	0.6403	0.1161	0.9674	Sand, MS, MSd, PSk, MK
59	13-Dv.R/CI/59	20.40	73.30	6.30	4.8208	1.3763	0.2241	1.4242	sandy silt, Z, PS, PSk, LK
60	13-Dv.R/CS2/60	4.00	79.40	16.60	5.9453	1.6786	0.4203	0.8588	Silt, Z, PS, VPSk, PK
61	13-Dv.R/FP/61	30.20	61.40	8.40	4.8727	1.7895	0.2600	1.2120	sandy silt, Z, PS, PSk, LK
62	14-Dv.R/CS/62	100	-	-	2.4881	0.6600	-0.1112	1.1169	Sand, FS, MSd, NSk, LK
63	15-Dv.R/CS/63	100	-	-	2.4943	0.7245	-0.0749	0.9942	Sand, FS, MSd, NSy, MK
64	15-Dv.R/RD/64	100	-	-	2.4727	0.4912	-0.1734	0.9915	Sand, FS, WS, NSk, MK
65	16-Dv.R/CS/65	1.00	89.90	9.10	5.6559	1.3915	0.3711	1.0845	Silt, Z, PS, VPSk, MK
66	17-Dv.R/CS/66	5.10	83.10	11.80	5.7565	1.5638	0.3775	0.9831	Silt, Z, PS, VPSk, MK
67	18-Dv.R/CS/67	100	-	-	1.9115	0.5374	0.1910	1.1111	Sand, MS, PS, PSk, LK
68	19-Dv.R/CS/68	2.10	84.00	13.90	5.8987	1.7321	0.4401	1.0953	Silt, Z, PS, VPSk, MK
69	20-Dv.R/CS/69	2.00	80.80	17.20	6.0931	1.9331	0.4389	1.0981	Silt, Z, PS, VPSk, MK
70	21-Dv.R/CS/70	34.20	56.70	9.10	4.8086	2.0087	0.1746	0.9248	sandy silt, Z, PS, PSk, MK
71	22-Dv.R/CS/71	1.40	85.30	13.30	5.8954	1.6671	0.4209	1.0597	Silt, Z, PS, VPSk, MK

The details of sample numbering pattern, for example 4-Kj.R/CS/14. First digits indicate station number i.e., 4; next letters indicate name of the river (MR: Mahanadi River, AMD: Apex of the Mahanadi Delta, Kj.R: Kathjodi River, SR: Serua River, BN: Basuli Nadi, Dv.R: Devi River); next letters indicate environment (CS: Channel sediment, PB: Point bar, RD: River dune, SB: Sediment bar, NL: Natural levee, FP: Flood plain, RB: River Bank, CI: Channel Island, PR: Paleo ridge, IRB: Island river bank): last digits indicate sample number i.e., 14.

The abbreviations used in remarks indicate:
CS: Coarse Sand; MS: Medium Sand; FS: Fine Sand; VFS: Very Fine Sand; Z: Silt; C: Clay; VWS: Very Well Sorted; WS: Well Sorted; MSd: Moderately Sorted; PS: Poorly Sorted; VPS: Very Poorly Sorted; EPS: Extremely Poorly Sorted; VNSk: Very Negatively Skewed; NSk: Negatively Skewed; NSy: Near Symmetrical; PSk: Positively Skewed; VPSk: Very Positively Skewed; VPK: Very Platy Kurtic; PK: Ptatykurtic; MK: Mesokurtic; LK: Leptokurtic; VLK: Very Leptokurtic; ELK: Extremely Leptokurtic.

Table. 2. Range and average values of grain size parameters of sediments of Kathjodi-Debi River and sub-environments.

River Name		Mean size (Ø)	Standard Deviation	Skewness	Kurtosis
Kathjodi-Debi River	Min	0.4721	0.5374	-0.4103	0.8588
	Max	6.0931	2.0087	0.4401	1.6940
	Av.	2.9817	1.1736	0.0829	1.1034
Point bar	Max.	2.6370	1.0079	0.3354	1.4233
	Min.	0.1720	0.3734	-0.2668	0.8034
	Average	1.3789	0.7275	-0.0454	1.0937
Flood plain	Max.	5.2756	1.7895	0.3880	1.3736
	Min.	1.5229	0.5762	0.1785	0.9650
	Average	4.1865	1.2521	0.2986	1.2185

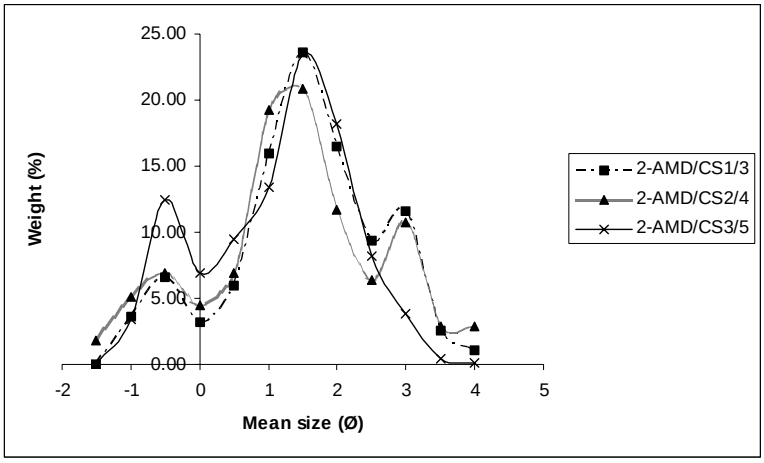

Fig.2. Frequency distribution curves of sediments near Apex of the Mahanadi River.

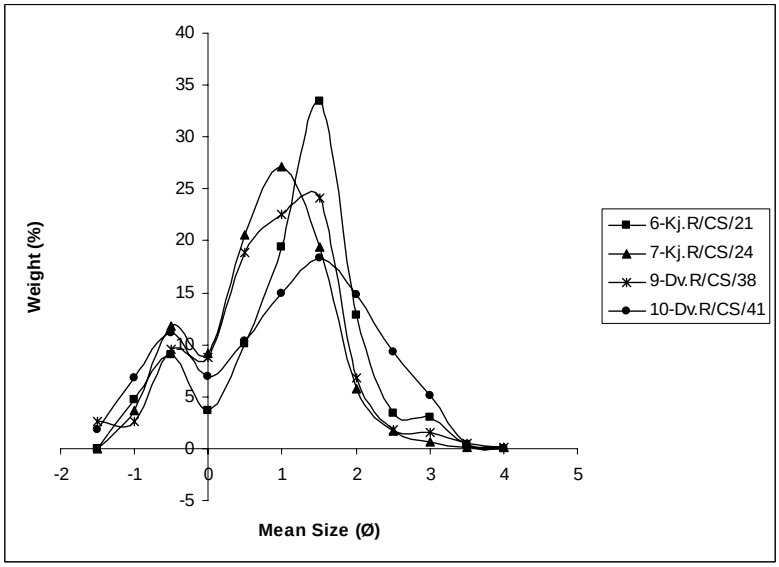

Fig. 3. Frequency distribution curves of upstream sediments of the Kathjodi-Debi River.

conspicuous peak is around medium sand (1.5 Ø). In the downstream of the Kathjodi-Debi River (fig. 4), the frequency distribution curve shows medium sand to very coarse silt (3-5 Ø), with unimodal nature. This clearly demonstrates that the grain size reduces gradually from upstream to downstream.

Heavy Mineral Distribution

The weight percentages of total heavy minerals in three size grades namely +60, +120 and +230 ASTM in different sub-environments are shown in Table.3.

Variations of total and fractionwise heavies along Kathjodi-Debi River from upstream to downstream are plotted in figures 5 and 6. These figures show that the percentages of heavies are increasing from upstream to downstream. The highest concentration of heavies is recorded in the lower delta-estuary, near the interface between the river and sea. Heavies are concentrated more in finer fraction (+230 ASTM) than in the coarser fraction and increase gradually from +60 to +230 ASTM. Heavy mineral abundance is inversely proportional to the grain size (Figs. 7 and 8). In each of the three size grades studied (+60, +120, +230 ASTM), the

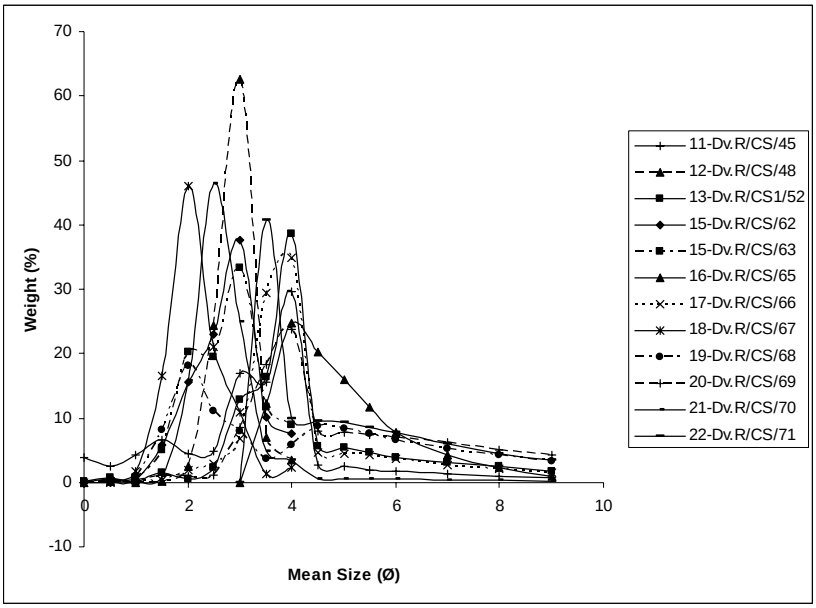

Fig. 4. Frequency distribution curves of downstream sediments of the Kathjodi-Debi River.

Table.3. The concentration (Wt %) of heavies in three size fractions and concentration of heavies in total sample in different sub-environments.

S.No	Station No.	Sub-environment	Heavies (%) - Fractionwise (Including Magnetite)			Magnetite (%) – Fractionwise			Heavies (%) - in total sample (Including Magnetite)
			+60	+120	+230	+60	+120	+230	
1	1	CS	1.63	12.10	30.78	0.00	0.14	0.10	3.91
2	3	CS	1.62	6.53	18.99	0.00	0.36	0.35	3.61
3	14	CS	1.33	15.30	21.06	0.00	0.45	0.35	2.64
4	15	PB	3.88	21.22	32.23	0.02	0.54	1.27	6.46
5	16	SB	1.67	9.85	25.08	0.01	0.30	1.52	3.25
6	38	CS	1.69	14.05	19.21	0.01	0.30	0.42	2.83
7	39	PB	1.03	7.80	8.48	0.01	0.12	0.27	1.50
8	40	FP	0.60	4.38	8.70	0.00	0.04	0.22	6.08
9	41	CS	1.54	11.99	18.64	0.01	0.26	0.69	3.28
10	42	SB	0.57	7.02	9.13	0.01	0.14	0.56	1.60
11	43	RB	3.01	5.84	4.45	0.00	0.34	0.12	4.59
12	44	FP	4.38	3.34	6.94	0.00	0.02	0.07	6.09
13	48	CS	1.95	5.18	12.82	0.00	0.10	0.28	3.55
14	49	PB	1.17	5.32	21.69	0.01	0.06	0.60	3.69
15	50	FP	0.88	5.08	9.43	0.00	0.03	0.09	2.89
16	51	PR	1.03	6.39	8.03	0.00	0.01	2.17	2.88
17	63	CS	3.69	9.52	15.78	0.02	0.13	0.31	10.33
18	66	CS	0.42	4.52	15.92	0.00	0.03	0.05	9.94
19	71	CS	1.72	7.94	14.68	0.23	0.46	1.30	6.30

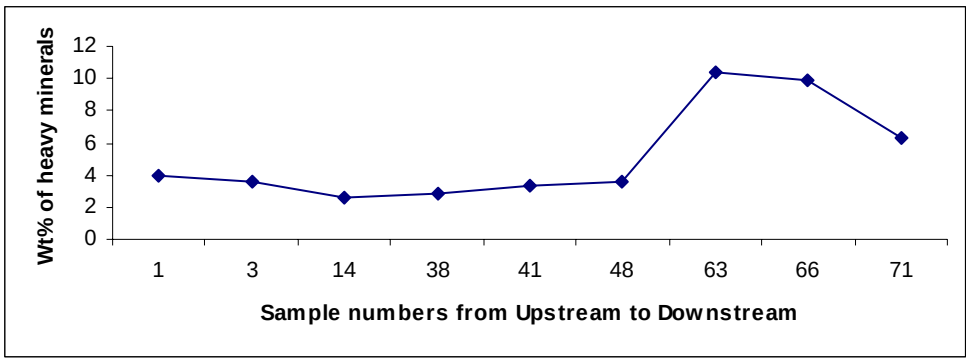

Fig. 5. Variation of total heavies in the sediments along the Kathjodi-Debi River.

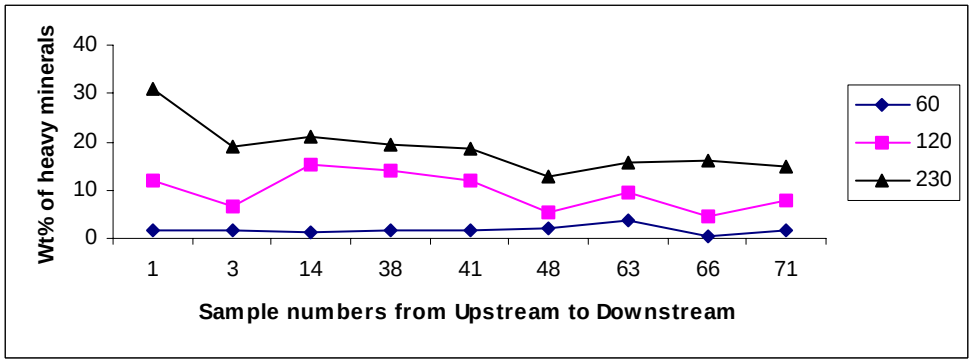

Fig. 6. Fractionwise variation of total heavies in the sediments along the Kathjodi-Debi River.

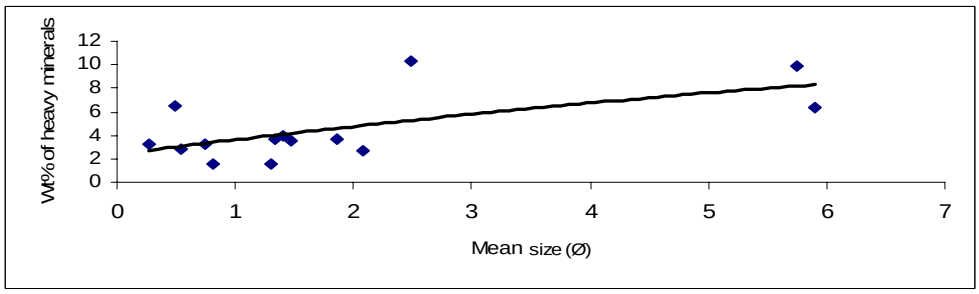

Fig.7. Variation of total heavies with mean size in the sediments of the Kathjodi-Debi River.

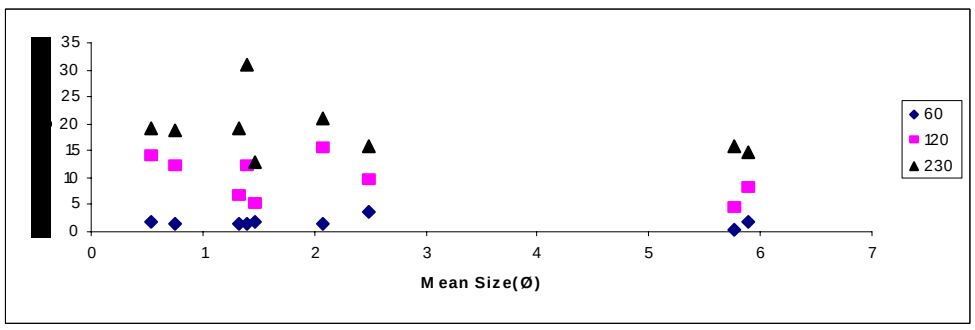

Fig. 8. Fractionwise variation of total heavies, with mean size in the sediments of the Kathjodi-Debi River.

concentration of heavies decreases in the river channel from apex of the delta.

Description and distribution pattern of Heavy minerals

The percentages of various heavy minerals in different size grades of the Kathjodi-Debi River sediments are given in table 4. Upstream to downstream, fractionwise number percentages of heavy minerals are presented in figures 9-11. It is observed that the predominant heavy minerals of the Kathjodi-Debi River sands consist of magnetite, opaques (other than magnetite), garnet, sillimanite and hypersthene. The less abundant heavy minerals are amphiboles, zircon, monazite, rutile, staurolite, tourmaline, epidote and biotite.

The salient features of the various heavy minerals are as follows. The concentration of magnetite is presented in weight percentage while the concentrations of other heavy minerals are presented in number percentage.

Magnetites: These grains are black and are rounded and sub-rounded in shape

Magnetites (Fig. 12) are concentrated more in finer fraction (+230 ASTM) than in the coarser fractions and increases gradually from +60 to +230 ASTM. In +60 ASTM fraction, the concentration of heavies (Wt. %) ranges from 0 to 0.23%, with an av. 0.03% (S.D – 0.08). In +120 ASTM fraction, the concentration of heavies ranges from 0.03 to 0.46%, with an av. 0.25% (S.D – 0.16). In +230 ASTM fraction, the concentration of

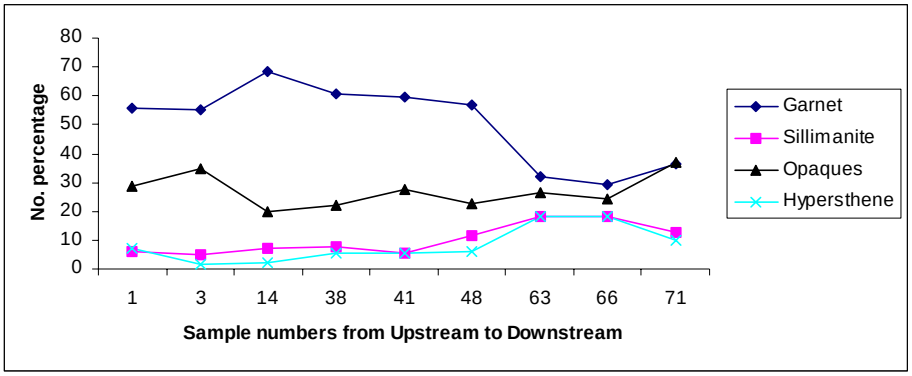

Fig. 9. Variation of heavy minerals in the sediments along the Kathjodi-Debi River (+ 60 fraction)

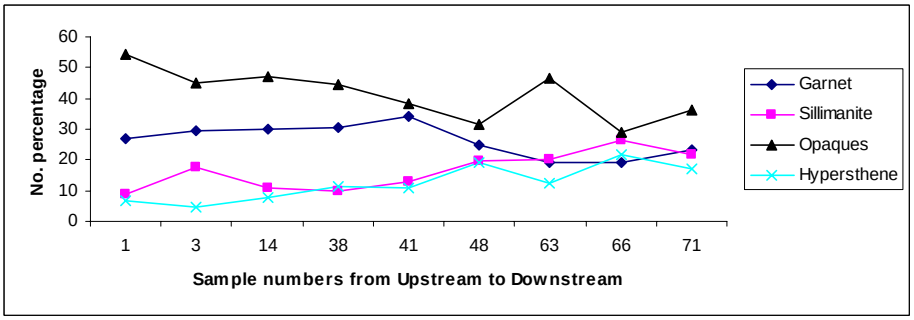

Fig. 10. Variation of heavy minerals in the sediments along the Kathjodi-Debi River (+ 120 fraction).

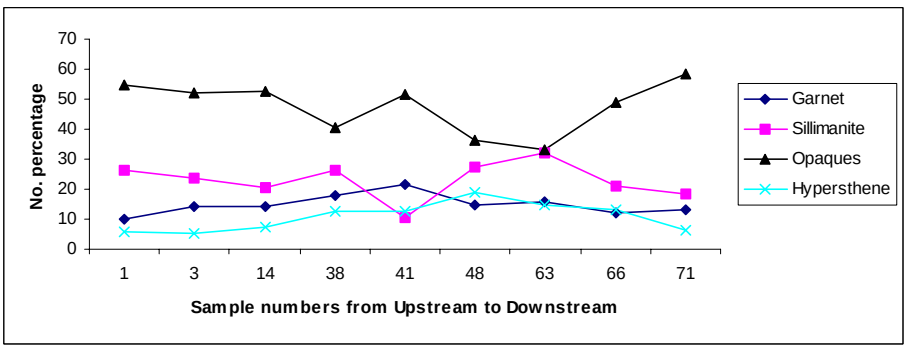

Fig. 11. Variation of heavy minerals in the sediments along the Kathjodi-Debi River (+ 230 fraction).

Table. 4. Number percentage of various heavy minerals in different sub-environments of the Kathjodi-Debi River sediments.

S.No	Fraction	Gnt	Slm	Opq	Hyp	Amp	Zr	Mnz	Rut	Str	Trm	Ep	Others	Total
1	+60	55.59	6.07	28.75	7.35	0.64	----	----	----	----	----	----	1.60	100
	+120	26.95	8.77	54.55	6.49	0.65	----	0.97	0.32	----	0.32	----	0.97	99.99
	+230	9.96	26.56	54.69	5.66	0.39	0.78	0.20	----	----	0.78	----	0.98	100
3	+60	54.95	4.95	34.90	1.82	1.04	----	----	----	----	0.52	0.26	1.56	100
	+120	29.48	17.69	45.20	4.59	1.09	----	0.22	----	----	0.66	----	1.09	100.02
	+230	14.38	23.89	51.99	5.31	0.44	1.55	0.22	----	----	1.33	----	0.88	99.99
14	+60	68.32	7.25	19.85	2.29	0.76	----	----	----	0.38	----	----	1.15	100
	+120	29.92	10.98	46.97	7.95	1.14	1.14	0.76	0.38	----	----	----	0.76	100
	+230	14.06	20.46	52.67	7.12	1.07	2.85	1.42	0.36	----	----	----	----	100.01
15	+60	64.73	5.57	25.75	3.48	----	----	----	----	----	----	----	0.46	99.99
	+120	29.00	7.55	55.59	3.93	0.91	0.60	0.60	0.60	----	----	----	1.21	99.99
	+230	15.81	20.53	56.87	0.59	0.74	2.81	0.59	0.15	0.15	1.33	----	0.44	100.01
16	+60	46.84	6.32	33.16	11.58	----	----	----	0.53	----	----	----	1.58	100.01
	+120	31.01	11.59	44.64	10.72	----	0.29	----	0.29	----	----	----	1.45	99.99
	+230	17.03	19.60	50.30	10.89	0.59	0.20	0.40	----	----	----	----	0.99	100
38	+60	60.69	7.51	21.97	5.78	1.73	----	----	----	0.58	----	----	1.73	99.99
	+120	30.43	9.94	44.72	11.18	0.93	0.62	0.93	0.31	----	----	----	0.93	99.99
	+230	18.15	26.24	40.59	12.71	0.66	0.33	0.33	0.50	----	----	----	0.50	100.01
39	+60	56.77	7.14	25.56	9.02	----	----	----	----	0.38	----	----	1.13	100
	+120	28.57	7.51	49.88	12.83	----	----	0.24	----	----	0.24	----	0.73	100
	+230	18.74	23.39	45.13	10.79	1.20	0.15	0.15	----	----	----	----	0.45	100
40	+60	----	----	----	----	----	----	----	----	----	----	----	----	----
	+120	23.97	30.99	26.63	17.43	----	0.24	----	----	----	----	----	0.73	99.99
	+230	12.05	30.29	46.25	9.12	0.98	0.33	----	----	----	----	----	0.98	100
41	+60	59.62	5.36	27.44	5.68	0.95	----	----	----	0.32	----	----	0.63	100
	+120	34.05	13.09	38.12	10.80	0.76	1.02	0.76	0.51	----	0.38	----	0.51	100
	+230	21.70	10.61	51.34	12.71	0.65	2.19	0.16	0.32	----	----	----	0.32	100
42	+60	53.41	8.71	27.29	10.59	----	----	----	----	----	----	----	----	100
	+120	33.95	13.27	39.20	11.11	0.93	0.31	----	0.31	----	----	----	0.93	100.01
	+230	15.42	22.72	47.43	12.44	0.66	0.17	0.33	----	----	----	---	0.83	100
43	+60	----	----	----	----	----	----	----	----	----	----	----	----	----
	+120	27.96	17.67	34.95	18.06	----	0.58	0.19	0.39	----	----	----	0.19	99.99
	+230	15.64	23.29	49.02	10.26	0.65	0.33	0.33	0.16	0.16	----	---	0.49	100.33
44	+60	----	----	----	----	----	----	----	----	----	----	----	----	----
	+120	15.97	28.01	32.18	20.83	1.39	0.69	----	----	----	----	----	0.93	100
	+230	12.33	31.12	45.35	8.54	1.52	0.19	----	----	----	----	----	0.95	100
48	+60	56.89	11.48	22.45	6.12	2.04	----	----	----	----	----	----	1.02	100
	+120	24.95	19.50	31.45	19.29	0.84	1.47	1.26	0.63	----	----	----	0.63	100.02
	+230	14.67	27.55	36.31	18.78	0.89	0.36	0.18	0.36	----	----	----	0.89	99.99
49	+60	51.49	13.06	24.25	11.19	----	----	----	----	----	----	----	----	99.99
	+120	27.56	16.10	34.63	18.78	1.22	0.24	0.49	----	----	----	----	0.98	100
	+230	20.45	23.70	52.76	1.30	0.65	0.16	0.16	----	----	----	----	0.81	99.99
50	+60	54.32	17.53	17.78	10.37	----	----	----	----	----	----	----	----	100
	+120	25.81	18.82	38.17	14.78	0.81	0.27	0.54	----	----	----	----	0.81	100.01
	+230	10.97	26.16	46.62	13.50	1.27	0.21	0.21	----	----	----	----	1.05	99.99
51	+60	56.69	13.91	16.27	12.60	----	----	----	----	----	----	----	0.52	99.99
	+120	26.32	19.84	37.25	16.19	----	----	----	0.40	----	----	----	----	100
	+230	17.66	26.09	43.21	9.51	1.63	0.27	0.54	----	----	----	----	1.09	100
63	+60	32.18	18.39	26.44	18.39	2.30	----	----	----	----	----	----	2.30	100
	+120	19.05	20.15	46.34	12.45	0.55	0.37	0.37	0.18	----	----	----	0.55	100.01
	+230	15.95	31.90	33.28	14.57	1.23	1.69	0.46	0.15	----	----	----	0.77	100
66	+60	29.27	18.29	24.39	18.29	6.10	----	----	----	----	----	----	3.66	100
	+120	19.32	26.37	28.98	21.93	0.78	0.52	0.52	0.26	----	----	----	1.31	99.99
	+230	12.33	20.85	48.71	13.24	0.91	2.89	0.30	0.15	----	----	----	0.61	99.99
71	+60	36.36	12.83	36.90	10.16	1.60	----	----	----	----	----	----	2.14	99.99
	+120	23.20	21.66	36.24	17.02	0.66	0.33	0.22	0.11	----	0.22	----	0.33	99.99
	+230	12.94	18.24	58.21	6.47	1.33	1.49	0.50	0.17	----	----	----	0.66	100.01

Gnt: Garnet, Slm: Sillimanite, Opq: Opaque (excluding magnetite), Hyp: Hypersthene, Amp: Amphibole, Zr: Zircon, Mnz: Monazite, Rut: Rutile, Str: Staurolite, Trm: Tourmaline, Ep: Epidote

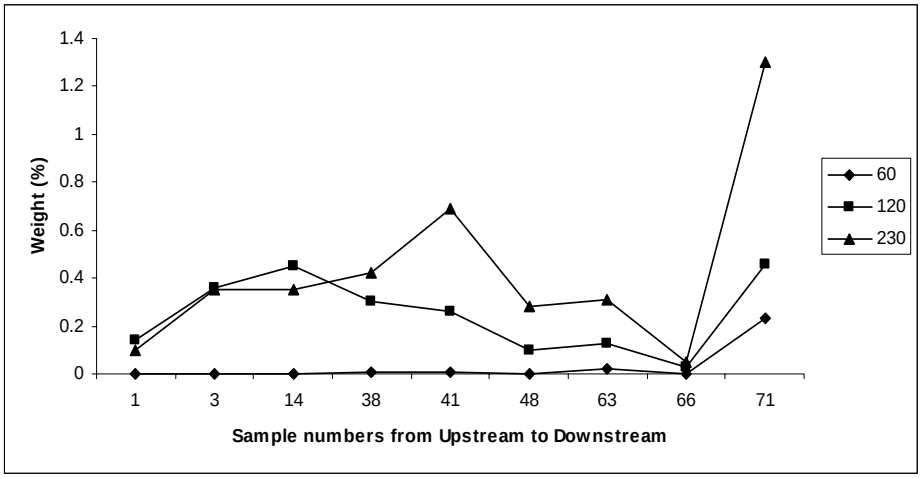

Fig. 12. Fractionwise variation of magnetite in the sediments along the Kathjodi-Debi River.

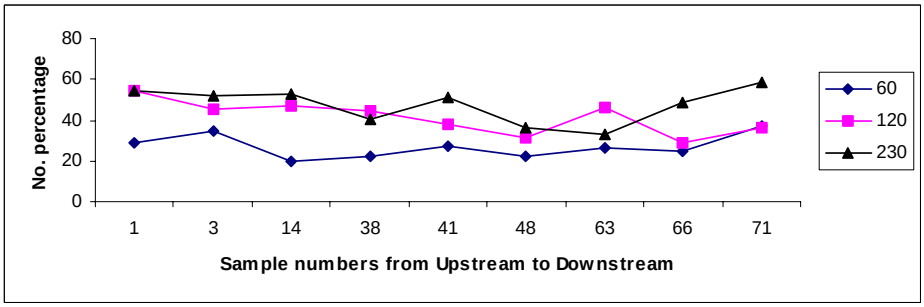

Fig. 13. Fractionwise variation of opaque (other than magnetite) in the sediments along the Kathjodi-Debi River.

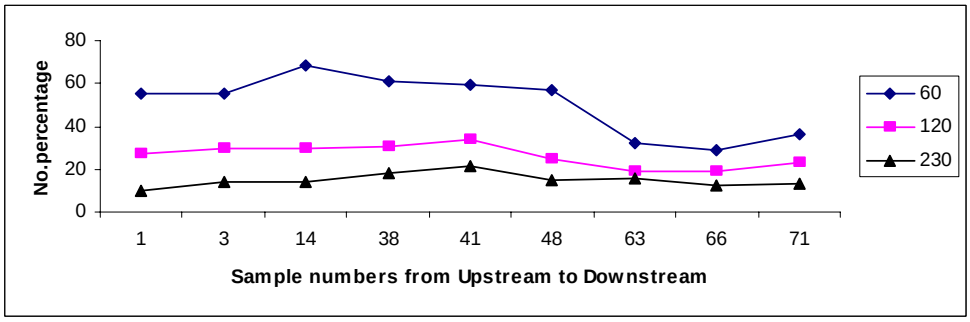

Fig. 14. Fractionwise variation of Garnet in the sediments along the Kathjodi-Debi River.

heavies ranges from 0.05 to 1.30% with an av. 0.43% (S.D – 0.38).

Opaques: These are present in good proportion and are mostly rounded or sub-rounded. The opaques consist almost entirely of ilmenite. It has been observed that a few grains show a dull grey luster in patches in reflected light indicating alteration to leucoxene.

Opaques (Fig. 13) are concentrated more in finer fraction (+230 ASTM) than in the coarser fractions and increases gradually from +60 to +230 ASTM in Kathjodi-Debi river. In +60 ASTM fraction, the concentration of heavies ranges from 19.85 to 36.90%, with an av. 27% (S.D – 5.79). In +120 ASTM fraction, the concentration of heavies ranges from 28.98 to 54.55%, with an av. 41.40% (S.D – 8.25). In +230 ASTM fraction, the concentration of heavies ranges from 33.28 to 58.21% with an av. 47.53% (S.D – 8.69)

Garnets: These are generally rounded and sub-rounded, and occasionally sub-spherical. The two varieties observed are almandine and grossularite. Almandine type is characterized by pink or purple red colour in them while grossularite type by light honey brown colour. Inclusions of iron oxides and zircon are observed occasionally. Both almandine and grossularite varieties occur mostly as fresh and unaltered grains.

Garnets (Fig. 14) are concentrated more in coarser fractions (+60 ASTM) than in the finer fraction and decreases gradually from +60 to +230 ASTM. In +60 ASTM fraction, the concentration of garnets ranges from 29.27 to 68.32% with av. 50.43% (S.D – 14.04). In +120 ASTM fraction, the concentration of garnets ranges from 19.05 to 34.05% with av. 26.37% (S.D – 5.17). In +230 ASTM fraction, the concentration of garnets ranges from 9.96 to 21.70% with av. 14.90% (S.D – 3.42).

Sillimanite: These grains are colourless and are either prismatic or acicular in shape. They show good relief and straight extinction. They have irregular terminations with no inclusions.

Sillimanite (Fig. 15) is concentrated more in finer fractions (+230 ASTM) than in the coarser fraction and increases gradually from +60 to +230 ASTM. In +60 ASTM fraction, the concentration of sillimanite ranges from 4.95 to 18.39% with an av. 10.24% (S.D – 5.30). In +120 ASTM fraction, the concentration of sillimanite ranges from 8.77 to 26.37% with an av. 16.46% (S.D – 6.05). In +230 ASTM fraction, the concentration of sillimanite ranges from 10.61 to 31.90% with an av. 22.92% (S.D – 6.24).

Pyroxenes: Hypersthene is the dominant mineral. It is characterized by short prismatic shape and often contains inclusions. Hypersthene exhibits strong pleochroism from pink to green.

Hypersthene (Fig. 16) is more in finer fractions than in the coarser fraction and increases gradually from +60 to +230 ASTM. In +60 ASTM fraction, the concentration of hypersthene ranges from 1.82 to 18.39% with an av. 8.43% (S.D – 6.14). In +120 ASTM fraction, the concentration of hypersthene ranges from 4.59 to 21.93% with an av. 12.41% (S.D – 5.91). In +230 ASTM fraction, the concentration of hypersthene ranges from 5.31 to 18.78% with an av. 10.73% (S.D – 4.74).

Minor Minerals: There are several minerals which occur only in some of the samples and in minor quantities. They include amphiboles, zircon, monazite, rutile, staurolite, tourmaline, epidote and biotite.

Amphiboles: Hornblende is the predominant mineral in the amphiboles. The green to greenish brown variety is the most common mineral. Grains are characterized by elongated form, platy cleavage and frayed ends. Hornblende grains exhibit uneven distribution of colour, thickest in the middle, becoming gradually thinner towards the boundaries. Pleochroism is generally variable from strong to weak.

Zircons: Zircon is colourless and usually oval shaped. Prismatic grains with pyramidal terminations are also observed. Zoning is a characteristic feature of these grains.

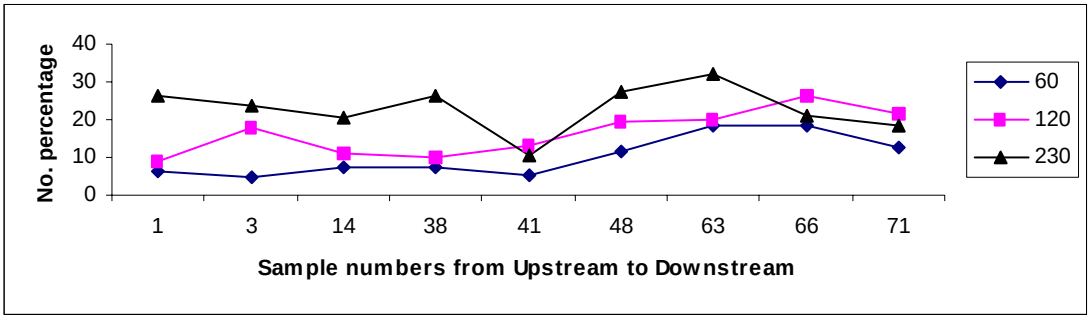

Fig. 15. Fractionwise variation of Sillimanite in the sediments along the Kathjodi-Debi River.

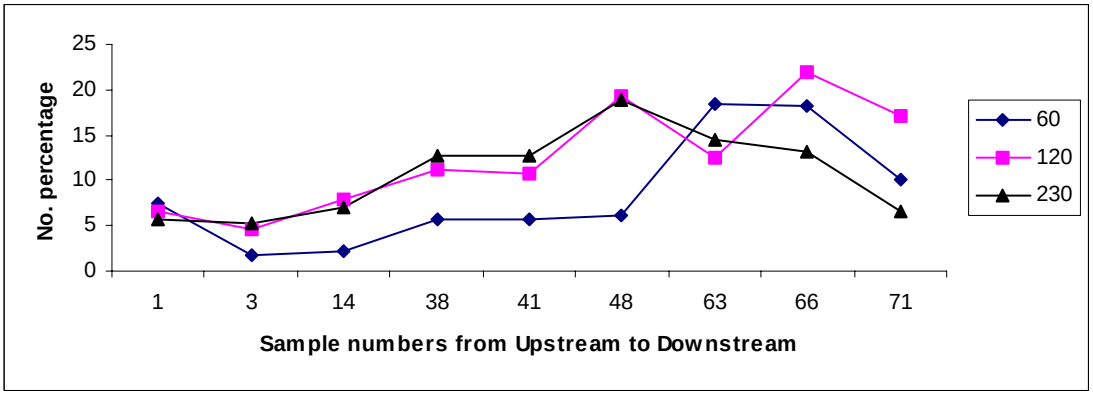

Fig. 16. Fractionwise variation of Hypersthene in the sediments along the Kathjodi-Debi River.

Monazite: These are mostly rounded grains with pitted surface. Light yellow colour is the characteristic property of this mineral. It shows high relief with distinct borders.

Rutile: Most of the grains are prismatic with pyramidal terminations. The grains exhibit reddish brown colour. They show high refractive index with thick borders. Hence the colour of the grain is visible only in the middle of the grain, characterized by straight extinction.

Tourmaline: Prismatic, some of the rectangular and a few euhedral pink varieties are observed. The body colour is usually dark brown. Pleochroism is strong from dark brown to honey yellow.

Epidote: The epidote grains are sub-rounded and sub-spherical in shape and shows greenish yellow colour with distinct pleochroism and high order interference colour and platy form.

The differences in specific gravity, settling velocity and differential transport play a major role in the distribution of heavy minerals (Komar and Wang, 1984). The concentration of opaques and garnets decreases, while the concentration of sillimanite increases in all the size grades i.e. +60, +120 and +230 ASTM in channel from upstream to downstream. This can be explained on the basis of specific gravity, as opaques (Sp.gr magnetite 5.2, ilmenite 4.7, and garnets (almandine 4.25 and grossularite 3.6) are heavier than sillimanite (Sp.gr 3.2). During deposition, heavier opaques settle down quickly because of their greater settling velocity. Hence, the lighter heavies increase in the downstream direction. The difference in shape of the heavy minerals also is a dominating factor in the downstream decrease of heavier heavies and increase of lighter heavies. Garnets are concentrated more in coarser fractions (+60 ASTM) than in the finer fraction and decreases gradually from +60 to +230 ASTM. Opaque, sillimanite and hypersthenes are concentrated more in finer fractions (+230) than in the coarser fraction and increase gradually from +60 to +230 ASTM.

Provenance

From the study of heavy mineral assemblage and their relative abundance in the Mahanadi River sediments, certain inferences have been drawn regarding the mineralogy of the source rocks of the drainage basin of the river and contribution of heavy minerals to the river sands. The details regarding geological formations of the drainage basin and their mineralogical characters are described below.

The drainage basin of Mahanadi River (Fig.1.3) is largely occupied by the granite suite of rocks (34%), Upper Gondwana sandstone, shale (22%), Lower Gondwana limestone and shale (17%), Charnockite (15%), Khondalite suite (7%) and Coastal sediment (cover 5%).

The granite contains quartz, orthoclase, microcline, biotite, muscovite, hornblende, magnetite, apatite and zircon. Sandstone, shale and conglomerate are the rock types in the Gondwana Formations. The charnockite region is characterized by the rocks of the granulite facies, which are the products of regional metamorphism of high pressure and temperature. The main rock types in this region are migmatised gneiss, granites, charnockites, pyroxene granulites, metagabbros, garnetiferous granulite, hornblende granulite and amphibolites. The common heavy minerals from these rock types in the middle to lower part of the drainage basin are hornblende, hypersthene, biotite, garnet, epidote, zircon, tourmaline and rutile.

The Mahanadi River in the lower reaches, i.e., before entering the Delta, flows through a gorge, known as Satkosia gorge, that is 23 km in leong, across the strike of the Eastern Ghats, made up of khondalites and charnockites. The khondalite group consists of quartz-feldspar-garnet-sillimanite gneiss, quartzites and calc-granulites. The charnockite series include hypersthene granite, hornblende-hypersthene granite, pyroxene granite, hornblende-pyroxene granite and pegmatites. The heavy minerals that would be essentially supplied by these rocks are sillimanite, garnet, hornblende, hypersthene, zircon, monazite and tourmaline.

From the above, it is clear that the sillimanite in Mahanadi River sands comes from khondalite series of Eastern Ghats. Garnet and hypersthene are mainly derived from the khondalites and charnockites of Eastern Ghats. Well rounded monazites come from the Eastern Ghats. This is based on the occurrence of monazite in pegmatites (Mahadevan and Satapati, 1948) and charnockites (Murthy, 1958) of Eastern Ghats. The various characters of the tourmaline, rutile and zircon suggest that each of these minerals has a multiple source. Tourmaline grains might have come from the pegmatites in the khondalite or charnockite rocks. Zircons are mostly rounded and sometimes euhedral in shape. These euhedral grains are mostly from granitic rocks and to a less extent from charnockites, whereas the rounded ones are mainly from khondalites and reworked sediments like gondwanas.

CONCLUSIONS

In the Kathjodi-Debi River (distributary of Mahanadi River), the sediments in the river channel and point bar show coarse grain size, indicating that they are deposited in high-energy environment while the sediments in flood plain show finer grain size, positive skewness, and poorly sorted nature indicating that they are deposited in low-energy environment.

Heavy minerals are concentrated more in finer fractions and in the estuary. The sediments predominantly consist of heavy minerals such as magnetite, opaque (other than magnetite), garnet, sillimanite and hypersthene whereas minerals such as

amphiboles, zircon, monazite, rutile, staurolite, tourmaline, epidote and biotite occur in minor quantities. The concentration of opaques and garnets decreases while the concentration of sillimanite increases in all the size grades, i.e., +60, +120 and +230 ASTM in channel from upstream to downstream. The heavy mineral assemblage suggests that it is mainly derived from Khondalite and Charnockite group of rocks.

Acknowledgement: This work forms part of the research project (Ref.No. KDMIPE/GFRD/Res.Proj./ 2(382)/2004) sponsored by KDMIPE, ONGC, Dehradun, and the authors gratefully acknowledge the financial support provided by ONGC. The authors also thank the Delta Studies Institute, Andhra University for providing the infrastructure facilities for carrying out the research work at Delta Studies Institute, Andhra University.

References

Acharya, B.C., Panigrahi, P.K., Nayak, B.B. and Sahoo R.K. (1998). Heavy mineral placer deposits of Ekakula beach, Gahiramatha coast, Orissa, India. Resource Geology, 48(2), 125-136.

Folk, R. L., (1968). Petrology of Sedimentary Rocks: Austin, University of Texas Publication.

Folk, R.L. and Ward, W. (1957). Brazos River Bar: a study in the significance of grain-size parameters. Jour. Sed. Petrol., 27, 3-26.

Gajapathi Rao, R., Sahoo, P. and Niroj K. Panda. (2001). Heavy mineral sand deposits of Orissa. Special Issue on "Beach and Inland Heavy mineral sand deposits of India. Exploration and Research for Atomic minerals, 13, 23-52.

Galehouse, J.S. (1969). Counting grain mounts number percentage Vs. number frequency. Jour. Sed. Petrol., 39, 812-815.

Galehouse, J.S. (1971). Sedimentation analysis. In Carver, R.E. (Ed.), Procedures in Sedimentary Petrology: New York (Wiley), 69-94p.

Ghosh, R.N., and De, S.K. (1984). Sedimentological analysis of coastal sands, Mahanadi Delta, Orissa. Geological Survey of India special publication, No.2, 345-358.

Hota, R.N., and Maejima, W. (2009). Heavy minerals of the Barakar Formation, Talchir Gondwana Basin, Orissa. Jour. of Geol. Soc. of India, 74, Sept., 375-384.

Jagannadha Rao, K., Subramanyam, A.V., Abhinav Kumar, Sunil, T.C., and Chaturvedi, A.K. (2008). Discovery of heavy mineral-rich sand dunes along the Orissa-Bengal coast of India using remote sensing techniques. Current Science, 94(8), 25 April, 983-985.

Komar, P.D., and Wang Chi. (1984). Processes of selective grain transport and the formation of placers on beaches. Jour. Geol., 92, 637-655.

Krumbein, W.C. and Pettijohn, F.J. (1938). Manual of sedimentary Petrography, New York, Appletpon century – Crofts, 549p.

Mahadevan, C. and Sathapati, N. (1948). The home of Monozites in the Vizagapatnam area. Curr. Sci., 17, p.297.

Mahalik, N.K., (2000). Mahanadi Delta, Geology, Resources & Biodiversity, AIT Alumni Association (India Chapter), New Delhi.

Murthy, M.S. (1958). Occurrence of monozites in the charnockites of Visakhapatnam. Curr. Sci., 27, 347-348.

Patro, B.C., Sahu, B.K., and Guru, S. (1989). A Study on heavy mineral sands of Gopalpur beach, Orissa. Jour. Geol. Soc. of Ind., 33, Mar., 243-252.

Pattnaik, M. (2000). Heavy minerals in recent sediments of Mahanadi River Delta. UGC sponsored state level seminar on Quaternary Geology and Archaeology of Orissa, Abstract Volume, p.15.

Prabhakara Rao, A., Prasad, W., Vijayanand, B and Ravi, G.S.(2005). A Note on the occurrence of rich heavy mineral beach placers along Gahiramatha coast, Kendrapara district, Orissa. Jour. Ind. Assoc. of Sed., 24(1&2), 59-64.

Rajasekhara Reddy, D., Karuna karudu, T., and Deva Varma, D.,(2008a).Textural Characteristics of the sediments of different micro-environments of Mahanadi Delta, Abstracts volume: XXV Annual convention of Indian Association of Sedimentologists & National Seminar on Sedimentary Basins of India – Their Geological Significance and Economic Prospects, 26th -28th Dec., 20-21.

Rajasekhara Reddy, D., Karuna Karudu, T., and Deva Varma, D.,(2008b). Textural characteristics of southwestern part of Mahanadi Delta, East Coast of India. Jour. Ind. Assoc. of Sed., 27 (1), 111-121.

Satyanarayana. K., (1973). Some aspects of the Modern Deltaic sediments of the Mahanadi River, India. Ph.D Thesis submitted to Andhra University, Waltair. (Unpublished).

Satyanarayana, K., and Poornachandra Rao, M. (1980). Heavy mineral assemblage in lower Mahanadi deltaic modern sediments. Proc. 3rd Conv., Ind. Assoc. Sed. (Abstract), p.49.

Tewari, R.C., and Trivedi, G.S. (2001). Heavy mineral assemblages vis-a-vis composition of provenance of Gondwana rocks of peninsular India. Ind. Jour. of Petrol. Geo., 10(1), July, 33-42.

Jour. Indian Association of Sedimentologists, Vol. 28, No. 1 (2009), pp. 31-37

Petrographic Studies of Noncoking Coals for Combustion Characterisation – A Case Study from Bukbuka Seam, South Central Sector of North Karanpura Coalfield, Jharkhand

DEBASHREE MANDAL and UDAY KUMAR
University Department of Geology, Ranchi University, Ranchi
E-mail: debashreedutta09@yahoo.com, kumaruday10@gmail.com

Absract: North Karanpura coalfield (NKCF) is a vast depository of non coking coals, which are rich in mineral matter content with a high percentage of inertinite, due to their allochthonous origin. These coals are mainly supplied to different Thermal Power Plants in India.

Assessment of the combustion characteristics of coal from the standard proximate and ultimate analysis often becomes difficult and it has widely been accepted that the petrographic characters have a crucial role in controlling the combustion characteristics. It has also been observed that not only vitrinite and liptinite are reactive macerals , as previously accepted but inertinites having mean reflectance values lower than 1.30% are also considered to be reactive, which show good burning behavior and they can even be more reactive than vitrinite.

In this paper four blocks viz. Ashok, K D Hesalong, Karkata and Piparwar of South central Sector of NKCF has been undertaken for the study, as the bukbuka seam (Seam-II) is common in all the four blocks. The results of the petrographic study of the coals of Bukbuka seam shows that the vitrinite content varies from 19.5% to 60.8%, liptinite from 5.2% to 17%, inertinite from 22% to 49.5%. The vitrinite reflectance values (Ro%) ranging from 0.46% to 0.58% show that the rank of these coals varies from lignito-bituminous to sub-bituminous. The percentage of reactive macerals (vitrinite, semivitrinite and liptinite) is high while the percentage of reactive inertinites having reflectance values < 1.30% is significant. Thus, the total content of reactive macerals indicates that these coals have good combustion characteristics and can be best used in the boiler if beneficiated and the ash percentage is reduced. This paper also highlights the importance of inertinites while assessing the combustion behavior of non-coking coals.

Key words: Coal petrography, combustion characters, reactive macerals, inertinite reflectance.

INTRODUCTION

North Karanpura Coalfield (NKCF), situated between latitudes 23^0 38'N - 23^0 56'N and longitudes 84^0 46'E - 85^0 23'E covering an area of 1230sq km is a storehouse of noncoking coals. The South Central Sector of this coalfield has drawn attention of the planners mainly after nationalization of coal industry. The area is gradually becoming a major coal supplier to Thermal Power Plants of north India. The coals of this area are characterized by high percentage of inertinite and high mineral matter content, due to its allochthonous origin (Stach et al., 1982).

The study area includes four adjoining blocks out of eleven blocks of the South Central Sector of NKCF, which are Ashok, K D Hesalong, Karkata and Piparwar (Fig.1). The area covers about 100 sq km. where the mining operation is active at present. In three blocks viz. Ashok, K D Hesalong and Piparwar, Seam I to Seam IV are present, while Seam V is present along with the other four in Karkata Block. All these seams, in the South Central Sector are termed as Seam I = Dakra, Seam II = Bukbuka, Seam III = Bisrampur, Seam IV = Karkata and Seam V = Raniganj. In the four blocks only a few seams are being mined at present among which Bukbuka seam is one.

Gondwana coals usually have high inertinite content but they can burn satisfactorily to give high heat value (Cloke and Lester, 1994; Choudhury et al., 2003). Assessment of the combustion characteristics of coal from the standard proximate and ultimate analysis often becomes difficult and it is widely accepted that the petrographic characteristics has a crucial role in controlling the combustion characteristics (Jones et al., 1985; Oka et al., 1987; Choudhury et al., 2003). The reactive macerals, viz. vitrinite and liptinite play a more predominant role during combustion than the inertinite content (Su et al., 2001; Kizgut and Yilmaz,2003). It has been discussed in ICCP (2001) that inertinite can show very good reactivity towards combustion, even higher than vitrinite (Oka et al., 1987; Phong-Anant et al., 1989; Thomas et al.,1993; Borrego et al, 1997). It has also been observed that not only vitrinite and liptinite are reactive macerals but also inertinites having mean reflectance lower than 1.30% are also considered to be reactive which show good burning behavior and they can even be more reactive than vitrinite(Bailey et al. 1990; Cloke and Lester,1994; Cloke et al., 2002b; Choudhury et al.,2004).

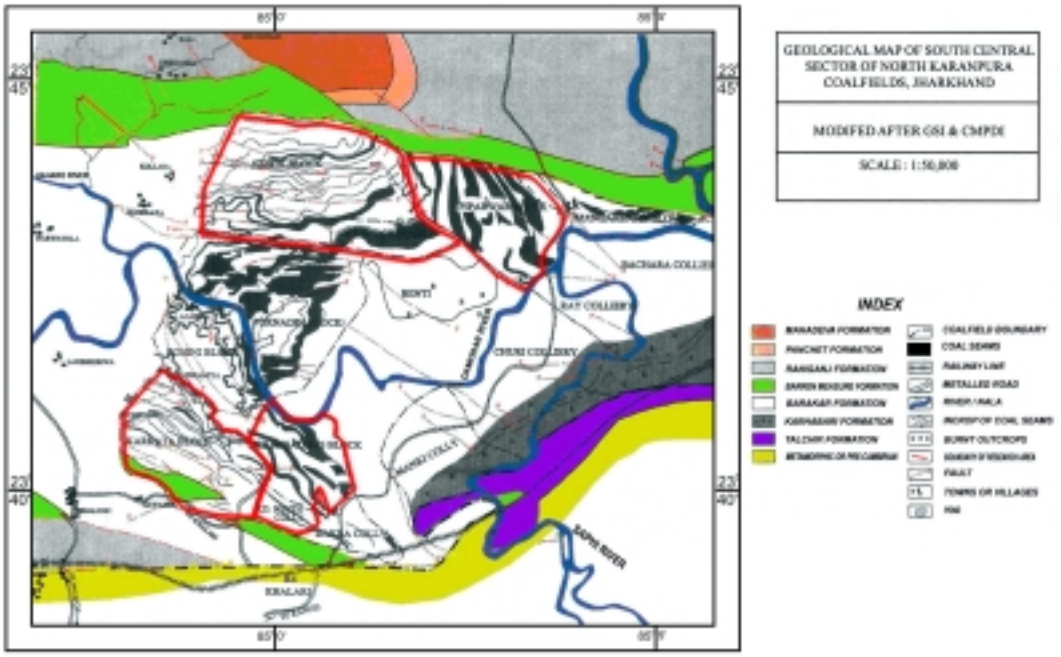

Fig.1. Geological Map of the Study Area.

(a) Bogen structure in Fusinite,×50

(b) Collotelinite with mineral inclusion,×50

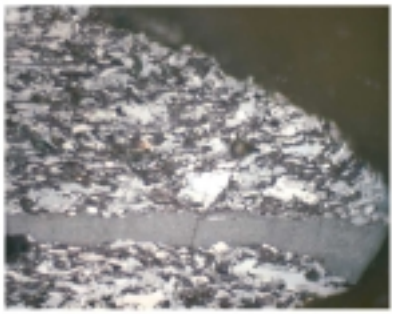

(c) Sporinite (under white light),×50

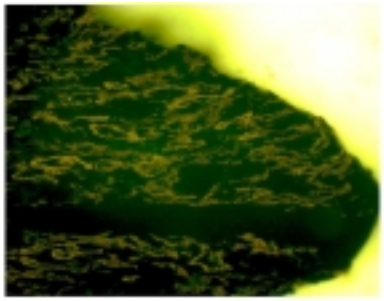

(d) Sporinite (under fluorescent light),×50

(e) Collodetrinite with semifusinite bands,×50

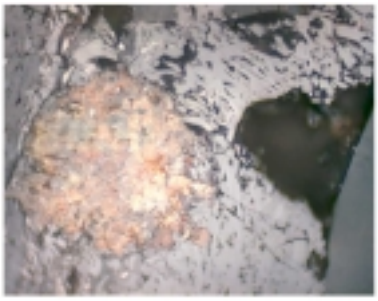

(f) Siderite Nodule (spherulitic),×50

Fig. 2 a-f. Macerals in the Bukbuka Seam, South Central Sector, NKCF.

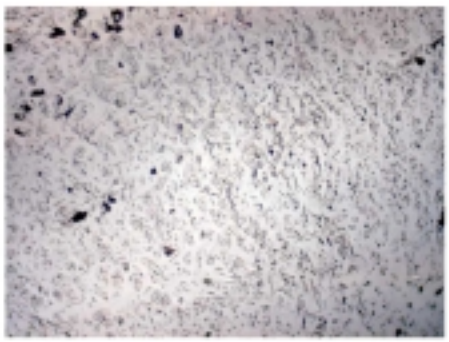

(a) Degradofusinite,×50

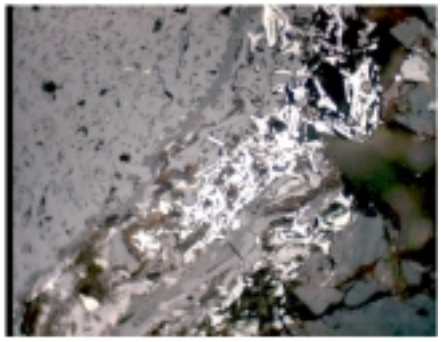

(b) Pyro- and Degradofusinite,×50

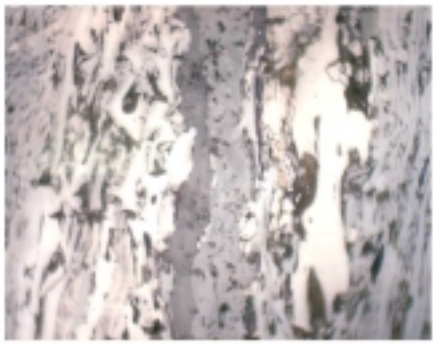

(c) Fusinite with variable reflectance,×50

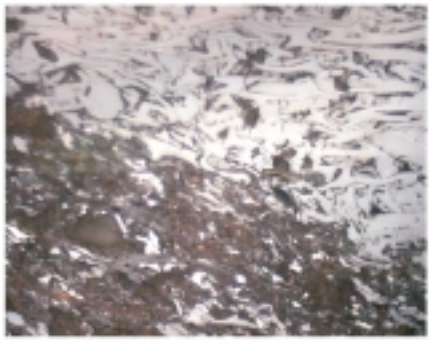

(d) Semifusinite,×50

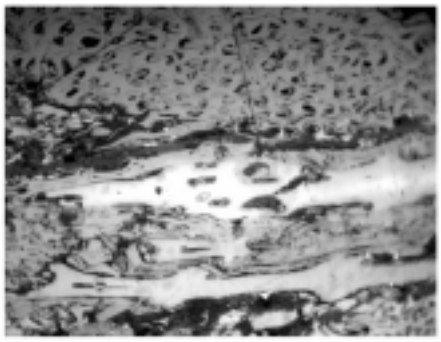

(e) Fusinite with semifusinite,×50

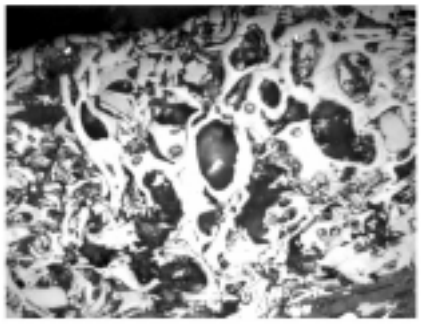

(f) Bogen structure in Pyrofusinite,×50

Fig. 3 a-f. Fusinite and Semifusinite with different values of reflectance.

METHODOLOGY

The channel samples were taken from the mine faces of the Bukbuka seam in all the four blocks. In total 24 samples were prepared and studied taking 6 samples from each block. The analytical techniques applied were Proximate analysis, maceral composition and vitrinite reflectance measurement. Following IS: 1350 (Part I) 1984, the proximate analysis was carried out. The maceral analysis and the reflectance measurement were carried out with a Leica DMRX polarized light microscope following IS: 9127 (part I): 1992 and IS: 9127 (part III): 1992. The reflectance measurement was done by MSP 200 software and the photomicrographs were taken using QWin Image analysis software.

RESULTS AND DISCUSSIN

Proximate Analysis

The Proximate analysis shows that the ash content ranges from 21.7% to 38.1% and the volatile matter ranges from 24.6% to 29%, while the moisture content ranges from 4.9% to 9%. A detail of the proximate analysis is given in the Table 1. The result of the proximate analysis shows that the

Table 1. Proximate analysis data of Bukbuka coal seam.

S.No.	Name of the Seams	Moisture %	Volatile Matter %	ASH %	Fixed Carbon %
1.	Bukbuka Seam, Piparwar	9.0	24.6	31.2	35.2
2.	Bukbuka Seam, Karkata	4.9	24.9	38.1	32.1
3.	Lower Bukbuka, Ashok	5.5	29.0	25.7	39.8
4.	Upper Bukbuka, Ashok	5.7	25.9	29.3	39.1
5.	Bukbuka Seam,K D Hesalong	7.6	28.6	21.7	42.1

Table. 2. Petrographic Analysis of Bukbuka Seam.

Block Name	Sample No.	Vitrinite	Liptinite	Reactives	Inertinites	Reactive Inertinites (R_r% <1.30)	Total Reactives	R_r%
Ashok	A1	41.5	9.8	51.3	35.4	26.2	77.5	0.47
	A2	54.4	13.2	67.6	25.4	21.2	88.8	0.49
	A3	45.8	17.0	62.8	30.6	23.9	86.7	0.46
	A4	26.2	15.5	41.7	42.5	26.0	67.7	0.55
	A5	19.5	16.7	36.2	49.5	29.1	65.3	0.56
	A6	23.4	14.8	38.2	44.7	27.3	65.5	0.52
K D Hesalong	KDH1	48.5	5.3	53.8	24.3	19.7	73.5	0.52
	KDH2	60.8	8.0	68.8	22.0	17.8	86.6	0.57
	KDH3	53.4	8.2	61.6	28.8	20.6	82.2	0.58
	KDH4	57.8	7.9	65.7	23.8	19.6	85.3	0.55
	KDH5	53.9	7.6	61.5	27.8	21.2	82.7	0.58
	KDH6	58.6	8.5	67.1	25.5	18.4	85.5	0.53
Karkata	KT1	22.9	12.1	35.0	49.5	33.6	68.6	0.47
	KT2	30.0	12.1	42.1	42.8	28.5	70.6	0.51
	KT3	28.7	11.6	40.3	45.6	30.6	70.9	0.46
	KT4	32.3	13.4	45.7	44.6	28.7	74.4	0.54
	KT5	23.4	12.5	35.9	48.8	30.1	66.0	0.49
	KT6	26.8	11.7	38.5	44.8	29.4	67.9	0.50
Piparwar	PP1	41.9	5.2	47.1	30.9	23.5	70.6	0.55
	PP2	43.8	11.3	55.1	28.5	22.4	77.5	0.51
	PP3	48.2	10.6	58.8	29.0	24.6	83.4	0.53
	PP4	45.7	9.6	55.3	27.6	24.2	79.5	0.56
	PP5	40.7	12.2	50.4	27.8	21.6	72.0	0.52
	PP6	42.3	11.8	54.1	25.6	22.7	76.8	0.55

coals are medium to high volatile, high moisture bituminous coals having high ash content.

Petrographic analysis

The petrographic analysis of these coals shows that vitrinite is the dominating maceral group. Collodetrinite is most common, which is followed by collotelinite and vitrodetrinite (Vitrinite Classification ICCP, 1994) as shown in Fig.2b & 2e. The percentage of vitrinite content is quite high in KD Hesalong block, while it is the lowest in Karkata block. In the two other blocks vitrinite content is intermediate. The total range varies from 19.5% to 60.8%. In the Liptinite group of macerals, sporinite is the only maceral observed abundantly in all the samples (Fig.2c & 2d). Cutinite is rarely observed and present in a very few samples of Piparwar and Ashok Block. The Bukbuka Seam of Ashok and Piparwar block shows a higher content of liptinites in comparison to other two blocks. The value of liptinite varies from 5.2% to 17%. The proportion of inertinite in these coals is quite high and it is just next to vitrinite. Inertodetrinite is the major component in all the samples followed by semifusinite and fusinite with bogen structure (Fig.2a). Micrinite is observed in almost all the samples in a very few numbers. The proportion of inertinite is the highest in Karkata block while in the other three blocks it is present in similar proportion. The range of inertinite varies from 22% to 49.5%.

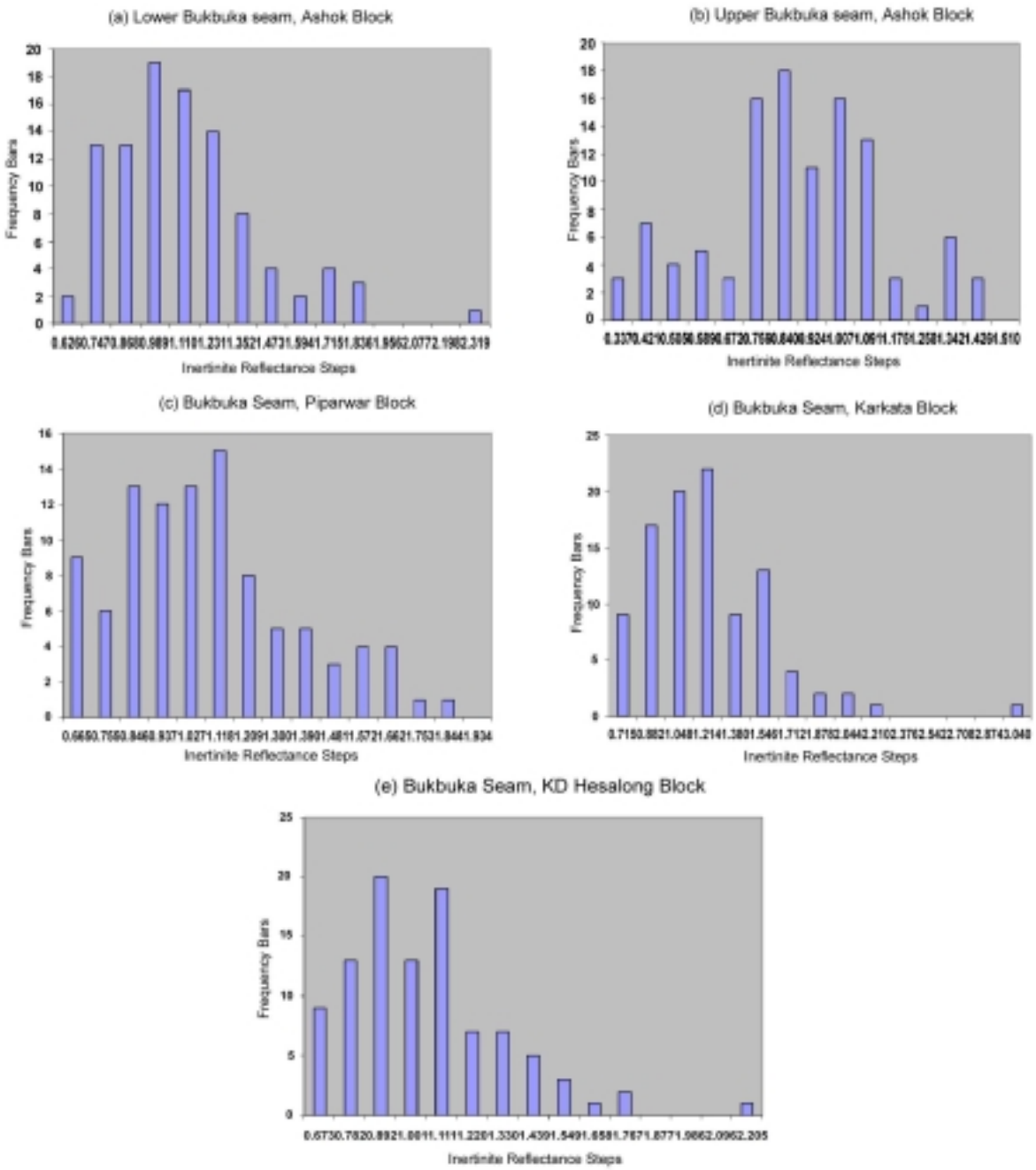

Fig. 4 a-e. Graphs showing Inertinite Reflectance of coals of the study area.

The mineral matter content in these samples is moderate to high. Clay mineral is most abundant followed by siderite and pyrite (Fig.2f).

The reflectance analysis of the samples clearly shows that the coals of the Bukbuka seam are subbituminous in nature. Detail of the reflectance values of the samples are presented in the Table 2. It ranges from 0.46% to 0.58%. Inertinites show variable reflectance values in different fusinites and semifusinites (Fig.3a-f). The reflectance values of the inertinites were taken randomly, which shows a wide range of values from <0.5% to 3.97%, (Fig.4a-e). The horizontal axis of the graphs shows the inertinite reflectance and the vertical axis shows their frequency. It is clearly observed in these graphs that the frequency of the inertinites, having Ro% values in between 0.7% to 1.0% is much higher than those inertinites having values lower than 0.7% or higher than 1.0%.

It has been observed that the frequency of those inertinites having reflectance value less than or equal to 1.3% is quite high than those of more than 1.3%. In most of the cases the percentage of such inertinites having lower reflectance values is more than 70% of the total inertinites.

It is observed that the percentage of total reactives (Vitrinite + Semivitrinite + Liptinite + Reactive Inertinite) is very high than the inerts which are less than one third of the total macerals. The percentage of total reactives range from 65.3% to 88.8% (Table 2). It is also observed that the percentage of total reactives is more in K D Hesalong block than the other three blocks, being least in Karkata block. In the Ashok block where the Bukbuka seam is splitted into two, the Lower Bukbuka seam has less reactives than the upper seam, which is due to the lower concentration of vitrinites. The difference may be due to the variation in the nature of depositional environment.

The petrographic study of the coals shows that the coals are rich in reactive macerals. Therefore, these coals will show good burning characteristics in the furnace. If these coals are properly washed and the mineral matter is removed they can be best used in thermal power plants.

CONCLUSION

Inertinite rich non-coking coals of Bukbuka seam of South Central Sector, North Karanpura Coalfield show good burning characteristics. The petrographic characters of these coals show that though they are rich in inertinites, the percentage of reactive macerals is significant due to the presence of not only vitrinite and liptinites but due to the presence of a good number of reactive inertinites having reflectance Ro% < 1.30. Thus, the total percentage of reactive macerals is very high. Moreover, it has also been found that the concentration of those inertinites having reflectance values ranging in between 0.7% to 1.0% is much higher than those inertinites with Ro% <0.7% or > 1.0%. Thus, if the reflectance of inertinite is considered to be a parameter for the reactivity of inertinites, then these contribute to the total number of reactive macerals and throw light on the burning characteristics of coals. It may be said that these coals can be best used in the boiler if beneficiated and the ash content is reduced. However, it is recommended that thermogravimetric analysis may be done to confirm the burning characteristics.

Acknowledgements: We are thankful to Dr. D. K Bhattacharya, Head of the University Department of Geology, Ranchi University, Ranchi for his support and encouragement in the research work. We also extend our sincere thanks to CMPDI, Ranchi for providing Laboratory facilities. Lastly, we extend our heartiest thanks to S. N Chaudhury and D.R Dutta of Petrology and Palaeontology Division, Coal Wing, Geological Survey of India, Kolkata and Mrs. Nandita Choudhury, CIMFR, for their suggestions.

References

Bailey. J. G. Tate, A, Diessel, C.F.K., Wall, T.F., (1990). a char morphology system with application to coal combustion. Fuel. 69, 225-237.

Choudhury, N., Chaudhari, S.G.,Chakraborty, C.C, Boral, P., (2004). Studies on char morphology in relation to petrographic characteristics of some Permian coals of India. Indian Journal of Scientific and Industrial Research, 63, 383 – 385.

Choudhury, N., Boral, P., Mitra, Tandra, Adak, A.K., Choudhury, A., Sarkar, P., (2007). Assessment of nature and distribution of inertinite in Indian coals for burning characteristics, International Journal of Coal Geology, 72 (2007), 141-152.

Cloke. M., Lester, E., (1994). Charaterization of coals for combustionusing petrographic analysis, A Review, Fuel. 73, 315 – 320.

Cloke, M., Lester, E., Thompson A.W., (2002b). Combustion characteristics of coals using drop tube furnace. Fuel. 81, 727-735.

ICCP, (1994). The New Vitrinite Classification, Fuel. 77(5), 341-358.

IS: 1350 (Part I) (1984). Methods of test for coal and coke – Proximate analysis.

IS: 9127(Part I): (1992) Methods of the petrographic analysis of coal – Definition of terms relating to petrographic analysis of coal.

IS: 9127 (part III) (1992). Method of the petrographic analysis of coal Microscopical determination of the reflectance of Vitrinite.

Jones , R. B., McCourt, C. B., Morley, C., King K., (1985). Maceral and rank influence on the morphology of coal char. Fuel. 64, 1460-1467.

Kizgut, S., Yilmaz, S. (2003). Characterization and non isothermal decomposition kinetics of some Turkish Bituminous coals by thermal analysis. Fuel Processing Technology 85, 103-111.

Oka, N., Maurayama, T., Matsuoka, H., Yamada, S, Yamada, t., Shinozaki, S., Shibaoka, M., Thomas, C.G. (1987). The influence of rank and maceral compostion on ignition and char burnout of pulverized coal. Fuel Processing Technology 15, 213-224.

Phong-anant, D., Salehi, M., Thomas, C., Baker, J., Canroy, A. (1989). Burnout and reactivity of coal macerals, Proceeding of International conference on Coal Science, NEDO, Tokyo, 253-256.

Stach, E., Mackowsky, M.T., Teichmuller, M., Taylor, G.H., Chandra, D., Teichmuller, R. (1982). Stach's Textbook of Coal Petrology, Gebruder Borntraeger, Berlin, Stuttgart, Third Edition.

Su, S., Phol J.H., Holcombe D., Hart J. A. (2001). A proposal maceral index to predict combustion behaviour of coal. Fuel. 80, 699-706.

Thomas, C.G., Gosnell, M.E., Gawronski, E., Phong-anant, D., Shibaoka, M. (1993). The behavior of inertinite maceral under pulverized fuel (pf) combustion conditions. Organic Geochemistry, 20, 779-788.

Jour. Indian Association of Sedimentologists, Vol. 28, No. 1 (2009), pp. 39-48

Significance of Size Parameters of the Carbonate Sands Between Dabhol and Jaigarh Creeks, Ratnagiri District, Maharashtra

MILIND A. HERLEKAR[1] and R.K. SUKHTANKAR[2]
[1]Department of Geology, University of Pune, Pune
[2]Department of Atmospheric & Space Science University of Pune, Pune
E-mail: milindk@unipune.ernet.in

Abstract: Textural studies of the tidal clastics, exposed along the coast in parts of Ratnagiri District, Maharashtra; have been carried out. The coastal tract is about 40 km. in length. The area under investigation is the narrow coastal tract, and lies between Dabhol creek in the north and Jaigarh creek in the south.

Representative sediment samples from the foreshore zone, backshore zone, raised marine terrace and beach dune were subjected to granulometric analysis and statistical parameters, such as; mean size, standard deviation, skewness and kurtosis have been computed from each geomorphic unit. These textural parameters have been examined to understand hydrodynamics of the depositional environment.

Keywords: Size Parameters, Carbonate Sands, Ratnagiri.

INTRODUCTION

The area bounded between Dabhol creek in the north and Jaigarh creek in the south, Ratnagiri district, Maharashtra has been investigated for the textural characters of the exposed Holocene sediments.

The study area extends for a distance of about 40 km. in length in NS direction, with an average width of about 15 km. and is bounded by the Dabhol creek (Lat. 17º, 35'N; Long.73º, 10'E) in the north and the Jaigarh Creek (Lat.17º, 16'N; Long 73º, 15'E) in the south. It is covered in the Survey of India topographic sheet No. 47 G/2, 47 G/3, 47 G/6 and 47 G/7 on the scale 1:50 000 (Fig. 1).

GEOLOGY OF THE AREA

The area under investigation forms a part of the major Continental Tholeiitic Province of India, represented by the Deccan basaltic lava flows. Two major lithological units, viz., the basalts, which are lateritised and the Quaternary (Holocene) sediments, are exposed in the study area.

Most of the area is covered by the basaltic lava flows. At number of places, laterite is developed as capping on basalts, which occurs at various altitudes. The beach sands occur all along the coast, but rather in discontinuous patches. There is an extensive linear beach, composed of unconsolidated carbonate sands, containing molluscan shell fragments in varying proportions. These sands occur in the foreshore and backshore zones, and in the form of berm, which is a raised marine terrace, well separated from the backshore zone and has elevation of about 3-4 m. w.r.t. sea-level.

The mudflats have developed on the southern bank of Vashishti river and the northern bank of Shastri river. These mudflats are quite extensive and can be traced in the inland region for a distance of about 4 to 5 km (Fig. 2).

METHOD OF STUDY

Representative samples from every micro-environment have been subjected to granulometric analysis on half phi interval, with the help of automatic ro-tap sieve shaker. The samples collected from the field were subjected to coning and quartering to obtain the desired sediment fraction. The fractions so obtained were weighed and then subjected to 1:10 dil. HCl acid to remove all the carbonates and molluscan shell fragments. The samples were then washed with distilled water to remove the traces of acid. It was then dried in an oven at 105º-110º C. After drying, weight of the sample was recorded. Difference in weight yielded the presence of carbonate.

In all, sixty eight sediment samples have been analysed for size studies, of which twenty samples each from foreshore zone, backshore zone and raised marine terrace and eight samples representing dune environment have been selected for the purpose.

RESULTS AND DISCUSSION

It is common practice amongst sedimentologists to apply grain size measures to identify and describe the depositional processes and depositional sedimentary environments. The theory of trends in grain-size measures, as suggested by McLaren (1991), has been applied to the intertidal zone sediments from the area under the present study to decipher sediment transport directions and nature of sedimentary processes in the light of hydraulic energy.

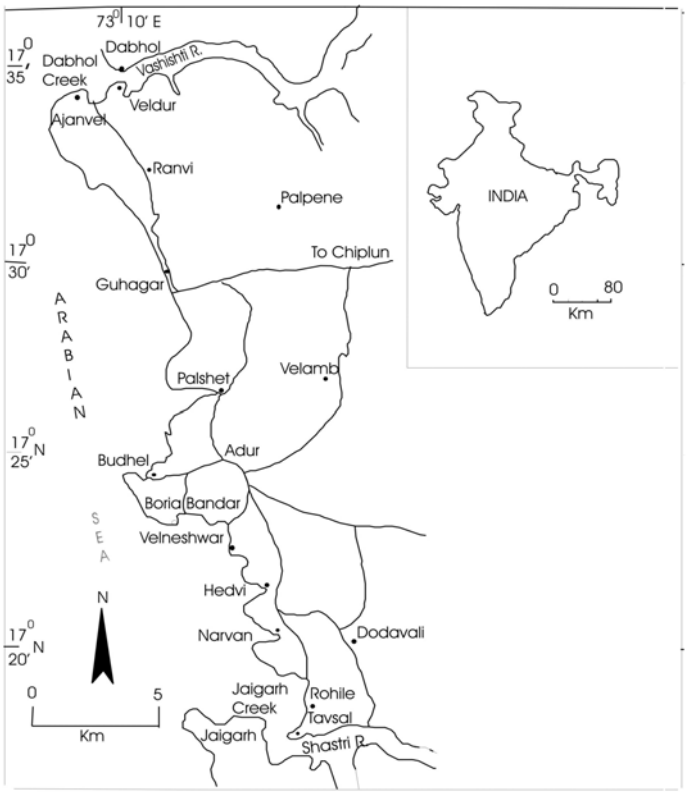

Fig. 1. Location map of the study area.

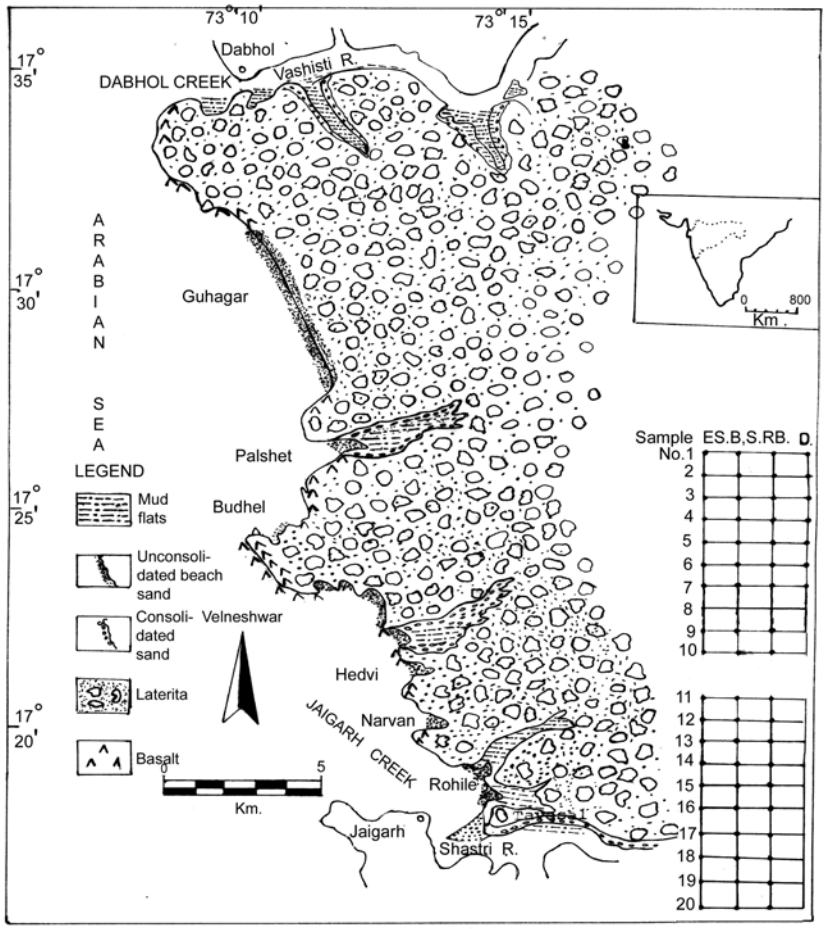

Fig. 2. Geological map of the area between Dabhol Creek and Jaigarh Creek. .

To the prevalent hydraulic energy, response of a particular sediment size fraction is its transport. Such a sediment size expresses the hydraulic energy, which is termed as 'hydraulic equivalence'. During the process of transport, as the hydraulic energy decreases, a particular sediment size fraction falls out of the hydraulic system. Therefore, there results a gradual decrease in sediment size as there is a fall in hydraulic energy. Such a phenomenon can very well be observed in a beach environment. Gradual decrease or increase in sediment size can be interpreted in terms of relative variations in hydraulic energy. An attempt is made accordingly to infer energy levels in the wave pattern on the beach under study. It is observed that coarse truncation seems to be better controlled and therefore seems to be a useful parameter in interpretation of hydraulic energy levels. The coarse truncation values, in phi units, therefore have been plotted at the respective sample locations and variations in hydraulic energy have been inferred. The results are presented in Fig. 3.

For the textural analysis, graphic measures following Folk and Ward (1957) have been computed. The interrelationship between different grain size parameters has been examined with the help of bivariate plots, as suggested by Friedman (1962, 1967). The inferences derived therefrom have been discussed in the following paragraphs.

Mean Size

Mean size of the different sediment samples has been computed and values so obtained have been presented in Table 1, 2, 3 and 4. For foreshore zone sediments, it is seen that mean size of the sediments varies from 1.88 Ø to 3.56 Ø, suggesting thereby that these are medium to very fine sand grade. Sediments from the backshore zone have mean size, ranging between 1.70 Ø to 3.53 Ø. These sediments are of medium sand to very fine sand grade. Raised beach sediments have the mean size variations in the range between 1.25 Ø to 3.63 Ø suggestive of the sediments being of medium sand to very fine sand grade; whereas, beach dune sediments have the mean size variations in the range between 2.70 Ø to 3.05 Ø, indicating that these are fine sand to very fine sand grade. It can be stated, therefore, that these beach sediments, in general, are of medium to very fine sand grade.

Standard Deviation

Higher the values of standard deviation poorer is the nature of sorting of sediments (Folk, 1974). Standard deviation of the different sediment samples has been computed and values so obtained have been presented in Table 1, 2, 3 and 4. It is found that values of standard

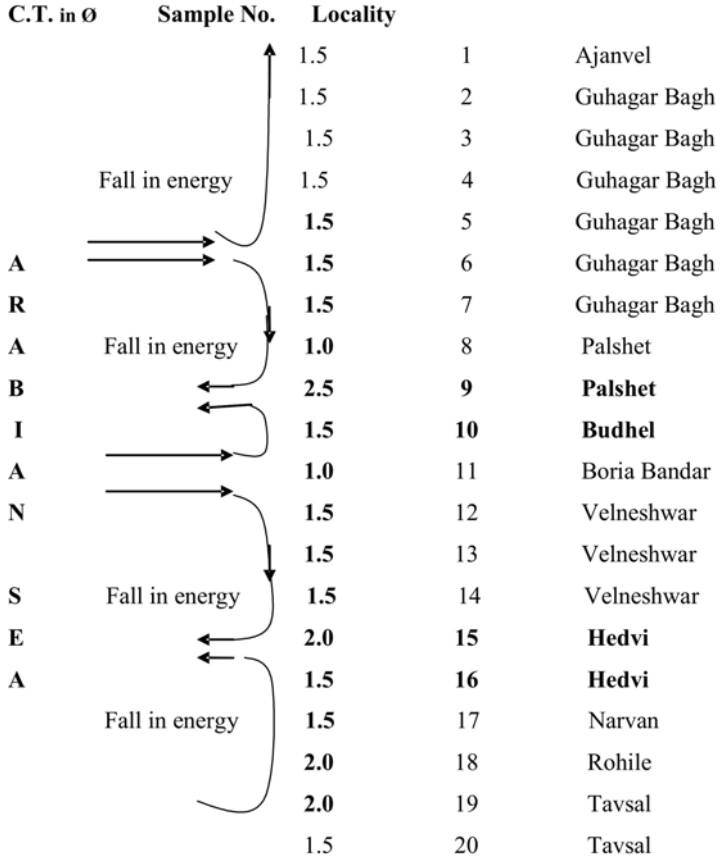

Fig. 3. Coarse Truncation (C.T.) points of the Raised Beach sediments indicating the probable wave refraction pattern.

Table 1. Graphic Measures of Foreshore Zone Sediments.

Sample No.	Mean	Mode	Median	Std. Deviation σ1	Skewness	Kurtosis	Coarse Truncation	Fine Truncation
1	2.62	3.00	2.60	0.4503	0.2556	1.7304	1.5	3.5
2	2.30	2.50	2.50	0.8803	-0.9642	2.3907	2.0	3.5
3	3.00	3.00	2.85	0.9587	0.5490	1.7687	2.0	3.5
4	2.93	3.00	2.80	0.6680	0.3888	0.8606	2.0	3.0
5	2.41	3.00	2.60	1.2193	-0.5103	2.8373	2.0	4.0
6	2.13	2.50	2.30	1.2000	-0.3135	1.5573	2.0	4.0
7	2.61	3.00	2.70	0.9678	-0.3237	1.6875	2.0	3.5
8	2.73	3.00	2.70	0.5075	0.3850	1.1612	2.0	3.5
9	2.51	2.50	2.50	0.4655	0.7142	1.8214	2.0	4.0
10	3.01	2.50	2.95	0.7659	0.1829	0.6147	2.0	3.5
11	3.01	3.00	2.95	0.5174	0.5913	0.9367	2.0	4.0
12	2.65	3.00	2.75	0.7287	-0.1927	1.3660	1.5	3.5
13	2.15	2.50	2.05	0.5227	0.4807	1.1349	2.0	3.5
14	2.16	2.00	2.00	0.5530	0.7250	1.6393	1.5	3.5
15	1.88	2.00	2.50	1.0150	0.4838	0.6193	1.5	3.0
16	2.85	3.00	2.75	0.5575	0.2720	0.9289	2.0	3.5
17	3.56	4.00	3.75	0.7867	-0.4574	1.4344	1.5	4.0
18	3.26	4.00	3.55	0.6253	-0.5516	0.7416	2.0	4.0
19	3.00	3.00	2.80	0.6678	0.4256	0.8424	1.5	4.0
20	2.60	3.00	2.60	0.6833	0.6810	1.000	1.5	3.5

Table 2. Graphic Measures of Backshore Zone Sediments.

Table 3. Graphic Measures of Raised beach Sediments.

Table 4. Graphic Measures of beach dune Sediments.

Sample No.	Mean	Mode	Median	Std. Deviation σ1	Skewness	Kurtosis	Coarse truncation in Ø	Fine truncation in Ø
1	2.70	2.50	2.60	0.7909	-0.6490	1.5047	1.5	4.0
2	3.41	3.00	3.10	0.5458	-0.2605	0.9196	1.5	3.5
3	3.13	3.50	3.15	0.6793	-0.1526	1.1269	1.5	4.0
4	2.63	2.50	2.80	0.6312	0.3382	0.5316	1.5	4.0
5	2.95	3.00	2.80	0.7312	0.2916	0.6706	1.5	4.0
6	2.83	2.50	2.70	0.5978	0.1234	0.8392	1.5	4.0
7	2.83	2.50	2.65	0.7090	-0.3146	1.1702	1.5	4.0
8	3.03	3.00	2.90	0.6886	0.3062	1.0920	1.5	4.0
9	2.10	2.00	2.00	0.7727	0.4910	2.1750	2.5	4.0
10	2.21	2.00	2.10	0.6988	0.3066	1.2568	1.5	3.5
11	3.01	3.00	2.90	0.6056	0.2235	1.1475	1.0	4.0
12	2.70	2.70	2.70	0.7887	0.6010	1.2054	1.5	4.0
13	2.20	2.00	2.10	0.5325	0.3421	0.8709	1.5	3.5
14	2.30	2.00	2.25	0.5276	0.4857	0.9562	1.5	3.5
15	1.25	2.00	2.17	1.2058	0.4422	1.2200	1.5	4.0
16	2.25	2.50	2.20	0.4625	0.2245	1.3295	2.0	3.5
17	3.63	4.00	3.75	0.6034	-0.3999	1.8422	2.0	4.0
18	2.88	3.00	2.80	0.5646	0.2326	0.5573	2.0	4.0
19	3.00	3.00	3.00	0.5928	0.1405	0.8919	2.0	4.0
20	2.72	3.00	2.75	0.7333	-0.2125	0.9490	1.5	3.5

deviation for the foreshore zone sediments vary between 0.43 Ø to 1.25 Ø, thereby suggesting that majority of these sediments are well sorted to poorly sorted in character. Standard deviation values for the backshore zone sediments, which range from 0.44 Ø to 1.16 Ø, suggest that these are well sorted to moderately well sorted sediments and few are poorly sorted. Sediments from the raised beach sections have the standard deviation varying between 0.55 Ø and 1.20 Ø and therefore these sediments are well sorted to moderately well sorted and few are poorly sorted. Sediments from the beach dune have the standard deviation values, ranging between 0.59 Ø to 0.79 Ø. Therefore, these sediments are moderately well sorted. It appears, therefore, that these beach sediments, in general, are well sorted to moderately well sorted in character.

Skewness

Skewness measures the asymmetry of the distribution (Folk, 1974). On the basis of skewness values, asymmetry of the distribution is described.

For the foreshore zone sediments, skewness values vary between 0.19 and 0.72 indicating thereby that these are very fine skewed to coarse skewed sediments. Skewness values of the backshore zone sediments vary between –0.21 to 0.83 suggesting that these are very fine skewed to coarse skewed. Sediments from the raised marine terrace have the skewness values varying between –0.31 to 0.60, therefore suggesting that these are very fine skewed to very coarse skewed, while the skewness values of the beach dune sediments lie between –0.14 to 0.29. It means that these are fine skewed to coarse skewed sediments. Thus, skewness

values suggest that these sediments, in general, are very fine skewed to very coarse skewed.

Kurtosis

Kurtosis describes the peakedness of the distribution. Based on the scale suggested by Folk (1974), it can be stated that the sediments from foreshore zone, having kurtosis values ranging between 0.61 to 2.83, are platykurtic to very leptokurtic in nature. Kurtosis values for the backshore zone sediments vary between 0.57 and 2.11, thereby suggesting that these sediments are very platykurtic to very leptokurtic in character. Kurtosis values of the raised beach sediments vary between 0.54 to 1.84, indicating that these sediments are leptokurtic to very leptokurtic, while kurtosis values of the beach dune sediments lie between are 0.86 and 1.57. These sediments are therefore platykurtic to very leptokurtic in nature.

Bivariate Plots

Size statistical parameters have been analysed with the help of bivariate plots, which have been used basically to discriminate the environments of deposition, such as; beach, dune and river. In the present studies, these bivariate plots have been tested to discriminate the microenvironments of the sediments collected from the known microenvironments.

The bivariate plots so employed are mean size vs. standard deviation, mean size vs. skewness, standard deviation vs. skewness and simple sorting measure vs. simple skewness measure.

I. Mean size vs standard deviation

The plot of mean size vs. standard deviation has been prepared for the sediments, collected from the foreshore zone, backshore zone, raised marine terrace. Average values of mean size and standard deviation for every microenvironment have also been plotted. It is seen that the sediments from each microenvironment form a separate envelope, however with little overlap of foreshore zone and backshore zone. The envelope formed by the sediments from raised marine terrace rather matches with that of the backshore zone (Fig. 4).

II. Mean size vs Skewness

The plot of mean size vs. skewness has been prepared for the samples from each microenvironment. In this case also, the sediment samples from every microenvironment formed a separate envelope, with overlap of foreshore zone and backshore zone envelopes. Envelope of the sediments from raised marine terrace rather overlaps with that of the backshore zone sediments (Fig. 5).

III. Standard Deviation vs Skewness

In Fig. 6, the values of standard deviation have been plotted against skewness values. Envelopes for foreshore zone and backshore zone also appear distinctly with little overlap. Envelope for the sediments from raised marine terrace closely matches with that of the backshore zone.

IV. Simple Sorting Measure vs Simple Skewness Measure

The plot of simple sorting measure vs. simple skewness measures has been made for the sediments from each microenvironment (Fig. 7). In this plot also, a distinct envelope for every microenvironment is formed, with the overlap of foreshore zone and backshore zone. Envelope for raised marine terrace as

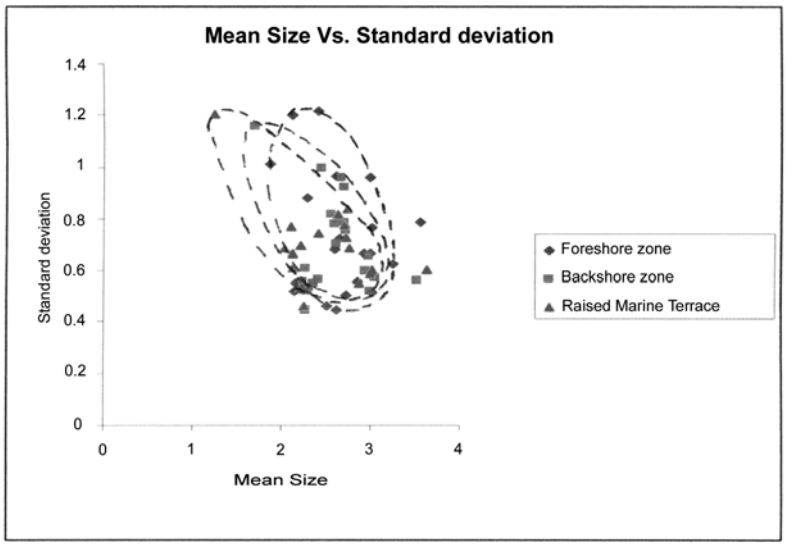

Fig. 4. Mean Size vs Standard Deviation.

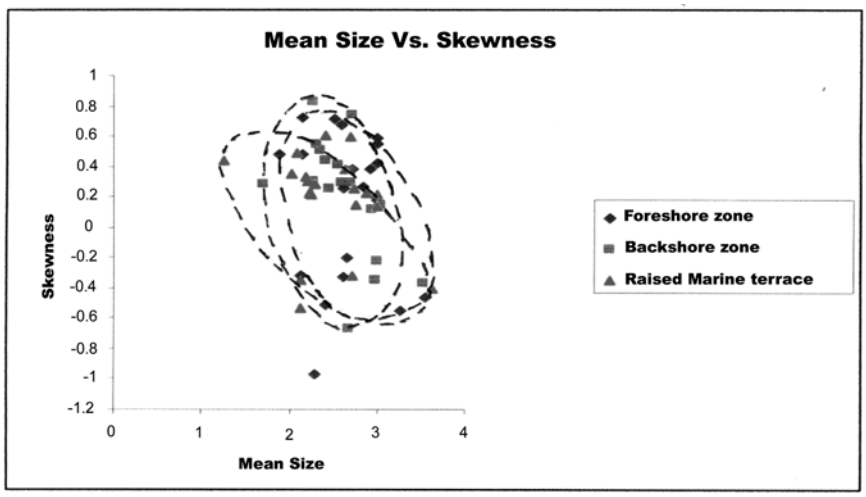

Fig. 5. Mean Size vs Skewness.

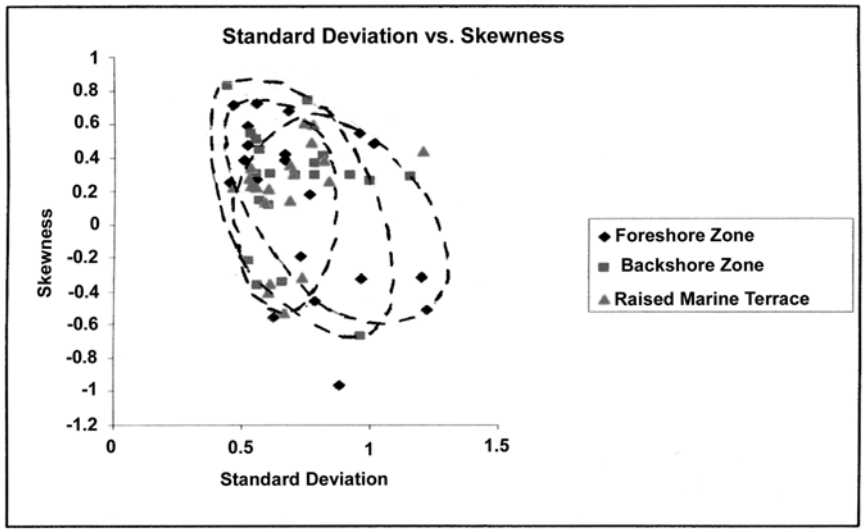

Fig. 6. Standard Deviation vs Skewness.

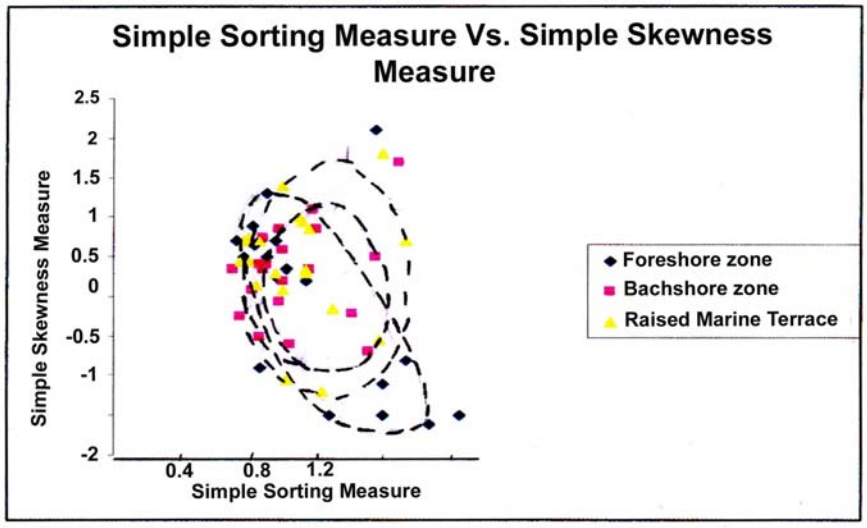

Fig. 7. Simple Sorting Measure vs Simple Skewness Measure.

Table 5. Simple sorting Measure and Simple Skewness Measure values for the Foreshore Zone sediments.

Table 6. Simple sorting Measure and Simple Skewness Measure values for the Backshore Zone sediments.

Sample Number	Simple Sorting Measure	Simple Skewness Measure
1	1.650	-0.70
2	0.825	-0.25
3	1.300	1.10
4	1.325	0.85
5	1.100	0.60
6	0.975	0.75
7	1.550	-0.20
8	1.075	0.85
9	0.950	0.40
10	1.700	0.50
11	1.075	-0.05
12	1.275	0.35
13	1.000	0.40
14	0.975	0.35
15	1.850	1.70
16	0.775	0.35
17	0.950	-0.50
18	1.150	-0.60
19	0.900	0.10
20	1.100	0.20

Table 7. Simple sorting Measure and Simple Skewness Measure values for the Raised marine terrace sediments.

Sample Number	Simple Sorting Measure	Simple Skewness Measure
1	1.25	0.35
2	1.100	1.40
3	1.425	-0.15
4	1.225	0.95
5	1.900	0.70
6	0.950	0.70
7	1.350	-1.20
8	1.200	1.00
9	1.725	-0.55
10	1.275	0.85
11	1.050	0.30
12	1.250	0.30
13	0.850	0.70
14	0.875	0.75
15	1.750	1.80
16	0.825	0.45
17	1.125	-1.05
18	0.875	0.45
19	0.925	0.15
20	1.100	0.10

Table 8. Simple sorting Measure and Simple Skewness Measure values for the Beach dune sediments.

Sample Number	Simple Sorting Measure	Simple Skewness Measure
21	1.400	0.80
22	1.200	-0.60
23	1.250	0.60
24	1.000	0.40
25	1.100	0.40
26	1.000	0.60
27	1.400	1.00
28	1.100	0.20

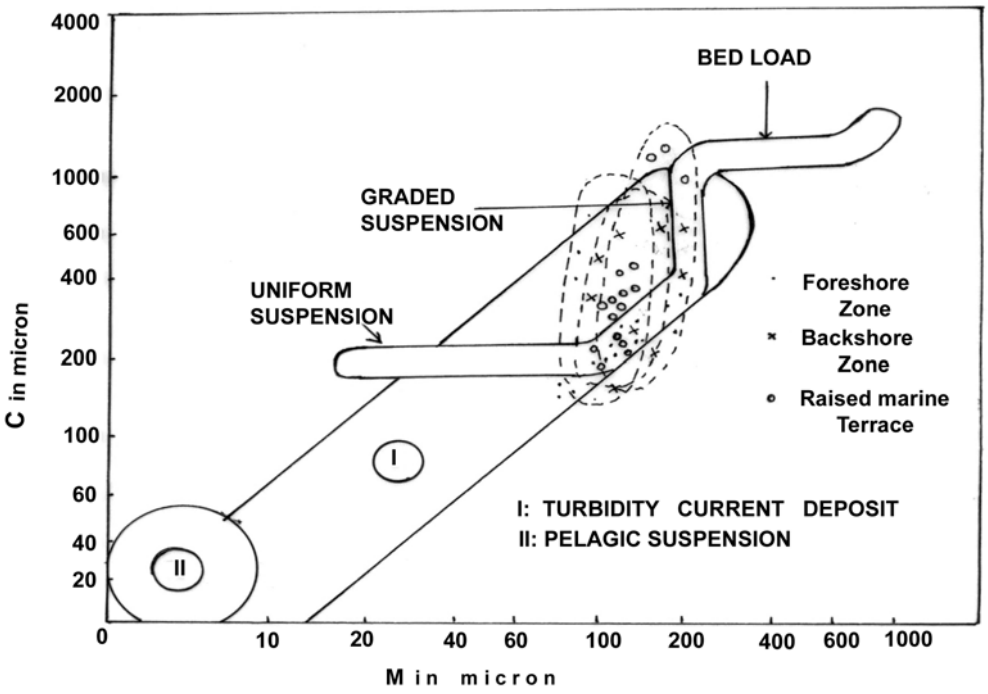

Fig. 8. C-M pattern of the sediments from the three microenvironments.

in the earlier cases closely matches with that of the backshore zone.

From the above discussion, it can be stated that the bivariate plots of size statistical parameters help to discriminate microenvironments. In the present case, microenvironments, viz., foreshore zone, backshore zone and raised marine sediments of the beach environment, can be distinguished.

CM Plots

Passega (1957, 1964 and 1977), has considered the relationship between C the first percentile and M-the median, the 50th percentile for the sediments from different environments. This relationship is presented as C-M plot. This plot has been employed to understand hydraulic energy conditions, under which these sediment have been deposited.

C-M plot suggested by Passega (1964) has later on been modified by Passega and Byramjee (1969), which Passega (1977) has further modified to indicate the hydraulic energy levels in the depositing medium. Sediment samples accordingly have been plotted in C-M plot and presented in Fig. 8, for foreshore zone, backshore zone and raised marine terrace which appear to have been deposited in hydraulic energy lower flow regime.

From the preceding paragraphs it is evident that the sediments from the raised beach sections appear more commonly deposited in the microenvironment, dominated by backshore zone.

CONCLUSIONS

In conclusion, it can be stated that analysis of size parameters of the sediments from each microenvironment suggest that there are of medium to very fine sand grade, well sorted to poorly sorted in character, very fine skewed to very coarse skewed and of very platykurtic to very leptokurtic in nature.

Bivariate plots of size statistical parameters help to discriminate microenvironments of beach environment with little overlap of each on other. Sediments from the raised marine terrace from the area under study indicate their deposition in backshore zone environment; whereas C-M plots suggest that these beach sediments from every microenvironment have been deposited in the lower flow regime, of the hydraulic energy.

Acknowledgement: The first author (MAH) is thankful to Prof. N. J. Pawar, Head, Department of Geology, University of Pune, Pune, for encouragement and providing the necessary facilities. We are extremely grateful to the journal referee for the critical comments and suggestions that helped to improve of the manuscript.

References

Folk, R.L. and Ward, W.C., (1957). Brazos River Bar: A study in the significance of Grain Size parameters. Jour. Sed. Pet., 27(1) 3-26.

Friedman, G.M., (1962). On sorting, sorting coefficient and the log normality of the grain size distribution of sandstones, Jour. Geol., 70, 737-753.

Friedman, G.M., (1967). Dynamic Processes and Statistical Parameters Compared for Size Frequency Distribution of Beach and River Sands. Jour. Sed. Pet., 37(2), 327-354.

McLaren, P. (1981). An interpretation of trends in grain size measure, Jour. Sed. Pet., 51, 611-624.

Passega, R., (1957). Texture as a Characteristic of Clastic Deposition, Am. Assoc. Petrol. Geol., Bull. 41(9): 1952-1984.

Passega, R., (1964). Grain size Representation by CM. Patterns as a Geological Tool., Jour. Sed. Pet., 34 (4), 830-847.

Passega, R., (1977). Significance of C-M Diagrams of Sediment Deposited by Suspension, Sedimentology, 24, 723-730.

Passega, R. and Byramjee, R., (1969). Grain size image of clastic deposit, Sedimentology, 13, 233-252.

Reineck, H.E. and Singh I.B. (1980). Depositional Sedimentary Environments, Springer-Verlag, Berlin Heidelberg New York, 549.

Sukhtankar, R.K. (1986). Trends in grain-size measure of the Quaternary sediments off the Vengurla coast, Maharashtra; with reference to beach morphology and tectonic evolution, Jour. Geol. Soc. India, 27: 419-427.

Visher, G.S. (1969). Grain Size Distribution and Depositional Processes, Jour, Sed. Pet., 30, 1074-1106.

Jour. Indian Association of Sedimentologists, Vol. 28, No. 1(2009), pp. 49-53

Soft Sediment Deformational Features (Seismites) as a Potential Tool for Seismic Hazard Assessment – A Case Study

A. R. CHAUDHRI
Department of Geology, Kurukshetra University, Kurukshetra 136 119, Haryana
Email: archaudhri@gmail.com

Abstract: Soft sediment deformation features in three sections namely, the Ghaggar River Section, the Patiali Rao Section and the Jainti Devi Ki Rao Section have been examined in the tectonically active Himalayan foothill region in the vicinity of Chandigarh for assessing seismo-tectonic character of the terrain. The main structures include kink folds, small scale faults, synclines and anticlines, plumes, sandstone dykes, pear drop (pillow) and flame structures. These structures are widespread in the region and are bounded by nearly horizontal Quaternary undeformed beds. These deformational features have developed as a consequence of liquefaction and shear stress generated by seismic activity in the Himalayan terrain that are evidenced by the presence of seismites.

Keywords: Seismites, Soft sediment deformation, Earthquake, Chandigarh Seismic Hazard.

INTRODUCTION

Soft sediment deformational structures formed during sedimentation or before compaction and cementation of sedimentary strata have been used in sedimentology for characterizing depositional processes, chaotic depositional episodes, paleocurrents and paleoslopes. These structures generally occur in coarse silt to fine sand size range sediments but occasionally silty clays also exhibit these structures. The formation of these structures is inherently related to grain cohesion, permeability and rate of deposition of the sediments which are the dominant factors in soil mechanics. Vertical displacing forces like liquefaction, reverse density gradation and slope failure along with horizontal deformational factor like shear stress represent the dominant mechanisms for their formation (Blatt et al., 1980). In nature, all these processes operate contemporaneously resulting in the production of deformational structures.

'Seismites' are considered as sedimentary evidences of past seismic activity (Sims, 1973, 1975; Sieh, 1978; Mills, 1982; Mohindra and Thakur, 1998; Chaudhri, 2007a, 2007b). Though there is no standard terminology to describe seismites (Lowe, 1975) yet, some of the more standardized structures whose genesis is attributed to seismic shaking include ball and pillow structure, pinch and swell bedding, lenticular boudins, pocket and pillar structures, pseudonodules or cycloids and flame structures. Therefore, to make a distinction between contorted strata produced by soft sediment deformational sedimentological processes and episodic seismogenic tectonic processes is often difficult. Nevertheless, Sims (1975) has suggested the criteria for correlating these structures with seismic events :

i. the deformational features occur in seismically active region,

ii. these are restricted to single stratigraphic layers separated by undeformed beds over a large area,

iii. the beds are near horizontal so as to exclude the possibility of slope failure as a potent trigger mechanism in their formation,

iv. presence of potentially liquefiable sediments,

v. the structures are similar to those described by Sims (1973) or formed experimentally by Keunen (1958).

Geological mapping of the foothill terrain in the vicinity of Chandigarh was carried out by the author and the field investigations reveal that the rocks comprising the Subathu Formation, the Lower Siwalik/Nahan Formation, and the Upper Siwalik sediments comprising the Tatrot, the Pinjore and the Boulder Conglomerate formations are exposed in the region (Fig. 1).

The Himalayan foothill terrain is tectonically active on account of the constant northward drift of the Indian plate. The Main Boundary Thrust, the Himalayan Frontal Thrust and the Piedmont fault are the weak zones in the crust which are prone to failure on account of compression and thrusting/faulting of the weakly consolidated to unconsolidated sedimentary strata which characterizes this zone. The Himalayan Frontal Thrust is a zone of brittle deformation between the alluvial plains and the steep slopes of the Siwalik sediments.

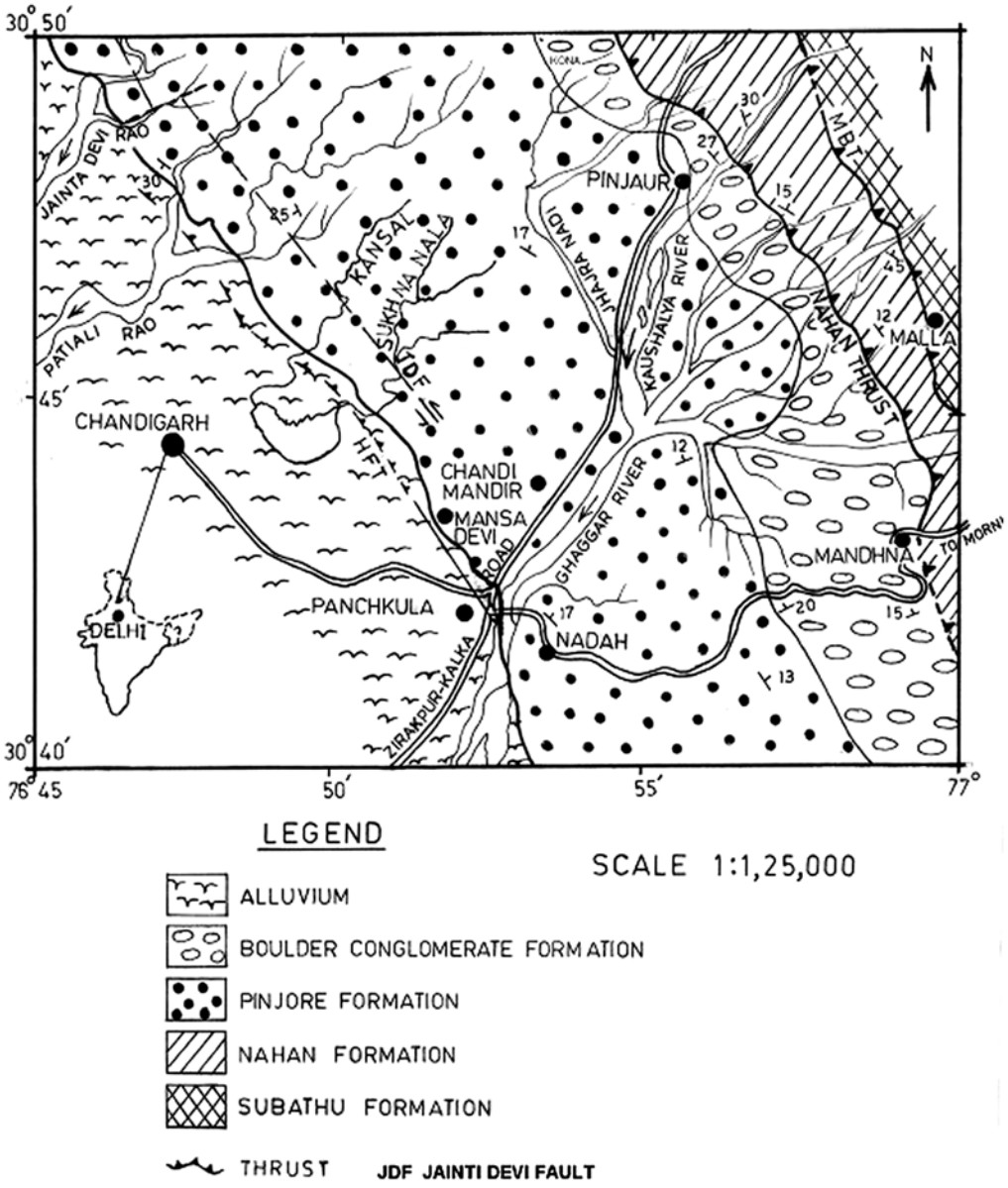

Fig. 1. Schematic geological map of the Himalayan foothill region East of Chandigarh showing the location of streams where soft sediment deformational features are located.

DEFORMATIONAL STRUCTURES

In the Himalayan foothill region in the vicinity of Chandigarh a variety of soft sediment deformational features have been examined in the Quaternary deposits exposed along the rivers and rivulets draining the region. The major streams around Chandigarh are the Jainti Devi Ki Rao, the Patiali Rao, the Kansal stream and the Sukhna stream (Fig. 1). Ghaggar is the major seasonal river draining the region and skirts the eastern boundary of Panchkula. The deformational structures occur throughout the sedimentary foothill terrain but are most common in the Ghaggar River Section, Patiali Rao Section and the Jainti Devi Ki Rao Section.

In the Ghaggar River Section, a reddish-brown laminated clayey silt bed with intercalated fine grained sand overlies a 80 cm thick flat bedded sand layer. The clayey silt-fine sand intercalated bed, which is at an elevation of about 1.5 m from the river bed, shows the development of kink folding (Fig. 2a). The kink folded linear zone in the bed is underlain by weakly folded sand laminae on the lower surface suggesting thereby that due to seismic shaking there was movement of water within the bed and the point of accumulation of water registered the maximum displacement due to low viscosity in that particular zone. The deformation is restricted to a 45 cm thick zone. The bed is overlain by a 1.2 m thick flat bedded un-deformed fine sand layer. The

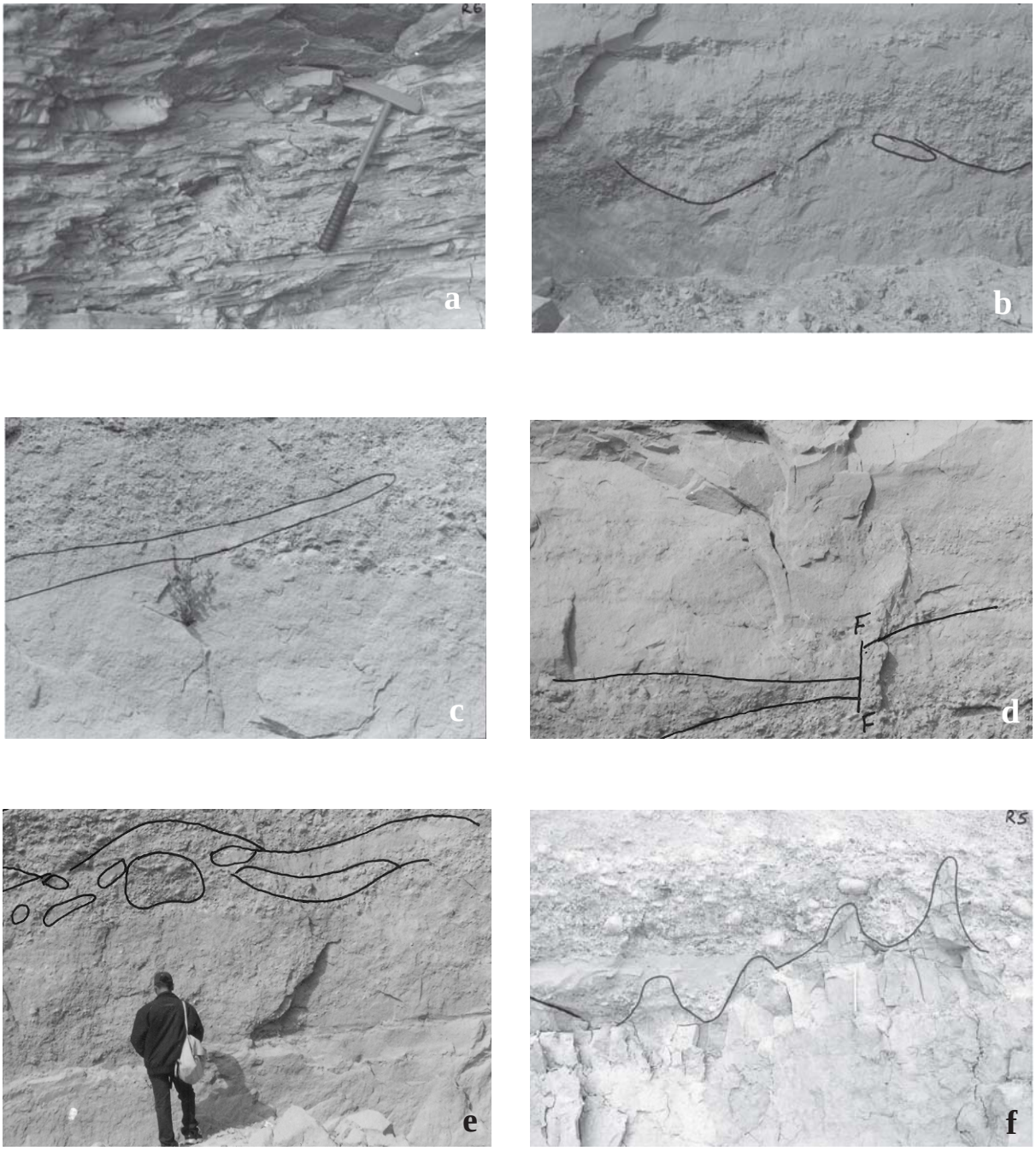

Fig. 2 a. Kink folding in clay rich silt bed exposed in Ghaggar river valley, **b.** Synclinal structures in fine grained sand exposed along Patiali Rao, stream, **c.** Low amplitude synclinal and anticlinal structures in fine grained sand exposed along Patiali Rao stream, **d.** Faulting in clay rich silt bed exposed along Patiali Rao stream, **e.** Pear drop (pillow) structure in fine to medium grained sand exposed along Patiali Rao stream, **f.** Flame structures in clay rich silt bed exposed along Jainti Devi ki Rao stream.

kink folding formed as a combined result of liquefaction and lateral shear stress generated due to the passage of seismic waves.

In the Patiali Rao Section, the deformation zone occurs 1.5 m above the stream bed and is confined to a 3.2 m thick grey coloured sandstone-silty clay intercalated unit. The light grey coloured sandstone bed measuring about 1.3 m in thickness shows development of synclinal structures. The synclines are very broad and disconnected with adjacent synclines at their top (Fig. 2 b). Individual synclinal structures are asymmetrical in character and extend for 3.5 m. A few meters ahead of this structure, the strata in the same layer are folded into low amplitude synclines and anticlines (Fig. 2 c). This structure has formed as a result of deposition of poorly laminated fine grained sand silt layer over a medium to coarse sand layer. Due to seismic shaking, liquefaction would have occurred resulting in a density gradient which caused the injection of a viscous mushroom shaped sediment plume of coarse material into the overlying fine sand silt layer. At places the plume truncated the fine lamination in the fine silt layer thus giving the appearance of truncated anticlines. Local sagging of the less viscous sediment resulted in the formation of synclinal structures. The pale grey sandstones exhibit the presence of 3 m long sandstone dykes. The dykes are composed of light brown fine to medium grained sandy material. The underlying bed from which these dykes generated are also visible. These dykes, which are about 20 cm to 30 cm in width, exhibit linear boundaries and make an angle of 25° to 30° with the horizontal. The dykes have been formed due to injection of liquefied fine grained sand into a sand silt layer. The ground shaking during the seismic episode resulted in widespread liquefaction which altered the density gradient and resulted in the rapid movement of water saturated non-cohesive material into the overlying dense silty sediment layer. The overlying 50 cm thick bed of clayey silt exhibits small scale faulting in localized area showing a displacement of about 25 cm (Fig. 2 d). This effect is confined to the lower bedding plane of the bed whereas the upper bedding plane is horizontal and does not show any effect of faulting. The faulting appears to be due to relatively more plastic nature of the lower layer of medium grained sand and the non-plastic nature of the faulted clay rich silt bed. This type of faulting within a bed reflects the characteristic response to seismic shaking of water under-saturated sediments. Further ahead, the pale grey sandstone bed exhibits the development of pear drop (pillow) structures. The elliptically rounded chunks of the sandstone bed measure 7 cm to 13 cm in diameter. These chunks have broken off their original bedding and have sunk into the underlying fine grained clay rich silt bed consequent to seismic shaking (Fig. 2 e). The pear drop structures are similar to those developed experimentally by Kuenen (1958). All these structures are quite widespread and are restricted to nearly horizontal beds with undeformed lower and upper units.

In the Jainti Devi ki Rao Section flame structures are very well developed. The structure consists of hydroplastic intrusion of the underlying sandy silt layer into the overlying coarse sand layer. The tongues of the intruded sandy silt layer have rounded to sharp upside down V shapes. The vertical thickness of the intruded flame like tongues of sandy silt layer varies from 7 cm to 24 cm (Fig. 2 f). The flame structure has been produced by seismically generated shear stress and reverse density gradation due to differential porosities of newly deposited poorly sorted medium to coarse sand layers and well sorted clay rich silt layers.

DISCUSSION AND CONCLUSIONS

The deformational structures (seismites) described in the Ghaggar River Section, the Patiali Rao Section and the Jainti Devi Ki Rao Section broadly confirm to the requisites proposed by Sims (1975) as these occur in seismically active Himalayan terrain, the beds containing these structures are overlain and underlain by un-deformed beds, the structures are similar to those described by earlier workers and produced experimentally and are quite widespread in the region. These structures have developed in nearly horizontal Quaternary sediments and are observed in loosely packed, friable, less cohesive sands and clayey silt beds. Such sediments are susceptible to failure upon episodic seismic shaking due to liquefaction. During earthquakes loose water saturated sands tend to decrease in volume, which produces an increase in their pore water pressures and consequently a decrease in shear strength, i.e. a reduction in effective stress. Sedimentary units that are likely to liquefy include well sorted Holocene sands and silts saturated with water. Such deposits are often found along riverbeds, beaches, dunes, and areas where windblown silt (loess) and sand have accumulated. The resistance of the cohesionless soil to liquefaction largely depends on the density of the soil; confining stresses; soil structure viz. its fabric, age and amount of cementation; the magnitude and duration of the earthquake loading; and the extent to which shear stress reversal occurs.

Since majority of the liquefaction processes are supposed to take place either at or close to the surface in sediment layers where overburden is negligible, the liquefaction in the foothill terrain is assumed to have taken place at shallow depths. The earthquakes that occurred in Niigata, Japan, Alaska, Loma Prieta and Kutch also recorded failure and liquefaction at depths less than 27 meters.

Kuribayashi and Tatsuoka (1975) and Youd (1977) suggested that a relationship exists between the Richter scale earthquake magnitude and the zone of influence from the epicentre in which liquefaction can occur.

Besides the magnitude of earthquakes, the duration of seismic shock is a significant parameter as repeated oscillations and sustained earthquake induced ground shaking causes liquefaction of otherwise stable sediments.

The frontal Siwalik sediments are tectonically active (Chaudhri, 2002, 2005; Delcaillau et al. 2006). During the past century, the City and its surrounding regions have experienced severe to moderate ground shaking during the 1905 Kangra (8), 1975 Kinnaur (6.2), 2001 Uttarkashi (6.6) , 2001 Bhuj (7.7) and 2005 Kashmir (7.6) earthquakes.

Thus, the soft sediment deformational features observed in the Himalayan foothill terrain in the vicinity of Chandigarh, are most likely to be seismogenic in nature. Further, the widespread presence of seismites in the foothill terrain points towards the vulnerable position of the densely populated City and its surrounding regions in the event of a large magnitude earthquake affecting the region. The subsurface lithology of the city comprises boulders, pebbles, gravel, sand, silt, clays and some kankar beds. The unconsolidated sand, silt and clay layers dominate at shallower depths which increases the risk of seismic wave amplification in the city and its neighbouring regions. The shallow depth of water table in southern sectors of the city and neighbouring regions accentuates the risk of liquefaction in the region. In view of the seismic hazard faced by the populated Himalayan foothills, proper incorporation of seismic design building codes in fresh constructions and retrofitting of old structures is imperative.

Acknowledgement: The financial grant received from Seismology Division, Department of Science and Technology, Govt. of India and Ministry of Earth Sciences, Govt. of India in the form of Research Projects is thankfully acknowledged. Discussions with Prof. Dr. R.S. Chaudhri, Ex. Director and Chairman, CAS in Geology, Panjab University, Chandigarh were fruitful. Dr. Mahavir Singh, ex-Project Assistant, assisted in field investigations. Work was carried out at Department of Geology, Kurukshetra University.

The author is grateful to the two anonymous referees for making positive suggestions which have improved the quality of this paper.

References

Blatt, H, Murray, G. and Middleton, R. (1980). Origin of Sedimentary Rocks. Prentice Hall, Englewood Cliffs, N.J., 782 p.

Chaudhri, A.R. (2002). Earthquakes – A potential natural hazard. In L.N. Gupta and G.S.Gill (eds.) Natural Hazards and their Mitigation, 61-70. Special Volume, Bulletin Indian Geologists Association, 35(2).

Chaudhri, A.R. (2005). Shutter ridges and sag ponds along the Chandigarh Fault, northwestern Himalaya. Department of Science & Technology, Sesimology Update, 1(4), 6.

Chaudhri, A R (2007a). Neotectonic activities in the Himalayan foothill region – A case study. In: O.P. Varma, A.K. Mahajan and Vikram Gupta (eds.), Natural Hazards, 73-83. Indian Geological Congress, Roorkee.

Chaudhri, A R (2007b). Seismo-tectonic characterization of the Himalayan foothill region – A case study. In: P.S. Saklani (ed.) Himalaya (Geological Aspects) 5, 41-50. Satish Serial Publishing House, New Delhi.

Delcaillau, B, Carroza, J.M. and Laville, E. (2006). Recent fold growth and drainage development: The Janauri and Chandigarh anticlines in the Siwalik foothills, northwest India, Geomorphology, 76(3-4), 241-256.

Keunen, P.H. (1958). Experiments in Geology. Geol. Soc. Glasgow, 23, 1-28.

Kuribayashi, E. and Tatsuoka, F. (1975). Brief Review of Liquefaction during Earthquakes in Japan. Soil Foundation, 15(4), 81-92.

Lowe, D.R. (1975). Water escape structures in coarse grained sediments. Sedimentology, 23, 285-308.

Mills, P.C. (1982). Genesis and diagnostic value of soft sediment deformation structures- a review. Sed. Geol., 35, 83-104.

Mohindra, R. and Thakur V.C. (1998). Historic large earthquake induced soft-sediment deformational features in the sub-Himalayan Doon valley. Geol. Mag., 135, 269-281.

Sieh, K.E. (1978). Prehistoric large earthquakes produced by slip on the San Andreas fault at Pallet Creek, California. Jour. Gephy. Res., 83(B8), 3907-3939.

Sims, J.D. (1973). Earthquake induced structures in sediments of the Van Norman Lake, San Fernando, California. Science, ½, 161-163.

Sims, J.D. (1975). Determining earthquake recurrence intervals from deformational structures in young lacustrine sediments. Tectonophysics, 29, 144-152.

Youd, T.L. (1977). Discussion of 'Brief Review of Liquefaction during Earthquakes in Japan' by E. Kuribayashi and F. Tatsuoaka. Soil Foundation, 17(1), 82-85.

Jour. Indian Association of Sedimentologists, Vol. 28, No. 1 (2009), pp. 55-71

Uranium Mineralisation Associated with Mesoproterozoic Semri Sediments of Vindhyan Supergroup along Kubari–Semariya–Marwa Fault, Sidhi district, Madhya Pradesh

M.K. Roy[1], Rahul Banerjee[1*], Mayank Agarwal[1] and P.B. Maithani[2]
Atomic Minerals Directorate for Exploration and Research
[1] AMD Complex, Central Region, Civil Lines, Nagpur–440 001
[2] 1-10-153/156, AMD Complex, Begumpet, Hyderabad–500 016
*E-mail: rahulbnrg@gmail.com

Abstract: The Mesoproterozoic Semri Group of sediments unconformably overlying Sidhi crystallines (a part of Chhotanagpur Granite Gneissic Complex; CGGC) are exposed in SW part of Sidhi in the environs of Son–Narmada North Fault (SNNF). This sector has been subjected to both pre-Vindhyan tectono-magmatic episodes resulting in emplacement of highly evolved younger felsic intrusives and post-Vindhyan deformations signifying substantial reactivation. ENE–WSW trending Kubari–Semariya–Marwa (KSM) fault (~20 km long) is an important structural feature in this sector and played significant role in mineralisation. Purple and whitish coloured brecciated and/or ferruginous shale, calc-tuffaceous rock and porcellanite (Semri Group) have recorded uranium anomalies along the KSM fault intermittently over a strike length of 2625m and analysed upto 0.088%U_3O_8 with negligible thorium (<0.005%ThO_2). Besides, borewell water samples from this zone have yielded upto 2260 radon counts/50sec (av. 296counts/50sec; n=529) forming two ENE–WSW trending anomalous clusters in eastern and western parts along the KSM fault while central part indicates NNW–SSE to NW–SE trend due to the presence of NW–SE trending cross faults. In addition, various lithounits in the vicinity of KSM fault have shown comparatively higher radioelemental abundance (sandstone: 22ppm, n=38; siltstone: 12ppm, n=28; calcareous tuffaceous shale: 9ppm, n=11; porcellanite: 29ppm, n=15; ferruginous breccia: 12ppm, n=41).

Based on geochemical data Semri sediments are mainly classified as lithic arenite, quartz arenite (arenaceous rocks) and shale and Fe-shale (argillaceous rocks) in log SiO_2/Al_2O_3) vs log(Fe_2O_3/K_2O) plot. Tectonic discrimination diagram based on SiO_2, K_2O and Na_2O relationship broadly indicates deposition of these sediments in Passive Margin (PM) setup while discriminant function analysis indicates their derivation from mafic and felsic igneous and quartzose sediment provenance, as also corroborated by the presence of Mahakoshal quartzites and metabasic rocks and CGGC granitoids in adjoining areas. Besides, chemical maturity (SiO_2 vs Al_2O_3+ K_2O+ Na_2O) diagram shows semi-arid to semi-humid depositional paleoclimate for siliciclastic and volcaniclastic sediments, which might have played vital role in retention of oxyphile elements, such as, uranium in the system.

Presence of favourable factors such as highly fertile Neoarchaean to Palaeoproterozoic basement-cum-provenance with labile uranium (40ppm, n=53), hiatus of 500-700 Ma before the deposition of thick pile of Mesoproterozoic cover sediments, episodic magmatism and basement reactivation including post-Vindhyan deformation provided channel-ways for hydrothermal activity and mobilisation of uranium finally leading to their fixation at suitable locales viz., unconformity planes and fracture zones.

Key words: Kubari-Semariya-Marwa (KSM) fault, Semri sediments, Vindhyans Supergroup, CGGC, Uranium mineralisation, Sidhi district, Madhya Pradesh.

INTRODUCTION

The Mesoproterozoic Semri Group (1.6–1.2 Ga: Anil Kumar et al., 2000, 2001; Rasmussen et al., 2002; Ray et al., 2002; Ray, 2006) of Vindhyan Supergroup deposited in an intracontinental basin developed along Son–Narmada mega rift zone in Son valley and forms an economically important domain for various mineral resources including uranium, especially in parts of Sidhi district, Madhya Pradesh. This constitutes the southern part of the largest Proterozoic basins i.e., Vindhyan basin (>1,00,000 sq km) of Central Indian shield and attracted the attention of several geoscientists since middle of the nineteenth century resulting in substantial contribution on stratigraphy, sedimentation, tectonics, geochronology and metallogeny (Auden, 1933; Soni et al., 1987; Rajurkar et al., 1990; Jain et al. 1984, 1995; Nair et al., 1995; Bose et al. 2001; Chakraborty and Bhattacharya, 1996; Ray et al., 2002; Chakraborty, 2006; Ray, 2006). Several phases of magmatism and tectonism, involving both basement and cover sediments have helped in mobilisation and remobilization of various metals leading to development of some important mineral deposits. This basin also provides a classical setup for

unconformity- related uranium mineralisation as Mesoproterozoic Semri sediments are deposited on highly fertile granitoids of Chhotanagpur Granite Gneissic Complex (CGGC; 3.7–2.9 Ga; locally known as Sidhi crystallines) and volcano-sedimentary sequence of Mahakoshal Group (2.6–1.9 Ga), and subjected to intense tectonic activity in the environs of Son–Narmada mega lineament. Based on favourable geological setup and time-bound character, exploration efforts by officers of Atomic Minerals Directorate for Exploration and Research (AMD) during last two decades have resulted in location of a number of uranium occurrences viz., Baskati, Khurmucha, Karahiya, Mankisar and Kathar in Semri sediments (Sesha Rao et al., 2004; Saxena et al., 2005; Abhinav Kumar and Banerjee, 2006; Bhattacharjee et al., 2008) and in intrusive syenite bodies associated with Sidhi crystallines at Bari and Ainthi (Saibaba et al. 1987, 1988) in parts of Sidhi district.

In the study area, thick pile of Semri sediments is resting over Sidhi crystallines while Mahakoshal metasediments are present in close vicinity. The area falls very close to the Son–Narmada North Fault (SNNF) and show signatures of pre-Vindhyan tectono-magmatic activities as well as post-Vindhyan deformations. The Semri sediments are traversed by nearly 20km long ENE–WSW trending Kubari–Semariya–Marwa (KSM) fault sympathetic to Son Narmada North Fault (SNNF; a part of Son–Narmada mega lineament), and form linear low mounds of brecciated rocks. This area is one of the important targets for uranium exploration due to its close proximity to basement with highly evolved and fertile granitoids and syenite bodies (40ppm U_3O_8, n=53). Besides, depth persistency of faults/fractures, concealed basic intrusives along unconformity contact, presence of carbonaceous matter and sulfides along faults/fractures etc., have also been indicated by geophysical surveys. Based on these positive factors, recent extensive prospecting work has resulted in discovery of radioactivity occurrence over a strike length of 2625m in purple and whitish coloured brecciated and/or ferruginous shale, tuffaceous rock and porcellanite along KSM fault. The present paper deals with the uranium mineralisation, its geochemical aspects and exploration efforts in the Kubari–Semariya–Marwa sector.

GEOLOGICAL SETTING

Regional Geology

In the Son valley region, arenaceous–argillaceous–calcareous sedimentary assemblages belonging to Semri Group are deposited in Vindhyan basin, which has developed along ENE–WSW to E–W trending Son–Narmada–Tapti lineament zone over a tonalite–trondjhemite basement (CGGC) representing ancient sialic crust, and lies to the north of the Central India Suture (CIS), a major ductile shear zone (Jain et al., 1995). The evolution of CGGC resulted in development of magmatic suites represented by migmatites, rhyodacite, alkaline intrusives and highly feldspathic gneisses. Fundamental faults tapping the mantle developed on pre-existing sialic crust have formed rift basin in which initially the sedimentation of Mahakoshal Group took place (Nair et al., 1995). The end of sedimentation witnessed post tectonic intrusion of granitic plutons (2.0-1.8 Ga) and alkaline suits of rocks (1.8 to 1.6 Ga). After a prominent hiatus, second spell of sedimentation in the form of Semris started around 1.4 Ga over a rugged basement of CGGC/ Mahakoshal. Subsequent to deposition of basal Vindhyan sequence, tectonic and magmatic activities became operative resulting in reactivation of basin margin faults and other tectonic elements (Chakraborty et al., 1996). Finally, these were overlain by Gondwana sediments and Deccan Trap. The generalized lithostratigraphic succession of Son valley area (after Rao and Neelkanthan, 1978; GSI, 2002) is given in Table 1.

Local Geology

The study area exposes Sidhi crystallines as an inlier between volcano-sedimentary sequence of Mahakoshal Group to the south and sedimentary sequence of Semri Group to the north (Fig 1 and 2). The Sidhi Crystallines comprise gneisses, migmatites and schists together with

Table 1. Generalised lithostratigraphic succession of Son Valley area.

Supergroup/Group		Formation/Lithology	Age
DECCAN TRAP		Vesicular Basalt	Cretaceous
GONDWANA		Sandstone, Shale, Clay, Coal Seam	Lr. Cretaceous – Up. Carboniferous
~~ Unconformity ~~~~~~~~~~~~~~			
VINDHYAN SUPERGROUP	BHANDER	Upper Bhander Sandstone Sirbu Shale Lower Bhander Sandstone Bhander Limestone Ganurgarh Shale	Neoproterozoic
	REWA	Upper Rewa Sandstone Jhiri Shale Lower Rewa Sandstone	Neoproterozoic
	KAIMUR	Sandstone and Shale	Mesoproterozoic
	~~ Unconformity ~~~~~~~~~~~~~~		
	SEMRI	Rohtas Limestone Rampur Shale Chorhat Sandstone Koldaha Shale Deonar Porcellanite Kajrahat Limestone Kanwari Shale Deoland Sandstone	Mesoproterozoic
~~ Unconformity ~~~~~~~~~~~~~~			
MAHAKOSHAL		Intrusive Granite, Quartz veins, Ultrabasic dyke, BHQ and BHJ, Metabasics, Phyllite, Quartzite and Tuffs	Palaeoproterozoic
~~ Unconformity ~~~~~~~~~~~~~~			
BASEMENT (CGGC)		Granite Gneisses and schists	Archaean

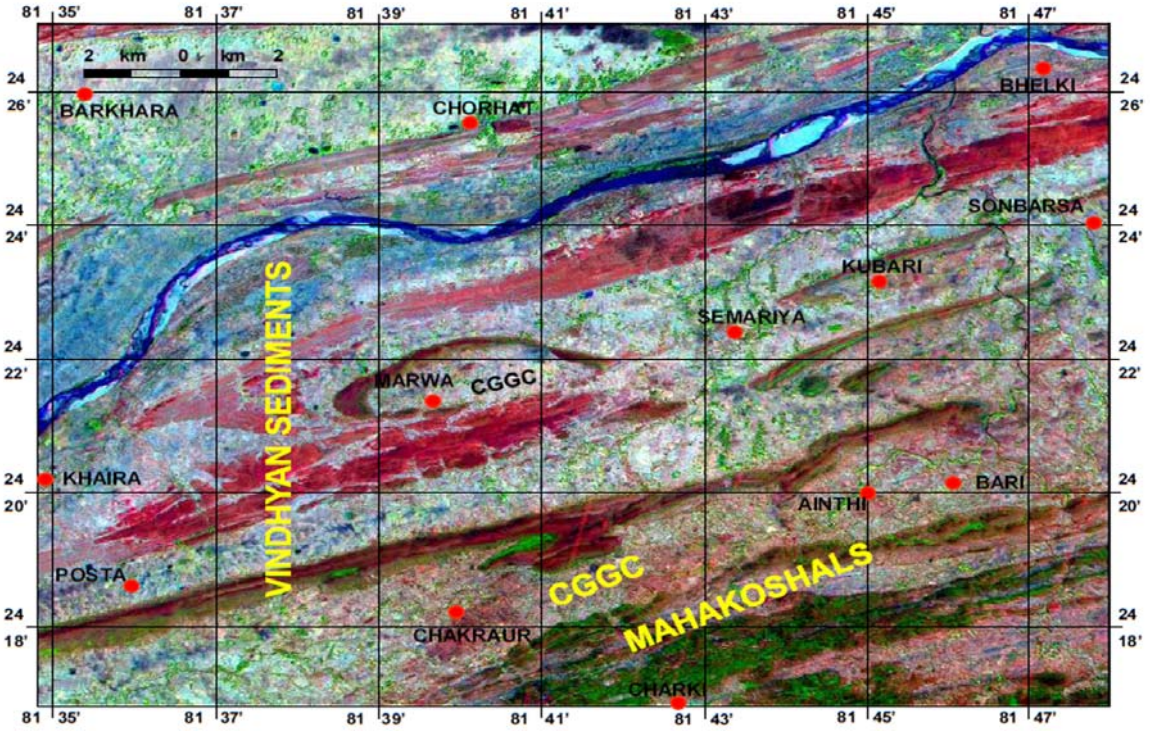

Fig.1. PAN sharpend LISS III image of Kubri-Semariya-Marwa-Posta Sector, District Sidhi,MP. Showing different lithounits (indicated by colour variation) and structural elements.

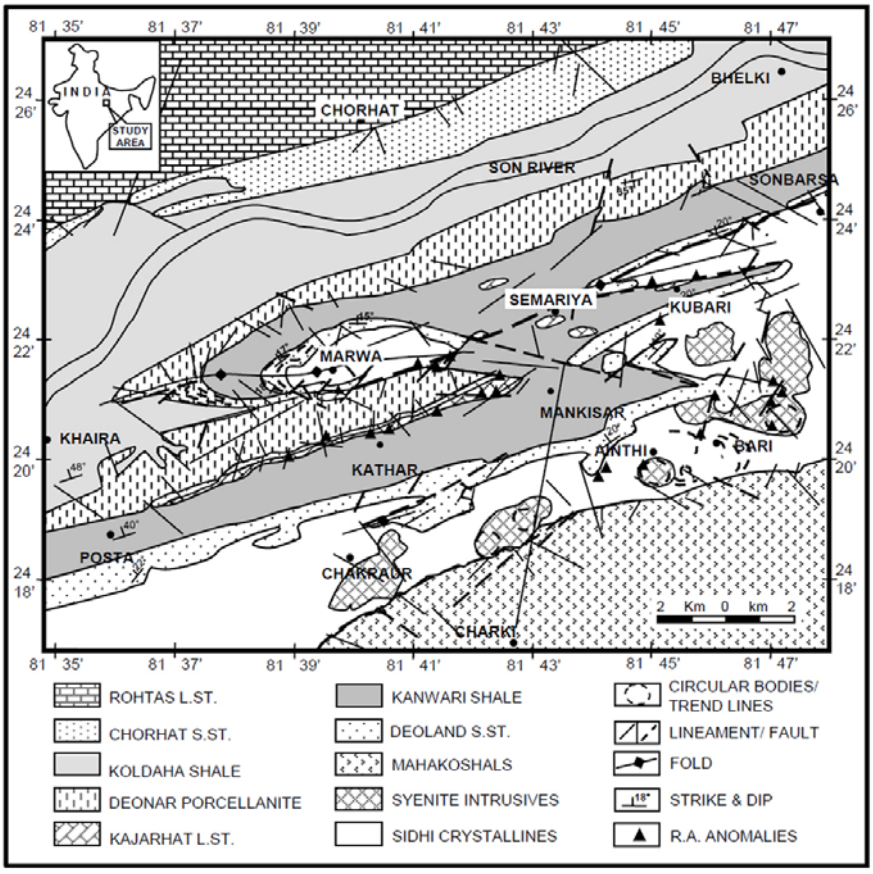

Fig. 2. Lithostructural map of Kubari-Semariya-Marwa-Posta sector, Sidhi district, M.P. showing radioactivity anomalies.

younger intrusives granitoids and syenites. The ENE–WSW trending Mahakoshal Group comprises quartzite, dolomite, phyllite and BHQ/BHJ and has faulted contact with Sidhi crystallines. Besides, mylonitized and hybrid rocks as well as ferruginous breccia have been observed at several places either confined to basement fractures or at the contact of basement rock with Semri sediments.

The Semri sediments (Lower Vindhyan) cover major part of the study area and generally follow ENE–WSW trending major structural grain sympathetic to Son–Narmada lineament. Linear sandstone ridge marks the southern contact with Sidhi crystalline while in the east faulted contact is delineated between crystallines and sandstone/shale. Brief Lithological details of various sedimentary formations exposed in the study area are given below:

Deoland Formation

It forms lowermost part of Semri Group and mainly comprises hard, compact, massive quartz arenite, pebbly arenite and conglomerate (quartz and jasper pebbles dominated) forming ENE–WSW trending linear ridge (Khenjua Hill range). The beds show vertical to sub-vertical dips along the contact zone with Sidhi crystallines while they have gentle northerly dips elsewhere. It rests unconformably over the basement rocks with localized faulted contact.

Kanwari/Arangi Formation

It consists of grey to buff coloured shale with intercalated greenish coloured micaceous siltstone, and exposed to the north of main Khenjua hill occupying broad valley around Kubari, Semariya and south of Marwa. This unit rests conformably over Deoland arenites and exhibit ENE–WSW trend with gentle to moderate northerly dips.

Kajrahat/Kuteshwar Formation

These are prominently exposed around Kubari, Semariya, Karondiya and Kathar areas and represented by 20–50 m wide lensoidal bodies of hard, Compact and massive grey coloured limestone and friable limonitic limestone/calcareous shale. The beds show ENE–WSW strike and moderate northerly dips.

Porcellanite Formation

These are exposed as small hillocks/mounds in the area and exhibit conformable relationship with limestone and shale units. At places it directly rests over Kanwari/Arangi shale. This formation consists of greyish coloured hard, compact and massive porcellanite, which at places show colour bands/laminations. Besides, thin bands of younger arenite, silver-grey coloured calcareous–tuffaceous shale and black coloured carbonaceous shale also occur as intercalations within porcellanites. The general trend of this formation is ENE–WSW to E–W while they exhibit variable dips due to highly folded nature.

Structure

The study area shows signature of significant tectonic activity in the form of substantial structural disturbances affecting almost all the lithounits. In fact, the study area forms a part of the SNNF zone and subjected to number of reactivation phases in the past, which are reflected in the form of younger intrusives, circular to semi-circular bodies, atleast two generation of folding and faulting etc. A detailed lithostructural map has been prepared based on satellite digital data interpretation (PAN sharpened LISS-III image of satellite data products IRS–1D, P101 R054) and ground validation (Fig. 1 and 2). Important structural features are given below –

Folds

Semri sediments (sandstone, shale and porcellanite units) exhibit significant folding as represented by the major anticlinal axis following nearly E–W trend. These units have undergone refolding which is reflected by N–S fold axis. These features are very well seen in the area along KSM fault zone. Trend lines around axial zone are also marked in sandstone and porcellanite units near Marwa. Fold limbs are dissected by faults at several places and dislocations are clearly visible. This has resulted in formation of small inliers of sandstone surrounded by younger shale unit.

Faults

The study area exhibit presence of number of major and minor faults. It is also apparent that some of these are marking the litho-contacts. Two major faults, i.e., crystalline–Mahakoshal contact fault in the south and 20 km long KSM fault within the Semris, are delineated. These have general ENE–WSW trend with slight swing in NE–SW direction towards east. The KSM fault is affected by a number of NE–SW, WNW–ESE and NW–SE trending minor faults which have dissected various lithounits of Semri Group. This feature is clearly visible in the form of apparent displacements along the fold limbs of sandstone and porcellanite units. Some of these post-depositional faults are also delineated upto Sidhi crystallines. Besides, a few faults are restricted within Sidhi crystallines and appears to be basement faults. Such faults present near Bari and between Marwa and Chakraur are very significant considering presence of circular/semicircular syenitic bodies emplaced in Sidhi crystallines in close proximity. These syenitic bodies show elevated radioelemental content suggesting that the faults might have provided the channelways for

movement of radioelements through hydrothermal solution. In addition, a number of minor faults, trending in NNE–SSW, NW–SE, NNW–SSE and E–W directions, are also delineated in Semri sediments.

Three sets of faults could be identified on the basis of mutual displacement. ENE–WSW major fault is the oldest in the area, which is traversed by younger NE–SW, NW–SE and WNW–ESE faults. The youngest set of fault is trending in nearly NNE–SSW direction and affecting both ENE–WSW and WNW–ESE older faults. This set of faults is delineated west and south of Semariya and seen traversing through Semri sediments and Sidhi crystallines.

Lineaments

A number of lineaments/linears are also delineated in the area, which are either represented by fracture/ joints and drainage trends vis-à-vis at places by litho-contacts. Apart from lineaments sympathetic to major structural grain, some other lineaments/linears trending in NNE–SSW, NNW–SSE, N–S and NW–SE directions are seen affecting almost all the lithounits of study area.

RADIOACTIVITY

Surface uranium anomalies have been recorded in purple and whitish brecciated and/or ferruginous shale (Kanwari Shale), calc-tuffaceous rock (Kajarhat Limestone) and porcellanite (Deonar Porcellanite) along the ENE–WSW trending KSM fault intermittently over a length of 750m near Kubari village (Fig. 1). Radiometric assay results of samples have indicated values upto 0.088%U_3O_8 (n=11) with negligible thorium (<0.005%ThO_2) (Table 2). Major part of its extension area is soil covered and hence a total of thirteen trenches (T1-T13) and one Pit (P1) has been excavated along KSM fault zone, which has established continuity of mineralisation over a strike length of 2625m. A total of 400 channel samples have been collected at a regular interval of 30cm from trench base (approx. 1.5m deep) and walls over a cumulative excavated length of 116.70m of these trenches. Most of the trenches, except T6, T7 and T13, have recorded anomalous abundance of uranium. The thickness of the mineralised band varies from 30 cm to 2.10m in different trenches and shielded probe logging of these trenches yielded upto 0.011%eU_3O_8.

Extensive systematic sampling was carried out in grid pattern (500m x 200m) along 500m spaced N–S sampling lines (W1–W38) starting from basement to main porcellanite hill and 774 samples were generated to identify the radioelemental distribution pattern. Radiometric assay data of samples indicates that the Semri sediments in the vicinity of the KSM fault are having anomalous abundance of uranium (sandstone:

Table.2. Radioelement data of KSM fault and adjoining areas.

Lithounit	n	Uranium (ppm)		Thorium (ppm)		Th/U	
		Range	Av.	Range	Av.	Range	Av.
General abundance (Non- mineralised)							
Arenite	74	0.5 – 5	1.58	1 – 13	6.44	0.5 – 10	4.58
Shale	93	0.5 – 5	1.91	2 – 17	10.20	3 – 10	7.10
Limestone	12	0.5 - 3	2.00	1 – 12	3.41	0.5 – 10	2.86
Calc Tuff. Shale	11	1 – 35	8.54	2 – 11	6.27	0.11 – 4	1.31
Ferrug. Breccia	20	0.5 – 19	10.65	1 – 25	9.70	0.5 – 4	2.16
Syenite	40	0.5 – 29	4.01	1 – 66	12.92	0.5 – 14	4.43
Granite	32	0.5 – 12	2.04	1 – 49	13.68	1 – 18	12.31
Abundance along KSM Fault (Mineralised/adjacent zones)							
Calc Tuff. Shale	12	**140 – 900**	**185**	<50			
Ferrug. Breccia	22	**150 – 880**	**230**	<50			
Arenite	38	2.75–107	21.70	2.75–116	38.36	0.5 – 32	6.70
Siltstone	28	2.75 – 63	12.21	2.75–108	39.69	0.15–39.3	8.78
Shale	9	2.75 – 5	3	2.75 – 64	20.89	1 – 23.7	7.29
Porcellanite	15	1 – 103	29	2 – 115	30	0.03–38.5	4.52

22ppm, n=38; siltstone: 12ppm, n=28; shale: 3ppm, n=9; calcareous tuffaceous shale: 9ppm, n=11; limestone: 5ppm, n=4; porcellanite: 29ppm, n=15; ferruginous breccia: 12ppm, n=41). This not only signifies derivation of the sediments from a fertile provenance but also mobilisation of uranium available in the system in response to various structural disturbances and hydrothermal activities. Finally, this leads to concentration and fixation along suitable structural aureoles under reducing environments as evidenced by mineralised bands along KSM fault zone.

Similarly, a total of 529 water samples (406 borewell and 123 dugwell samples) were generated and subjected to water radon measurement to assess the possibility of concealed radioactive zone beneath soil covered area along KSM fault zone. These water samples have yielded 12 to 2260 radon counts/50sec (Mean: 296counts/50sec; SD: 291counts/50 sec.) with 23 values above threshold (878 counts/50 sec.). Water radon contours show three major concentric nuclei viz., ENE–WSW trending anomalous clusters in eastern and western parts parallel to the KSM fault while another cluster in central part indicates NNW–SSE to NW–SE trend probably due to the influence of NW–SE trending cross fault (Fig. 3). It is also apparent from the study that most of the higher water radon values (>500 counts) are concentrated in porcellanite/tuffaceous shale country in Semariya–Marwa sector, possibly indicating presence of sub-surface mineralisation, especially in the intersection zone of KSM fault and NW–SE fault. The water radon anomalies are also in conformity with the hydrouranium anomalies (1.9 to 156 ppb U) reported by Murugan and Choudhury (1992) based on 233 water sample data generated over 530 sq. km area in the vicinity of KSM fault. They have identified two anomalous halos in Kathar–Karondiya (8 x 1km) and Semariya–Kubari (3 x 1km) sectors.

GEOCHEMISTRY AND PETROGENESIS

Four hundred eighteen samples of Semri sediments and basement rocks were analysed for major and trace elements using Philips X'unique II–WDXRFS (Wavelength Dispersive X-Ray Fluorescence Spectroscopy) controlled by computer with X-40 and Super Q software. The GFPC and SD detector based instrument consists of LiF220, 200, Ge, PET, TLAP, PX-1 and PX-4 crystal assembly and uses Rh target as a source of primary radiation. The details of sample preparation for analysis by WDXRF are dealt in detail elsewhere (Vishwanathan, 1989). Overall precision and accuracy, as determined by replicate analyses, are estimated 2–5% (RSD) for major elements with >0.5% concentrations whereas 5% (RSD) for trace elements with >50 ppm and 10% (RSD) for <50 ppm concentrations. Some selected samples were repeated using wet chemical methods of silicate analysis by Shapiro and Brannock (1962), Hounslow and Moore (1966) and others for major element determination with the help of titration, flame photometer and FAAS (Varian AA-20, Australia). Uranium was also determined in these samples using fluorometric procedure after its selective separation from the matrix. Chemical uranium data was used to compare the physical assay data.

Geochemical data (major element: n=274; and trace element: n=418) of systematic grid samples of Semri sediments and provenance area have been utilized for different characterisation and their implication on

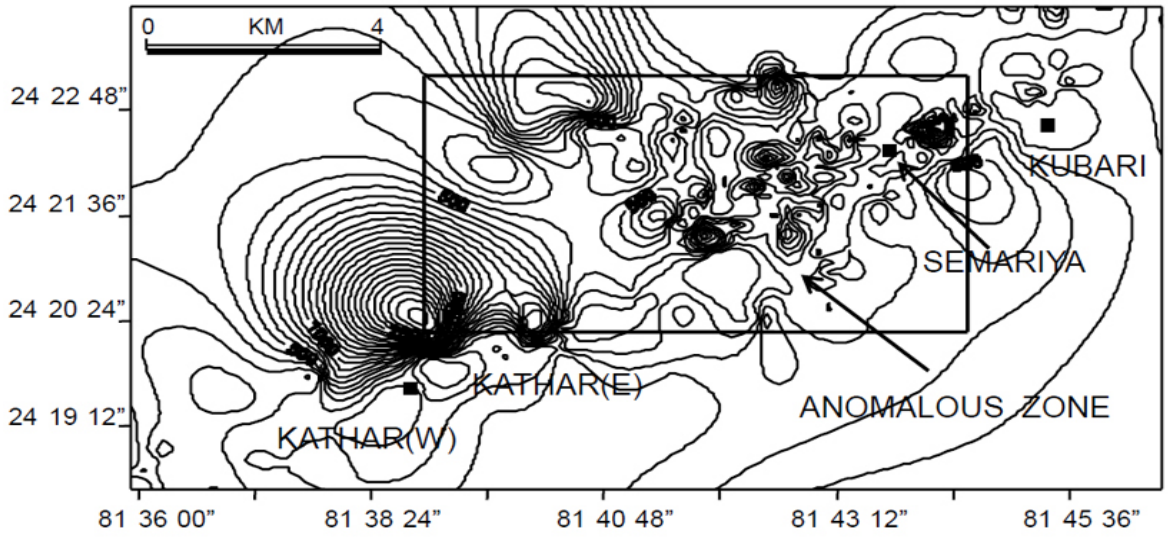

Fig.3. Chemical composition of arenaceous and argillaceous sediments of KSM fault zone and their classification as per sand class scheme.

Table. 3. Major oxide and Trace Element data of various lithounits of Kubri–Semariya–Marwa Sector.

Major oxide values in wt%

Sm. No.	W1/7	W1/8	W1/9	W1/10	W1/14B	W1/15	W1/16	W1/17	W1/18	W1/19	W1/20	W1/21	W2/23	W2/24	W2/25	W
	ARENITES (DEOLAND FORMATION)															
SiO_2	88.67	91.62	95.25	78.33	92.33	88.29	62.28	92.81	96.17	95.50	95.20	94.36	96.68	64.20	65.67	
TiO_2	0.09	0.22	0.18	2.58	0.12	0.25	0.82	0.10	0.07	0.07	0.04	0.08	0.16	0.72	0.28	
Al_2O_3	4.12	5.56	0.08	4.52	3.60	0.49	16.39	3.74	0.12	1.90	0.60	1.45	0.11	17.38	5.54	
FeO_t	4.49	1.20	3.23	12.32	2.01	7.50	10.75	2.36	0.95	0.60	1.05	1.82	1.57	5.89	3.34	
MgO	0.32	0.10	0.07	0.57	0.19	0.21	4.36	0.12	0.07	0.10	0.10	0.28	0.18	2.34	1.32	
MnO	0.02	0.01	0.01	0.01	0.01	0.01	0.02	0.01	0.01	0.01	0.01	0.01	0.01	0.02	0.04	
CaO	0.11	0.05	0.05	0.20	0.16	0.06	1.14	0.07	0.07	0.08	0.51	0.06	0.09	1.30	9.55	
Na_2O	0.25	0.08	0.06	0.01	0.18	0.17	1.00	0.19	0.03	0.07	0.26	0.30	0.01	1.71	0.13	
K_2O	0.05	0.01	0.01	0.98	0.13	1.37	1.26	0.01	0.01	0.01	0.94	0.75	0.41	3.54	1.89	
P_2O_5	0.04	0.01	0.01	0.11	0.01	0.01	0.08	0.01	0.03	0.08	0.31	0.01	0.01	0.42	0.56	
Total	98.16	98.85	98.95	99.63	98.74	98.36	98.10	99.41	97.52	98.42	99.02	99.12	99.22	97.52	88.32	
	Trace Elements (in ppm)															
V	17	11	35	18	47	23	56	12	23	3	9	7	21	98	30	
Cr	169	89	149	465	159	168	124	127	78	53	181	158	159	214	125	
Co	3	54	3	19	3	6	18	3	39	29	3	3	10	2.75	2.75	
Ni	123	74	99	69	93	107	95	89	49	46	116	145	104	60	103	
Cu	70	30	16	9	40	20	41	23	29	22	28	24	25	27	26	
Zn	8	3	3	17	3	3	44	3	3	5	3	3	3	37	203	
Ga	3	3	3	3	3	3	9	3	3	3	3	3	3	11	6	
As	14	12	10	11	12	12	11	11	11	12	13	12	11	13	11	
Rb	22	38	38	39	45	34	49	3	20	34	39	23	57	82	89	
Sr	9	33	19	14	41	21	79	3	41	61	49	20	30	80	22	
Y	16	3	3	32	3	24	20	33	3	3	3	3	<	12	2.75	
Zr	84	119	163	996	127	130	174	67	63	62	48	77	194	223	90	
Nb	33	6	3	16	3	3	11	3	3	3	3	3	3	6	2.75	
Ba	101	127	3	87	120	503	253	141	60	103	60	3	3	476	282	
Ce	3	3	3	3	3	3	3	3	3	3	3	3	3	2.75	2.75	
Pb	16	29	22	38	36	34	28	35	31	40	19	35	33	29	46	
Th	3	12	38	61	39	20	88	3	24	101	74	4	86	25	2.75	
U	8	3	3	3	58	3	3	3	84	65	18	60	3	10	2.75	

Table 3 Contd...

Major oxide values in wt%

Table 3 Contd...

Major oxide values in wt%

Sm. No.	W11/28	W11/29	W11/30	W11/31	W11/32	W11/33	W12/4	W12/5	W12/6	W12/10	W12/11	W12/12 A	W12/12 B	W13/1	W14/2	W
	SILTSTONE (KANWARI FORMATION)															
SiO_2	61.39	48.89	60.37	62.09	62.07	69.83	62.70	63.73	70.04	70.15	60.42	61.34	60.17	77.96	68.57	7
TiO_2	0.97	0.43	1.05	0.82	1.08	0.86	0.98	0.88	0.81	1.28	1.00	0.89	0.94	0.72	0.76	0
Al_2O_3	18.64	13.36	18.70	19.52	18.60	12.43	18.14	14.54	14.52	11.27	20.09	16.63	18.08	9.98	13.82	1
FeO_t	8.77	6.71	10.85	6.82	8.81	8.17	8.45	11.86	6.67	9.09	7.24	10.52	10.87	2.76	9.56	3
MgO	3.12	3.77	2.74	2.70	2.80	2.78	2.35	3.74	1.91	1.75	3.37	3.77	3.76	0.87	2.47	1
MnO	0.06	0.23	0.03	0.18	0.03	0.10	0.03	0.02	0.01	0.09	0.03	0.01	0.02	0.03	0.02	0
CaO	0.65	11.55	0.74	0.62	0.53	0.72	0.43	0.80	0.62	0.74	0.66	1.21	0.83	0.98	0.82	0
Na_2O	1.04	0.38	0.79	0.04	1.07	1.85	1.14	0.84	0.01	2.72	0.95	1.30	1.22	2.20	1.72	3
K_2O	4.29	3.66	3.65	5.86	3.47	1.25	4.22	2.34	3.91	1.16	4.60	1.73	3.24	2.22	1.06	0
P_2O_5	0.06	0.34	0.05	0.05	0.05	0.07	0.06	0.08	0.31	0.18	0.06	0.14	0.11	0.55	0.07	0
Total	98.99	89.32	98.97	98.70	98.51	98.06	98.50	98.83	98.81	98.43	98.42	97.54	99.24	98.27	98.87	9
	Trace Elements (in ppm)															
V	78	28	127	62	86	59	73	82	61	52	61	59	60	28	30	
Cr	267	66	193	166	233	182	187	181	155	176	163	294	243	119	112	1
Co	21	11	28	13	22	16	12	34	17	23	25	17	30	8	19	
Ni	100	51	80	60	87	78	99	107	81	66	66	128	109	429	83	
Cu	20	23	34	22	33	40	72	27	12	95	94	103	16	60	58	
Zn	97	68	128	60	85	90	79	104	40	95	191	116	99	23	81	
Ga	17	15	17	25	17	13	15	10	8	5	15	14	8	3	6	
As	14	10	12	0.5	13	12	13	1	11	1	11	11	12	12	1	
Rb	176	101	121	194	135	36	155	58	69	32	153	43	106	56	59	
Sr	71	26	69	37	87	104	85	75	23	94	43	89	56	61	38	
Y	18	14	42	19	6	25	19	3	14	18	19	37	17	27	19	
Zr	141	95	218	137	198	254	146	123	188	227	145	107	98	243	165	1
Nb	15	2.75	2.75	5	11	10	3	3	20	3	5	3	8	3	3	
Ba	342	482	315	382	242	206	249	187	294	270	316	280	192	251	160	
Ce	2.75	2.75	2.75	2.75	2.75	2.75	3	3	3	3	3	3	3	3	3	
Pb	29	34	20	21	27	28	26	23	38	42	32	32	30	32	19	
Th	33	6	2.75	2.75	47	23	3	91	40	79	23	3	69	53	72	
U	40	2.75	2.75	2.75	2.75	2.75	3	3	16	48	3	3	63	18	3	

Table 3 Contd...

Major oxide values in wt%

Major oxide values in wt%

Table 2 Contd...

Sm. No.	W7/26	W7/28	W7/29	W7/30	W7/31	W8/4	W8/5	W8/6	W8/7	W8/17	W8/20	W8/21	W8/21A	W8/22	W9/1A
	PORCELLANITE (DEONAR FORMATION)														
SiO_2	94.57	74.35	73.11	71.46	79.14	85.98	95.15	94.00	83.62						
TiO_2	0.06	0.19	0.14	0.65	0.11	0.26	0.13	0.13	0.43						
Al_2O_3	0.01	14.24	17.03	17.81	11.07	7.39	0.95	2.27	9.08						
FeO_t	1.83	2.31	1.65	1.82	3.90	1.62	1.00	1.26	0.82						
MgO	0.12	0.41	1.64	1.78	1.29	0.87	0.39	0.28	0.80						
MnO	0.03	0.03	0.02	0.01	0.13	0.01	0.01	0.01	0.01						
CaO	0.09	0.18	0.17	0.46	0.14	0.26	0.15	0.10	0.15						
Na_2O	0.16	6.26	0.19	0.09	2.64	0.21	0.15	0.14	0.14						
K_2O	0.09	1.73	4.50	4.57	0.49	2.17	0.64	0.30	3.13						
P_2O_5	0.02	0.03	0.07	0.12	0.01	0.07	0.04	0.01	0.01						
Total	96.98	99.73	98.52	98.77	98.92	98.84	98.61	98.49	98.19						
	Trace Elements (in ppm)														
V	34	30	21	246	10	11	42	94	213	19	86	13	36	107	440
Cr	161	150	28	72	60	103	106	125	71	109	81	89	115	44	112
Co	3	3	3	3	24	3	8	7	2.75	3	20	5	5	19	3
Ni	151	122	27	38	96	85	57	62	30	109	57	66	57	22	37
Cu	26	16	21	36	28	22	36	38	29	27	42	44	27	18	81
Zn	8	29	74	33	57	14	84	45	8	12	34	32	19	22	56
Ga	3	3	17	13	3	3	2.75	2.75	10	3	3	8	3	3	20
As	1	1	1	1	12	1	16	15	12	0.5	11	0.5	11	10	12
Rb	13	43	163	190	47	49	49	42	100	22	41	81	18	51	83
Sr	47	50	26	269	70	39	18	24	50	14	29	31	58	22	66
Y	3	21	41	3	3	32	11	2.75	18	16	29	37	33	14	29
Zr	42	105	147	148	97	314	86	66	123	37	46	183	78	66	111
Nb	3	12	14	12	5	12	11	2.75	8	3	3	3	5	3	3
Ba	81	348	730	461	445	102	357	2.75	268	158	141	662	478	164	159
Ce	3	3	3	3	3	3	2.75	2.75	2.75	25	132	79	25	25	25
Pb	39	41	23	40	29	37	33	14	31	25	58	26	26	35	49
Th	46	61	115	23	61	77	2.75	2.75	2.75	3	3	3	15	3	3
U	16	36	45	20	47	3	95	31	15	3	103	3	3	3	3

mineralisation. However, only selected major and trace element data of different lithounits of Semri Group (arenites, n=38; shale, n=9; siltstone, n=28; limestone, n=4; porcellanite, n=15) is given in Table 3. Analytical results indicate wide scatter in major and trace element distribution patterns of different lithounits. Synthesis of major element data indicates higher SiO_2 content in arenites (62.28–97.20%; av. 89.62%) and porcellanites (71.46 –95.155; av. 83.49%) while siltstone (48.89–77.96%; av. 64.47%) and shale (48.69–70.32%; av. 60.80%) have comparatively low content. This behaviour is commensurate with low Al_2O_3 and $FeO_{(total)}$ contents in arenites(2.95% and 3.11%) and porcellanite (8.87% and 1.10%) and comparatively high contents in siltstone (15.50% and 8.46%) and shale (16.86% and 9.11%). The general trace element abundance pattern in these rocks indicates higher content of LILE viz., U (upto 107 ppm), Th (upto 116 ppm), Zr (upto 996 ppm), Rb (upto 205 ppm) and Ba (upto 785 ppm). These rocks are also enriched in ferromagnesian trace elements, such as, Ni (upto 429 ppm) and Cr (upto 465 ppm).

Chemical classification of sandstone based on log (SiO_2/Al_2O_3), and log(Fe_2O_3/K_2O) ratios and CaO (Herron, 1988) indicates that arenaceous rocks of study area belong to lithic arenite to quartz arenite and Fe-sand while argillaceous rocks are categorized as shale and Fe-shale (Fig. 4). The use of chemical log data is helpful in minimizing the influence of tectonic setting, depositional environment and source material (Pettijohn et al., 1972), which results in close match of chemical and petrographic categorization of sediments. This observation also holds true for the arenaceous rocks of present study area. However, chemical composition of Semri sediments is influenced, at places, by the effects of alterations viz., ferruginisation, chloritisation etc. which has marginally modified the original composition. This is evident from clustering of a large number of samples in Fe-sand and Fe-shale fields.

Very high content of SiO_2 vis-à-vis very high (>10; except 4 samples) SiO_2/Al_2O_3 ratio (CMI, Potter, 1978) of arenites show high order of chemical maturity, whereas siltstone's CMI varies from 3 to 7.8 signifying their immature nature. Besides, implication of climatic conditions on the chemical maturity has also been studied using bivariant plot of Suttner and Dutta (1986) i.e., SiO_2 vs $Al_2O_3 + K_2O + Na_2O$ diagram, which shows semi-arid to humid depositional paleoclimate for siliciclastic and volcaniclastic sediments (Fig. 5). This indicates multicyclic origin of arenaceous sediments of study area similar to the ancient quartz as suggested by Suttner et al. (1981). Quartz arenites perhaps represent the first-cycle sediments produced in tropical climates. The climatic conditions might have also played vital role in retention of oxyphile elements, such as, uranium in the system.

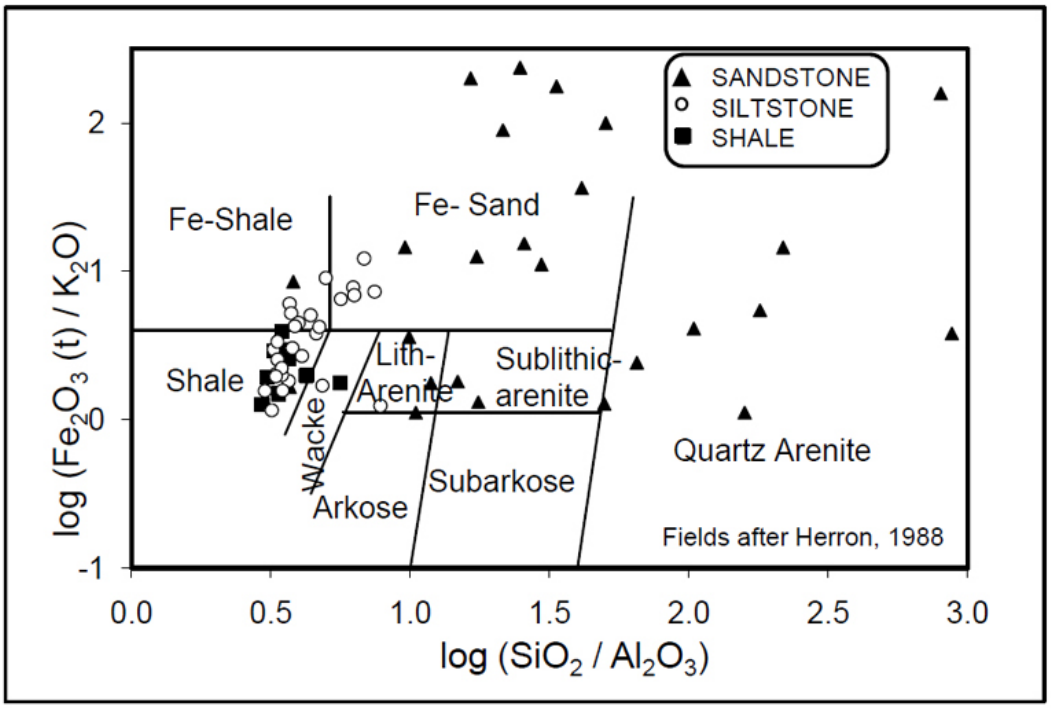

Fig. 4. Chemical composition of arenaceous and argillaceous sediments of KSM fault zone and their classification as per sand class scheme.

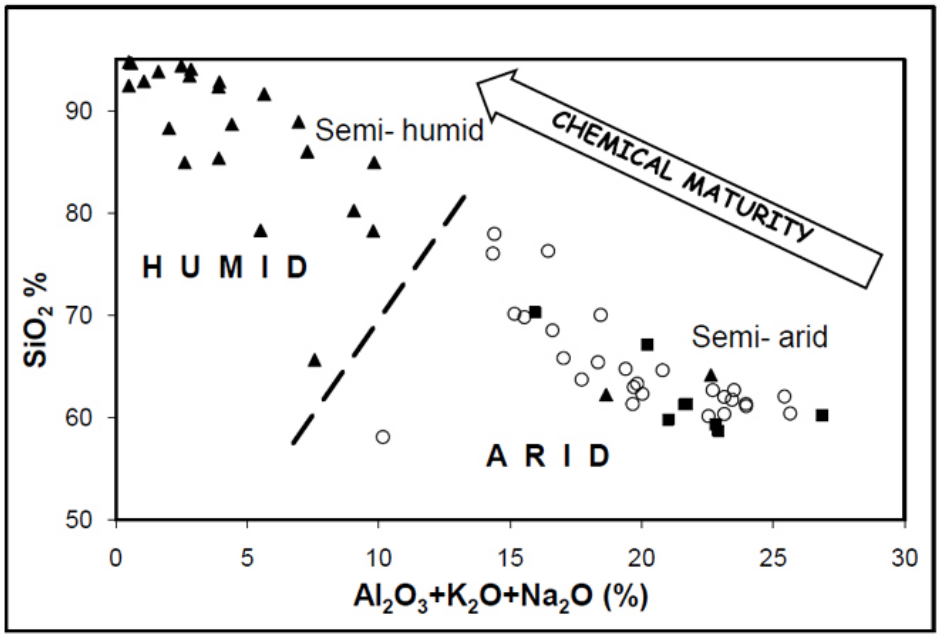

FIg.5. Chemical maturity of sedimentary suites of KSM fault zone expressed as function of SiO_2 % and total % of Al_2O_3, K_2O and Na_2O (fields after Suttner and Dutta, 1986) Symbols, same as in Fig.4.

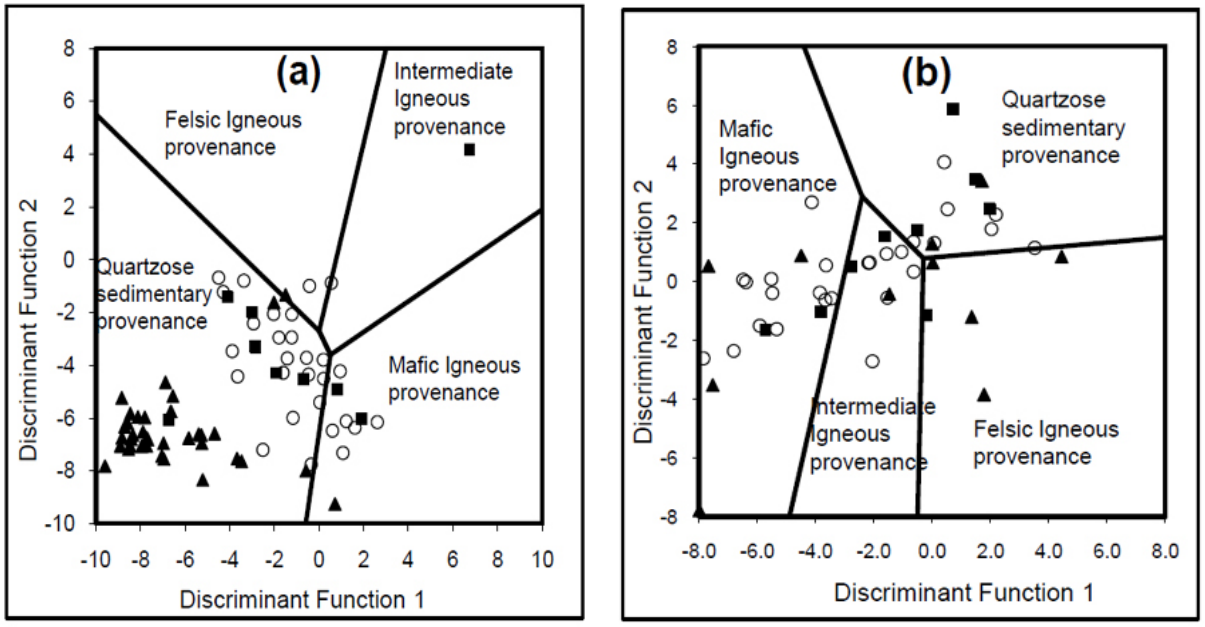

Fig.6 a. Discriminant function plot based on major oxide factor scores F1 and F2 for identification of sediment provenance, **b.** Ratio discriminant plot for sedimentary suites of KSM fault zone (Fields are after Roser and Korch, 1988) Symbols same as in Fig.4.

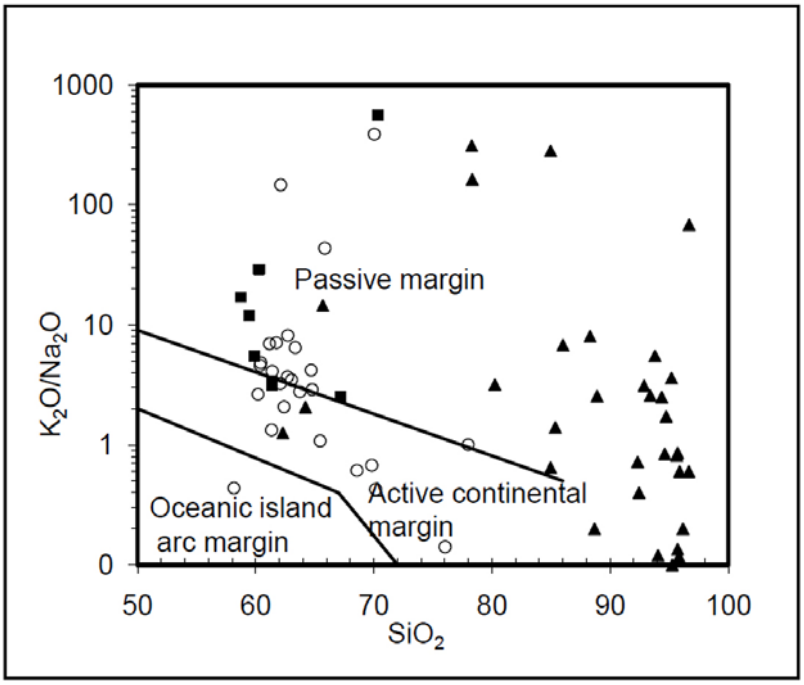

Fig.7. Tectonic discrimnation diagram for sedimentary suites along KSM fault zone (fields after Roser and Korsch, 1986) Symbols same as in Fig.4.

Table. 4. Average Chemical Composition of Basement and Cover Rocks.

	Arenite	Porcell-anite	Siltstone	Calc Tuff. shale	Lime stone	Ferrug. Breccia	Syenite	Granite
n	73	15	28	11	12	42	40	53
	Major oxides in wt%							
SiO_2	88.35	83.49	64.47	55.00	64.47	70.00	66.00	70.00
TiO_2	0.24	0.23	0.98	0.60	0.98	0.32	1.00	0.34
Al_2O_3	4.19	10.00	15.50	7.00	15.50	5.00	11.00	16.00
FeO_t	3.79	2.00	8.46	6.00	8.46	18.00	13.00	3.00
MgO	0.62	1.00	2.66	3.00	2.66	2.00	2.00	1.00
MnO	0.08	0.03	0.08	0.09	0.08	0.19	0.06	0.04
CaO	0.69	0.19	1.38	10.00	1.38	1.19	0.94	1.00
Na_2O	0.29	1.00	1.21	0.22	1.21	0.37	0.54	4.00
K_2O	0.82	2.00	2.87	1.00	2.87	1.52	4.65	4.00
P_2O_5	0.31	0.05	0.13	1.00	0.13	0.46	0.45	0.11
	Trace elements in ppm							
V	29	93	74	205	36	183	119	47
Cr	137	95	187	70	64	746	859	97
Co	21	13	20	10	15	26	23	18
Ni	89	68	86	65	32	170	187	67
Cu	29	33	40	57	15	69	52	45
Zn	44	35	88	107	35	111	52	42
As	7	7	8	12	8	10	9	14
Rb	49	66	99	63	67	47	102	8
Sr	50	54	66	61	45	84	91	93
Y	21	26	22	18	14	38	28	175
Zr	147	110	173	85	60	77	165	26
Nb	13	10	11	7	9	10	13	145
Ba	320	325	341	206	160	1851	855	18
Pb	29	34	28	29	32	28	28	679
Th	7	11	10	6	4	17	13	42
U	2	4	2	9	2	16	4	40

Discriminant function analysis using major oxides (after Roser and Korsch, 1986) were attempted to identify provenance for Semri sediments. Classification plot based on unstandardised Discriminant function coefficients using TiO_2, Al_2O_3, $FeO_{(t)}$, MgO, Na_2O and K_2O i.e., F1 and F2 scores (Fig. 6a) indicates that arenite sediments are mostly derived from quartzose sedimentary provenance while shale and siltstones show additional input from mafic igneous provenance. Similarly, ratio Discriminant function F1 and F2 plot (Fig. 6b) based on ratios of major oxide versus Al_2O_3 points toward derivation of Semri sediments from a mixed mafic and felsic igneous and quartzose sediment provenance. This is corroborated by the presence of CGGC granitoids, Mahakoshal quartzite and metabasic rocks in adjoining areas. Petrographic studies of Semri sediments also support this observation.

The provenance signature in the chemistry of sediments allows effective discrimination of tectonic environment at the time of sedimentation (Roser and Korsch, 1986). Based on this analogy, the Semri sediments were subjected to tectonic discrimination plots using SiO_2, K_2O and Na_2O relationship, which broadly indicates derivation of the sediments in Passive Margin (PM) setup (Fig. 7). This is corroborated by quartz-rich nature and deposition of these sediments in intracratonic basin in close proximity to the provenance.

DISCUSSION AND CONCLUSION

Integrated field exploration and laboratory studies of Son valley area in parts of Sidhi district, Madhya Pradesh, an important geological domain, reveals a complex evolutionary history of CGGC, Mahakoshals and Vindhyans involving atleast five magmatic phases (Saxena et al., 2005). These pre- and post- Vindhyan magmatic and tectonic activities have led to large scale potash metasomatism of basement together with emplacement of highly evolved acid, alkaline and mafic intrusives, development of pyroclastic and felsites in Vindhyan sequences vis-à-vis alteration of basement rocks/cover sediments. This has also influenced the sedimentation patterns. These activities have accelerated mobilisation of various elements such as base metals, precious metals, radioelements, REEs etc., some of which have ultimately led to formation of deposits of economic significance (GSI, 2002; Bhattacharjee eta al., 2008; Bhattachraya et al., 2008; Saxena et al., 2005; Sesha Rao et al., 2004).

The study area, forming a part of the Son–Narmada mega rift zone, exposes Neoarchaean to Palaeoproterozoic basement complex over which a thick pile of Mesoproterozoic Vindhyan sediments were deposited. Substantial structural disturbances in the form of major faults/fractures including KSM fault sympathetic to Son–Narmada lineament is significant as this provides an ideal geological setup for unconformity- related and/or fracture- controlled uranium mineralisation. This is evident from uranium mineralisation along KSM fault zone. Apart from surface radioactive occurrences, water radon anomalies indicate sub-surface continuation of the mineralisation. Another striking feature is association of uranium mineralisation mostly with ferruginous breccia zones developed along reactivated faults/fractures in close proximity to tectonised unconformity contact between Sidhi crystallines and Vindhyan sediments. This signifies the role of KSM and other associated faults/fractures in mobilisation of radioelements.

Geochemical distribution pattern of uranium in different lithounits exposed along KSM fault zone and adjoining areas indicates normal to slightly higher intrinsic values (Table 2 and 4). However, it is significant to mention that average uranium content of arenite (22 ppm), siltstone (12 ppm), porcellanite (29 ppm), calc tuffaceous shale (9 ppm) and ferruginous breccia (12 ppm) adjacent to mineralised zones is much higher than the normal abundances. This probably indicates mobilisation of available uranium in the system during different deformational episodes, where faults/fractures provided a good network of channelways for fluid movement. Post- Vindhyan reactivation of faults might have provided the thermal gradient for further remobilization of uranium from fertile basement granites (40 ppm U; n=53) as well as cover sediments, which finally concentrated and fixed in suitable locales.

Field observation, petromineralogical details and chemical data indicates that the provenance for the supply of Semri sediments in the environs of KSM fault zone comprises acid and mafic igneous suites and quartzose sedimentary rocks. These are confirmed by the presence of angular to sub-angular grains of quartz, feldspar, granite, syenite, quartzite, schist and basic rock fragments in lower arenaceous units. Besides, some contribution from mafic volcanic parentage is indicated by high abundance of Ni and Cr. This marks the Sidhi crystallines, Mahakoshal metasediments and various intrusives present at the immediate vicinity of Semris as the provenance rocks, which is further supported by the higher intrinsic radioelemental content of the sediments. The deposition of Semri sediments in a passive margin tectonic environment signifying limited transportation is corroborating above inference while semi-arid to semi-humid depositional paleoclimate have helped in retention of oxyphile elements, such as, uranium in the system. Uranium inventory of Semri sediments was further increased by deposition of volcaniclastic beds viz., porcellanite, calc tuffaceous shale etc.

Presence of favourable factors such as highly fertile Neoarchaean to Palaeoproterozoic basement-cum-provenance with labile uranium, hiatus of 500-700 Ma before the deposition of thick pile of Mesoproterozoic cover sediments, episodic magmatism and basement reactivation including post-Vindhyan deformation

provided thermal gradient and channel-ways for mobilisation/redistribution of uranium in the system. This finally led to epigenetic mineralisation by fixation of uranium at suitable locales viz., unconformity planes and fracture zones. Required reducing environments were created by oxidation of magnetite into ferric oxide minerals, whereas at places, pyrite acted as reductant. Hence, the KSM fault zone and its environs indicate high potential for uranium mineralisation.

Acknowledgment: The authors are thankful to Dr. Anjan Chaki, Director, Atomic Minerals Directorate for Exploration and Research, Hyderabad for permission to publish this paper. Analytical support from AMD laboratories is also acknowledged with thanks.

References

Abhinav Kumar and Banerjee Rahul (2006) A report on integrated studies of Remote Sensing, AGRS, Aeromagnetic and Ground radiometric data, in parts of Sidhi district, M.P. (Unpublished Annual Report), AMD, Hyderabad.

Anil Kumar, Gopalan, K. and Rajgopalan, G. (2000) Mesoproterozoic age of the Vindhyan sediments, Central India from Glauconite Rb–Sr systematics. Jour. Conf. Abst., 5, no. 2, p. 608.

Anil Kumar, Gopalan, K. and Rajgopalan, G. (2001) Age of the Lower Vindhyan sediments, Central India. Current Sci.,81, 806–809.

Auden, J.B. (1933) Vindhyan sedimentation in Son Valley. Mem. Geol. Surv. India,62, pt.2,. 141–250.

Bhattacharjee, I., Agarwal, M., Yadav, O.P., Roy, M.K. and Saxena, V.P. (2008) A note on the phosphatic tuffaceous shale hosted uranium mineralisation in Semri Group of sediments around Mankisar–Kathar area, Sidhi district, Madhya Pradesh. Jour. Geol. Soc. India,72, 215–218.

Bhattacharya, D., Joshi, G.B., Sharma, G.S. and Sen, D.B. (2008) A note on the uranium mineralisation along Jamual–Markundi fault, Sonbhadra and Sidhi districts, Uttar Pradesh and Madhya Pradesh. Jour. Geol. Soc. India, 71, 125–128.

Bose, P.K., Sarkar, S., Chakraborty, S. and Banerjee, S. (2001) Overview of the Meso- to Neoproterozoic evolution of the Vindhyan basin, Central India (1.4 – 0.55Ga). Sedimentology, 40, 79–85.

Chakraborty, C. (2006) Proterozoic intracontinental basin: The Vindhyan example. Jour. Earth Syst. Sci. 115,(1), 3 – 22.

Chakraborty, C. and Bhattacharya, A. (1996) The Vindhyan Basin: An overview in the light of current perspective. Mem. Geol. Soc. India, 36,301–312.

Chakraborty, T., Sarkar, S., Chaudhari, A. and Dasgupta, S. (1996) Depositional environment of Vindhyan and other Purana basins: a reappraisal in the light of recent findings. Mem. Geol. Soc. India, no. 36, 101–126.

Das, L.K., Mal, R.P. and Lal, J.K. (1995) Geological and geophysical studies in the Son valley and the Gangetic Plains. Geol. Surv. India, Spl. Pub., no. 10, 249–284.

G.S.I. (2002) District Resource Map, Sidhi District, Madhya Pradesh. Geol. Surv. India, Central Region, Nagpur.

Herron, M.M. (1988) Geochemical classification of terrigenous sands and shales from core or log data. Jour. Sed. Petrol.,58(5), 820–829.

Hounslow, A.W. and Moore, J.M. Jr., 1966. Preparations and Analysis of Silicate Rocks and Minerals. Carlton University Geological Paper, No. 66.

Jain, A.K., Nagar, A. and Singhal, D.C. (1984) Crustal evolution of the Narmada –Son lineament and associated shear zone of the Indian lithosphere. Ind. Jour. Earth Sci., CEISM Sem.,. 125–148.

Jain, S.C., Nair, K.K.K. and Yedekar, D.B. (1995) Geology of the Son–Narmada–Tapi lineament zone in Central India. Geol. Surv. India, Spl. Pub., no. 10,. 1–154.

Jain, S.C., Nair, K.K.K. and Yedekar, D.B. (1995) Tectonic evolution of the Son–Narmada–Tapi lineament zone in Central India. Geol. Surv. India, Spl. Pub., no. 10, . 333–371.

Murugan, C. and Choudhury, D.K. (1992) A report on detail radiometric survey, mapping and hydrogeochemical survey in Bari–Ainthi–Kusumahar area, Sidhi district, M.P. (Unpublished Annual Report), AMD, Hyderabad.

Nair, K.K.K., Jain, S.C. and Yedekar, D.B. (1995) Stratigraphy, structure and geochemistry of Mahakoshal Greenstone Belt. Mem. Geol. Soc. India, 31, 403–432.

Pettijohn, F.J., Potter, P.E. and Siever, R. (1972) Sand and Sandstone. Springer –Verlag, New York, 618p.

Potter, P.E. (1978) Petrology and Chemistry of modern big river sands. Jour. Geology, 86, 423–449.

Rajurkar, S.T., Bhate, V.D. and Sharma, S.B. (1990) Lineament fabric of Madhya Pradesh and Maharashtra and its tectonic significance. Geol. Surv. India Spl. Pub., no. 28, 241–259.

Rao, K.S. and Neelkanthan, S. (1978) Stratigraphy and sedimentation of Vindhyans in parts of Son Valley area, M.P. Rec. Geol. Surv. India, 110, pt. 2, . 180–193.

Rasmussen, B., Bose, P.K., Sarkar, S., Banerjee, S., Fletcher, I.R. and McNaughton, N.J. (2002) 1.6 Ga U –Pb zircon age for the Chorhat Sandstone, Lower

Vindhya, India: Possible implications for early evolution of animals. Geology, 30, no. 2, . 103–106.

Ray, J.S. (2006) Age of the Vindhya Supergroup: A review of recent findings. Jour. Earth Syst. Sci., 115, no. 1, 149–160.

Ray, J.S., Martin, M.W., Veizer, J. and Bowring, S.A. (2002) U–Pb zircon dating and Sr isotope systematics of the Vindhyan Supergroup, India. Geology, 30, 131–134.

Roser, B.P. and Korsch, R.J. (1986) Determination of tectonic setting of sandstone-mudstone suites using SiO_2 content and K_2O/Na_2O ratio. Jour. of Geol., 94, 635 – 650.

Roser, B.P. and Korsch, R.J. (1988) Provenance signatures of sandstone-mudstone suites determined using Discriminant function analysis of major element data. Chem. Geol., 68, 119 – 139.

Saibaba, M., Fahmi, S. and Khare, M.K. (1987) A report on radiometric survey in parts of Sidhi district, M.P. (Unpublished Annual Report), AMD, Hyderabad.

Saibaba, M., Fahmi, S. and Nagabhushanam, B. (1988) A report on detail radiometric survey, mapping and prospecting in Bari–Ainthi area, Sidhi district, M.P. (Unpublished Annual Report), AMD, Hyderabad.

Saxena, V.P., Sinha, R.M., Yadav, O.P. and Sesha Rao, R.V.S. (2005) Geochemical modeling for the unconformity-related uranium mineralisation: A case study from Baskati area, Madhya Pradesh, India. In: Proc. Uranium production and raw materials for the nuclear first cycle supply and demand, economics, the environment and energy security. IAEA, 141–151.

Sesha Rao, R.V.S., Deshpande, M.S.M. and Shivkumar, K. (2004) A note on the occurrence of uraniferous phosphatic ferruginous breccia in the Lower Vindhyan sediments of Son-valley, around Baskati, Sidhi district, Madhya Pradesh. Jour. Geol. Soc. India, 64, 685–688.

Shapiro, L. and Brannock, W.W. (1962) Rapid analysis of silicate, carbonate and phosphate rocks. U.S. Geol Surv. Bull., No. 1144-A, 1–56.

Soni, M.K., Chakraborty, S. and Jain, V.K. (1987) Vindhyan Supergroup – A review. Mem. Geol. Soc. India, 6, 87–138.

Suttner, L.J. and Dutta, P. (1986) Alluvial sandstone composition and paleoclimate, I. Framework Mineralogy. Jour. Sed. Petrol.,56(3), 329 – 345.

Suttner, L.J., Basu, A. and Mack, G.H. (1981) Climate and the origin of quartz arenite. Jour. Sed. Petrology, 51, 1235 – 1246.

Vishwanathan, S. (1989) Wavelength-dispersive X-ray fluorescence spectrometry in exploration and research for atomic minerals. Expl. Res. Atomic Min., 2, 247–268.

Jour. Indian Association of Sedimentologists, Vol. 28, No. 1 (2009), pp. 73-83

Grain-size Analysis and Depositional Environment of Lameta Sediments Exposed at Salbardi and Belkher, Amravati District, Maharashtra and Betul District, Madhya Pradesh

ASHOK K. SRIVASTAVA* and RUPESH S. MANKAR
P.G. Department of Geology, SGB Amravati University, Amravati - 444602
E-mail: ashokamt2000@hotmail.com

Abstract: Grain-size analysis of sixteen sandstone samples from two exposures of Lameta sediments (Upper Cretaceous) laying at Salbardi (lat. $21^0$25'15'' N: long.$78^0$00'00''E) and Belkher area (lat. $21^0$21'48'' N: long.$77^0$31'23''E) has been carried out to measure the textural and statistical parameters. The sandstones of both the successions are mainly medium to fine-grained, moderately-sorted, near-symmetrical to fine-skewed and mesokurtic in nature. Inter relationships of various parameters show unimodal to bimodal nature of the sediment, of which, the medium-sand size grains are the principal mode. Based on the granulometric analysis, the environment of deposition is adjudged to be fluviatile for sandy units.

Keywords: Lameta, Granulometric analysis, Depositional environment, Salbardi, Belkher.

INTRODUCTION

The Lameta lithounits are exposed as isolated patches at three near-by places viz., Salbardi (lat. $21^0$25'15'' N: long.$78^0$00'00''E), Bairam (lat. $21^0$22'25'' N: long.$77^0$37'23''E) and Belkher area (lat. $21^0$21'48'' N: long.$77^0$31'23''E), close to the boundary of Madhya Pradesh and Maharashtra (Fig. 1). The sediments are mainly represented by greenish, brownish and yellowish clay; friable to hard, reddish-brown, brownish to greenish, medium-grained sandstones; and, siliceous, brecciated and nodular limestones constituting 34m, 39m and 47m thick lithocolumns, respectively, at above-mentioned localities. However, at Bairam area, the sandy unit is not well developed. So far, all the three lithounits are never subjected to detailed sedimentological investigation and bear only casual reports about their occurrences with minor details (Srivastava et al., 1995, 1996, 1999, 2001, 2003; Saxena, 1987; Ravishankar et al., 1991; Gawande 2003; Rawale, 2004).

In the present study, the sandstones of Salbardi and Belkher areas are considered for detailed grain-size analysis apart from establishing detailed sedimentological log. Various parameters viz., mean, standard deviation, skewness and kurtosis and, their inter-relationships have been worked out to decipher the nature of sediments and environment of deposition. As, the data is generated from the sandy units only, therefore, interpretations are also limited to the same.

GEOLOGY AND STRATIGRAPHY OF THE AREA

The Lameta successions along with the upper most Gondwana are exposed due to roughly E-W trending Satpura Fault, which is locally known as the Salbardi Fault, in Salbardi area (Ravi Shankar et al., 1991). The Salbardi area lies at about 60 km east of Bairam-Belkher area. Both the sedimentary lithounits are still very less explored for their sedimentological and palaeobiological details, however, the underlying Gondwana has been referred to in a few earlier works (Pascoe, 1959; Adyalkar, 1975; Bhusari, 1979), which reflect a controversy about the age and stratigraphic position of these sediments. Recently, the Gondwana succession of Bairam-Belkher area has been assigned an Early Cretaceous age on the basis of rich and diversified mega-floral assemblage including *Ptilophyllum, Taeniopteris, Elatocladus, Pagiophyllum, Brachyphyllum, Araucarites* etc. (Srivastava et al., 1995, 1999, 2001, 2003 and Gawande, 2003). The same age has also been assigned to the Gondwana succession of Salbardi area, mainly on the basis of its similarity in lithological set-up including pebbly horizons in topmost part of the successions and facies architecture with those of the Bairam-Belkher area (Srivastava and Mankar, 2008).

Stratigraphically, the Lameta overlies the Gondwana with a disconformable contact. The Deccan Trap overlies the succession forming a regional exposure of vesicular

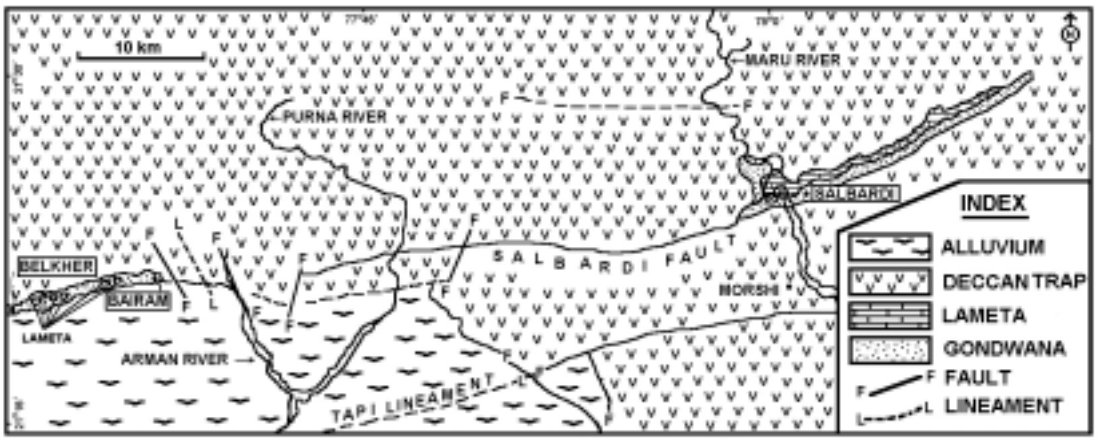

Fig.1. Generalized geological map of Bairam, Belkher and Salbardi area, (modified from district resource maps of Amravati and Betul, GSI, 2001, 2002).

Table 1. General stratigraphy of Salbardi and Belkher area. At Belkher, Achaean not exposed.

Age Quaternary	Lithounits	Roc types Soil and Alluvium
----------Unconformity----------		
U. Cretaceous to Eocene	Deccan Trap	Non-porphyritic and porphyritic basalt
----------Unconformity----------		
U. Cretaceous	Lameta	Sandstone, shale and limestone
----------Disconformity----------		
U. Cretaceous		Upper Gondwana Sandstone, siltstone, Conglomerate and clay
----------Unconformity----------		
Archaean		Quartzo-feldspathic gneiss with dolerite intrusions

to non-vesicular basalts. The trap is overlain by soil and alluvium of Quaternary and Recent age, which forms the top most horizons. The basement to Gondwana is of quartzo-feldspathic gneiss of Archaean age, which is exposed at Salbardi area (Deshpande, 1998) (Table 1).

LAMETA SUCCESSIONS OF THE AREA

The Lameta of Belkher and Salbardi area is almost similar, represented by limestone, calc-marl and arenaceous units (Figs. 2 & 3), however, the succession of Belkher area is comparatively well developed. At Belkher, it constitutes ca. 47m thick lithocolumn, of which, the lower part shows preservation of thinly-bedded, brownish to reddish, medium to fine-grained, loose to compact sandstones (Figs. 2, 4A & 4B). Bioturbated zones are also recorded. The upper part of succession is dominantly calcareous represented by nodular, brecciated and chertified limestones. At Salbardi, the lower sandy horizons is represented by only 12m thick unit, whereas, the upper calcareous part is similar to Belkher area, making a lithocolumn of ca. 34m thickness (Figs. 3, 4C & D). The Bairam area shows good development of only calc-marl unit. The arenaceous unit, though present, but less developed.

SAMPLING AND METHODOLOGY

A total of sixteen sandstone samples have been analyzed, of which, eleven belong to Belkher area and rest of five to Salbardi area. The samples are collected at close intervals, depending on bedding geometry, grain-size and colour variations.

Sieving technique as proposed by Ingram (1971) is applied to separate grains of various size-classes from the sediment admixture. Initially, 100gm of sample is prepared by removing carbonates and organic matters by treating it with 10% dilute hydrochloric acid and 6% hydrogen peroxide, respectively. The samples, completely free from carbonate and organic matter are subjected to sieve analysis. The sample was placed in the BSS sieves arranged at half phi (ϕ) interval, starting from 8 mesh (-1.25 ϕ), 12 mesh (-0.75 ϕ), 16 mesh (-

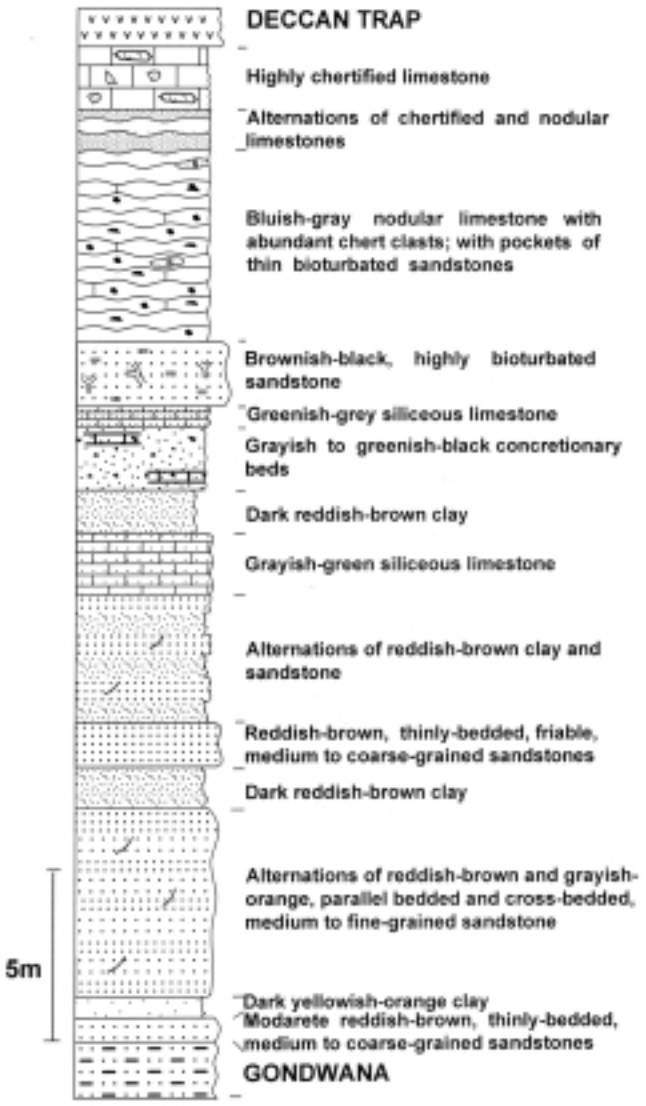

Fig. 2. Detailed sedimentological-log of Lameta succession exposed at Belkher area.

0.25 ϕ), 22 mesh (0.35 ϕ), 30 mesh (0.75 ϕ), 45 mesh (1.50 ϕ), 60 mesh (2.00 ϕ), 85 mesh (2.60 ϕ), 120 mesh (3.0 ϕ), 170 mesh (3.50 ϕ), 240 mesh (4.10 ϕ) and -240 mesh (4.25 ϕ), and was shaken for thirty minutes in sieve-shaker. The retained fractions on each sieve i.e., weight percentage, served as the basic data for the reconstruction of the cumulative curves, which are further applied to generate various statistical parameters as proposed by Folk (1980), Reinick and Singh (1980), Pettijohn (1984), Lindholmn (1987) and Sengupta (1996). Various graphical and statistical parameters of the sediments of both the successions are given in Table 2.

RESULTS AND DISCUSSION

Cumulative weight percentage frequency curves

The cumulative weight percentage frequency curves of the sediments belonging to both Belkher and Salbardi exposures show the dominance of medium to fine-grained sediments, and exhibit almost similar trend i.e., little sorting of grains and dominance of medium sand-size fraction (Fig. 5).

Statistical parameters

Inclusive Graphic Mean (Mz)

Graphic mean (Mz) is a measure of central tendency. The average mean value of Salbardi sediments is a little higher than that of the Belkher sediments i.e., 1.92ϕ and 1.53ϕ respectively, however, the general tendency is the dominance of medium sand-size sediments. Solitary sample (BLL-3) showing lower value i.e., 0.97ϕ is because of comparatively higher fractions of coarse-grained sediments (Fig. 6A). It may be due to the temporary increase in the energy condition of depositional environment.

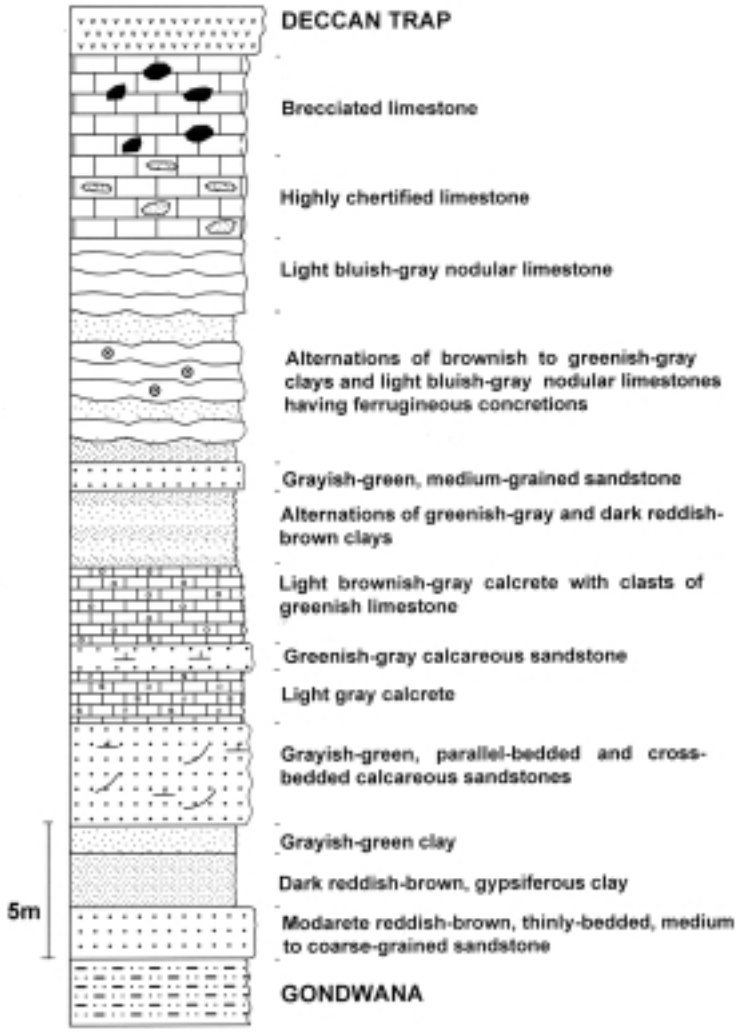

Fig. 3. Detailed sedimentological-log of Lameta succession exposed at Salbardi area.

Table 2. Graphical and statistical measures of the sediments belonging to Belkher and Salbardi area.

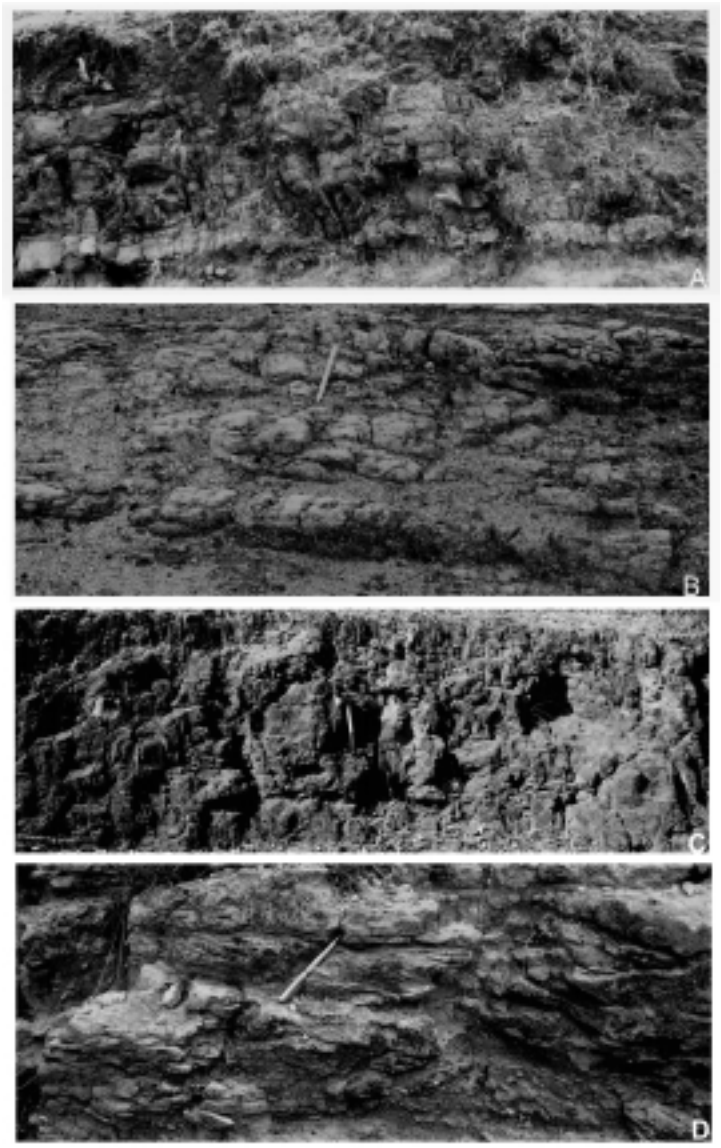

Fig. 4. Field photographs showing - A & B) thinly-bedded, medium-grained sandstone (Belkher area), C) thinly-bedded, fine-grained, friable sandstone (Salbardi area) and D) medium-grained, cross-bedded sandstone (Salbardi area).

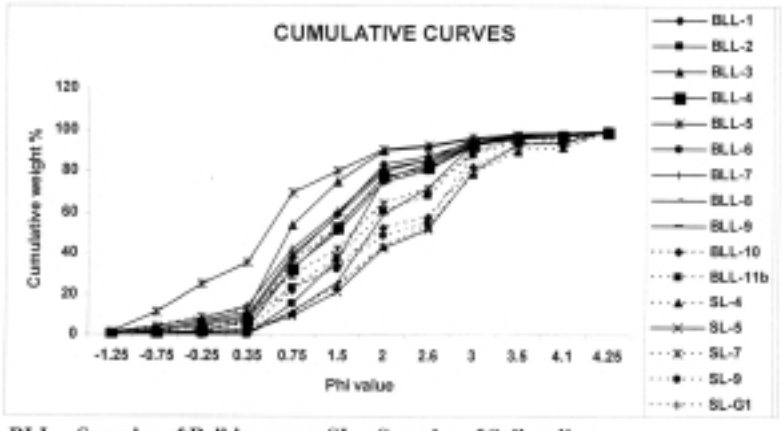

BLL – Samples of Belkher area, SL – Samples of Salbardi area

Fig 5. Cumulative curves showing trend of all samples.

Inclusive Graphic Standard Deviations (σ_1)

The graphic standard deviation (σ_1) measures the sorting or uniformity of particle-size distribution. In general, the sediments show poor to moderate sorting with an average standard deviation of 1.03ϕ (Fig. 6B). The sediments of Salbardi area are poorly-sorted (av. 1.26ϕ) whereas, the Belkher sediments are poor to moderately-sorted with an average of 0.95ϕ.

Inclusive Graphic Skewness (Sk_1)

The graphic skewness (Sk_1) measures the asymmetry of distribution i.e., predominance of coarse or fine-sediments. The negative value denotes coarser material in coarser-tail i.e., coarse-skewed, whereas, the positive value represents more fine material in the fine-tail i.e., fine-skewed.

The skewness values range from 0.01ϕ to 0.50ϕ for the Belkher sediments, whereas, 0.01ϕ to -0.25ϕ for Salbardi sediments, falling together between near-symmetrical to very fine-skewed categories (Fig. 6C). However, the complete assemblage shows the dominance of fine-skewed category, followed by near-symmetrical category shown by six and five samples, respectively. Very fine and coarse-skewed categories are represented by one and three samples, respectively.

Inclusive Graphic Kurtosis (K_G)

The graphic kurtosis (K_G) is the peakedness of the distribution. It measures the ratios between the sorting in the tails and central portion of the curve. If the tails are better sorted than the central portion, then it is termed as leptokurtic, whereas, it is platykurtic in opposite case, or mesokurtic if sorting is uniform both in tails and central portion. The values obtained from both the successions range widely between 0.56ϕ to 2.84ϕ (Fig. 6D). However, there is a dominance of very leptokurtic sediments represented by six samples, followed by leptokurtic to mesokurtic sediments represented by four samples each. The platykurtic condition is represented by only two samples. It shows that both coarse and fine fractions of most of the sediments are subjected for the sorting by the depositing medium to some extent.

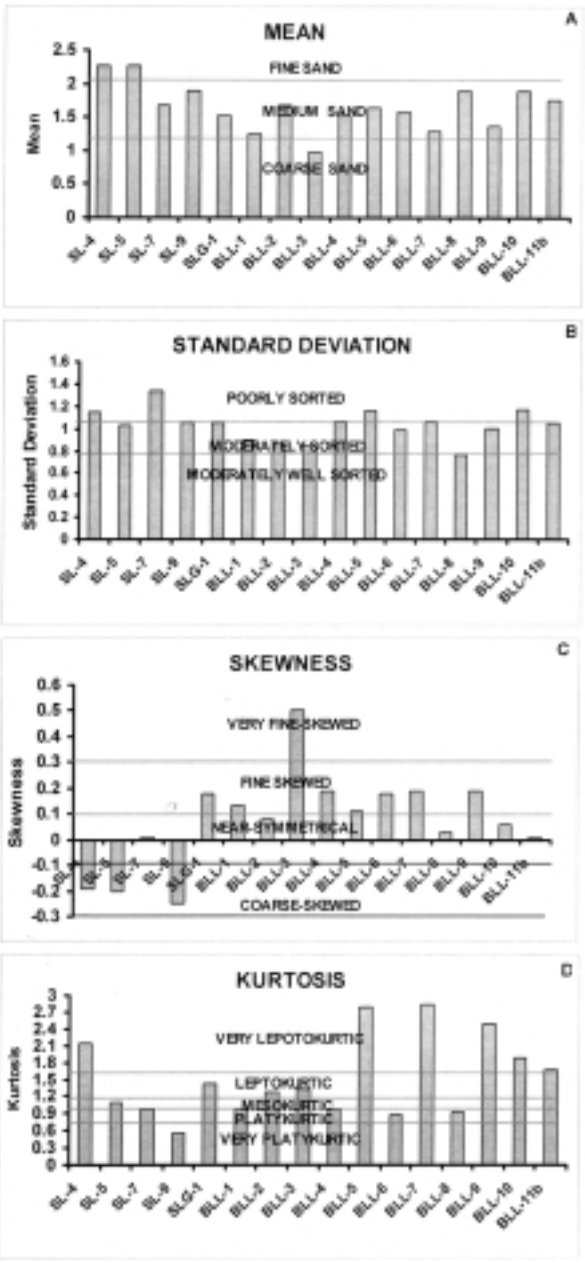

Fig 6. Comparative histograms of all samples showing trends of - **A.** mean, **B.** standard deviation, **C.** Skewness, and **D.** kurtosis values.

Bivariate plots

The basic idea behind the inter-relationship analysis is the fact that changing patterns of the textural parameters of the sediments have an established relationship with environmental set-up (Folk and Ward, 1957; Friedman, 1961, 1967; Moiola and Weiser, 1968). Plots between certain parameters are also helpful to interpret the energy conditions, medium of transport, mode of deposition etc. (Passega, 1957; Visher, 1969). In the present study, these plots are basically used to interpret the nature of sediments, environment of deposition and energy condition of the medium of transpotation.

i. Plots Showing Nature of Sediments

The nature of sediment admixture is interpreted by inter-relationship plots of mean, standard deviation, skewness and kurtosis, as proposed by Folk and Ward (1957). The scatter between mean vs. standard deviation shows either 'V' or inverted 'V' trend, which denotes very smaller size-range (Folk and Ward, 1957). Accordingly, the present values show a very small size-

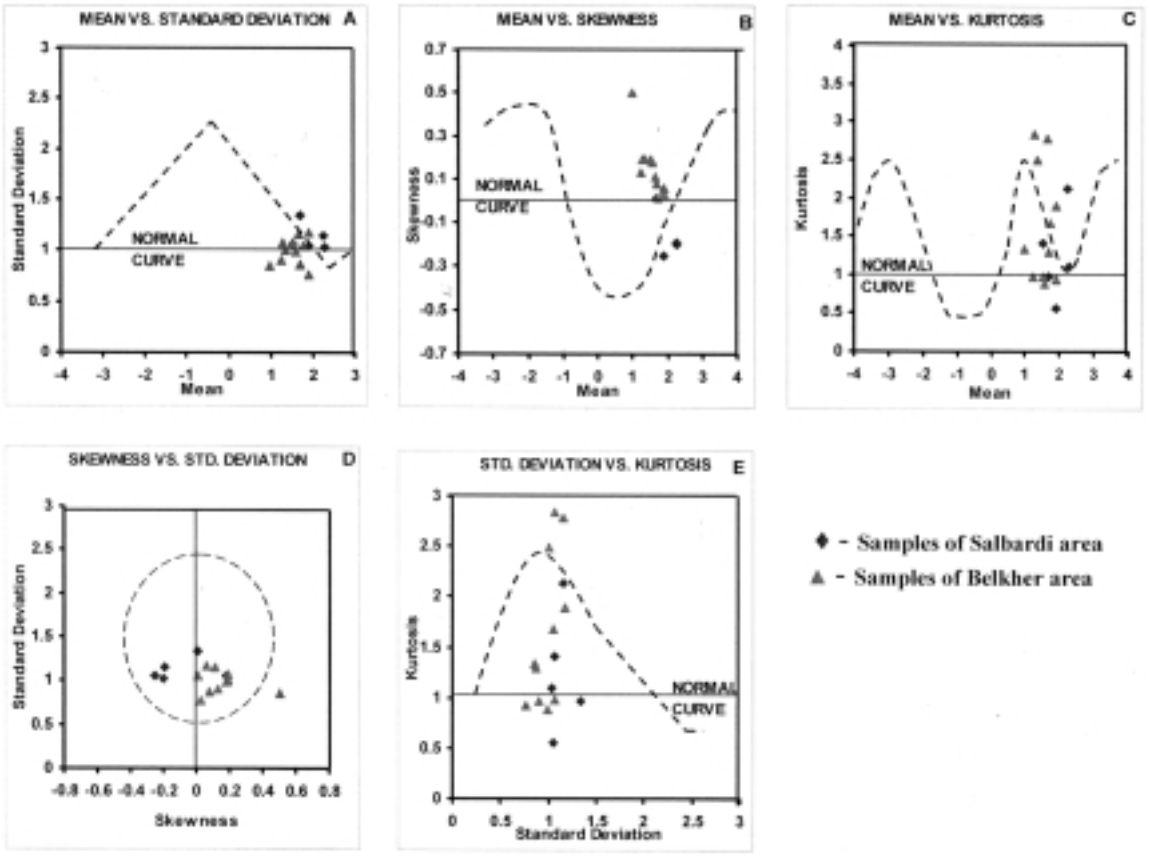

Fig. 7. Bivariate plots showing the placement of present samples in the model plot of Folk and Ward (1957) for- A) mean vs. standard deviation, B) mean vs. skewness, D) Skewness vs. standard deviation and E) standard deviation vs. kurtosis.

range, as the points are concentrated near the extreme end of the right limb of inverted V-shaped established trend of Folk and Ward (1957) (Fig. 7A). It is also supported by the average graphic mean value, which also confirms the dominance of medium sand-size sediments. A close observation of the mean vs. skewness plot (Fig. 7B) shows that the present data correspond to the established sinusoidal curve of Folk and Ward (1957). This established sinusoidal curve (Folk and Ward, 1957) is based on the proportion of two size-classes in the admixture of the sediment e.g., gravel and sand, which may produce either positive or negative skewness depending upon the proportions of size-classes in the admixture, otherwise, symmetrical in case of equal fractions. The present plot shows that the points are mostly clustered near normal graph in the range of near-symmetrical category of skewness, however, a few negative as well as positive-skewed samples are also represented, falling in the mean-size range of 1.0 to 2.09ϕ. Overall, the assemblage shows two categories of samples i.e., one having large number of samples shows unimodal nature of sediments whereas, second with less samples is bimodal. The medium-sand is the principal mode which looses the symmetrical distribution because of the addition of coarse or fine-sediments in the admixture, resulting in bimodal nature of the sediments.

The mean-size vs. kurtosis is also an important criterion to differentiate the mode of size-classes in an admixture of the sediments (Folk and Ward, 1957). It depicts the mixing of two or more size-classes and is a determining factor of the sorting in peak and tails i.e., index of kurtosis. The scattering of points give rise to an inverted 'V' shape trend, which depends on the proportion of two modes in the mixture. The scatters of present values indicate the dominance of mesokurtic (0.90ϕ to 1.11ϕ) condition, whereas, sorting in peak as well as in tails is almost equal (Fig. 7C). But, in certain samples, mixing of the finer mode in varying proportions is clearly visible, as the points above the normal curve goes up to 2.49ϕ value, i.e., very leptokurtic condition. Similarly, sediment admixture with coarser material is also represented, but very less.

Both, skewness vs. standard deviation and standard deviation vs. kurtosis are also used to interpret the presence of various size-modes in the sample (Folk and Ward, 1957). The skewness and standard deviation bear a mathematical relationship because both are the

functions of mean-size. The plot of these two variables produce nearly circular ring in the case of either unimodal samples with good sorting, or, equal mixture of two modes (Folk and Ward, 1957). In the present plot, most of the points are within the circular ring, concentrating in lower half, almost equally distributed on both sides of the normal curve, in the range of moderate to poorly-sorted category (Fig. 7D). It denotes that the samples, though, dominantly unimodal but, subordinate mode is also well represented in a few samples, hence, bimodal. The same is also supported by standard deviation vs. kurtosis plot (Fig. 7E).

ii. Plots Showing Depositional Environment

The depositional environment is interpreted as per the criteria proposed by Friedman (1967) and Moiola and Weiser (1968). The inter-relationship between mean vs. standard deviation and standard deviation (horizontal axis) vs. skewness (vertical axis) are considered to be significant tools to differentiate between beach and river environments (Friedman, 1967; Moiola and Weiser, 1968). Accordingly, both the plots show that the deposition of Lameta sediments took place under river influence, as all the points are falling in river-sediment sector of both the plots (Figs. 8A, B). Similarly, Friedman (1967) proposed the plot between SOS = ½ (ϕ_{95} - ϕ_5) and SKS = (ϕ_{95} + ϕ_5) - 2 ϕ_{50} to differentiate between beach and river environments. This criteria also confirms fluvial environment of deposition, as all the points in the present cross-plot of both the successions are restricted in the river sector of the standard plot as proposed by Friedman (1967) (Fig. 8C).

Based on the above-mentioned plots, it is concluded that the sandstone units of both the successions are a product of fluvial environment. This interpretation is specific to the sandstone units only, as the overlying and underlying lithounits of different composition may shows different environmental set-up. The lower part of both the successions show preservation of greenish-brownish-yellowish clay, which is lithologically correlatable with lacustrine facies of Nand-Dongargaon, (Mohabey and Samant, 2005). Similarly, the chertified, brecciated carbonate unit (Raiverman, 1995; Kumar et al., 1999; Tandon and Andrews, 2001), calcrete horizons and bioturbated unit with long, slender, branched burrows in the upper part are also correlatable with the lithological architecture of Lametas in the type area of Jabalpur (Kumar and Tandon, 1978, 1979).

iii. Plots Showing Energy Condition

The C-M scatter, C- coarser one percentile value in micron, and M- median value in micron, plotted on log-probability scale, as proposed by Passega (1957) is an important tool to evaluate the hydrodynamic forces working during the deposition of the sediments. The present interpretation is based on Passega (1957, 1964) and Passega and Byramjee (1969). The plot shows that most of the samples fall in N-O and O-P regions of sector I, which indicates dominantly rolled sediments, followed by a few suspension sediments, representing their deposition through traction currents (Fig. 9). The C-value, in general, is more than one millimeter. A few samples, falling in II and IV sectors, show mainly rolled and suspension categories, which may be due to comparatively more percentage of coarse or fine-grained material respectively, in the admixture.

Visher (1969) proposed log-probability curves, which provide an idea about the relationship of grain-

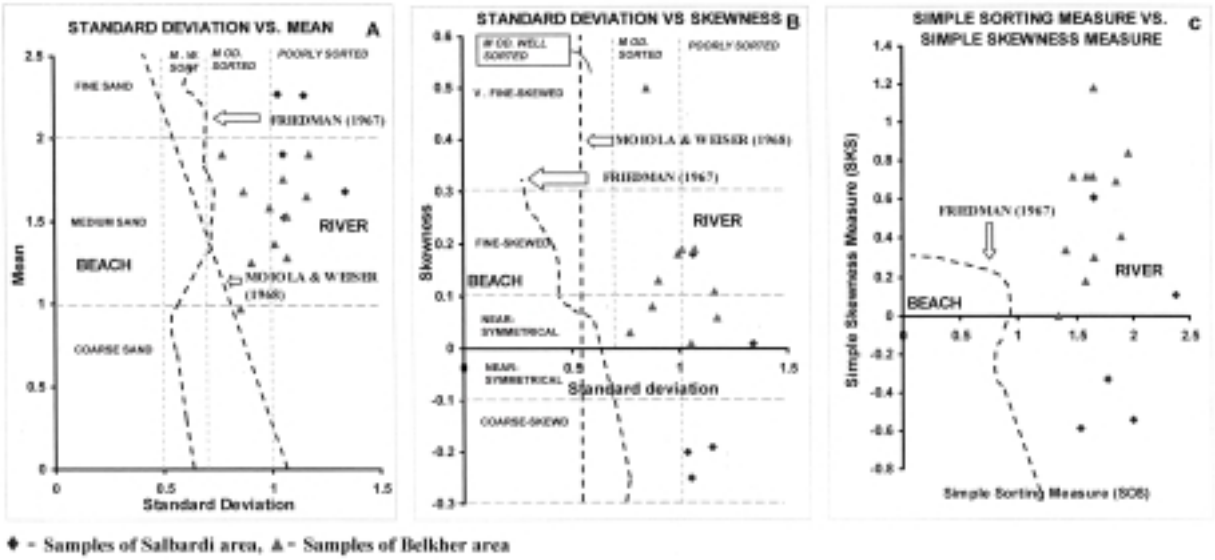

Fig.8. Bivariate plots showing environment of deposition - A) standard deviation vs. mean, B) standard deviation vs. Skewness, and C) simple sorting measure (SOS) vs. simple skewness measure (SKS).

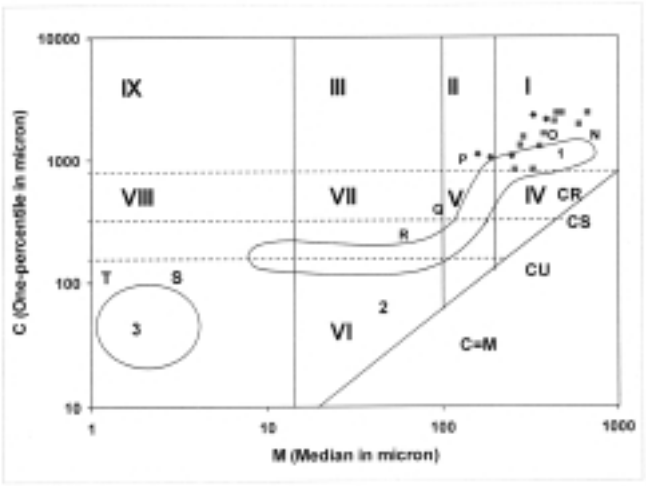

♦ - Samples of Salbardi area, ■ — Samples of Belkher area

Fig. 9. C-M plot showing concentration of grains in upper right corner.

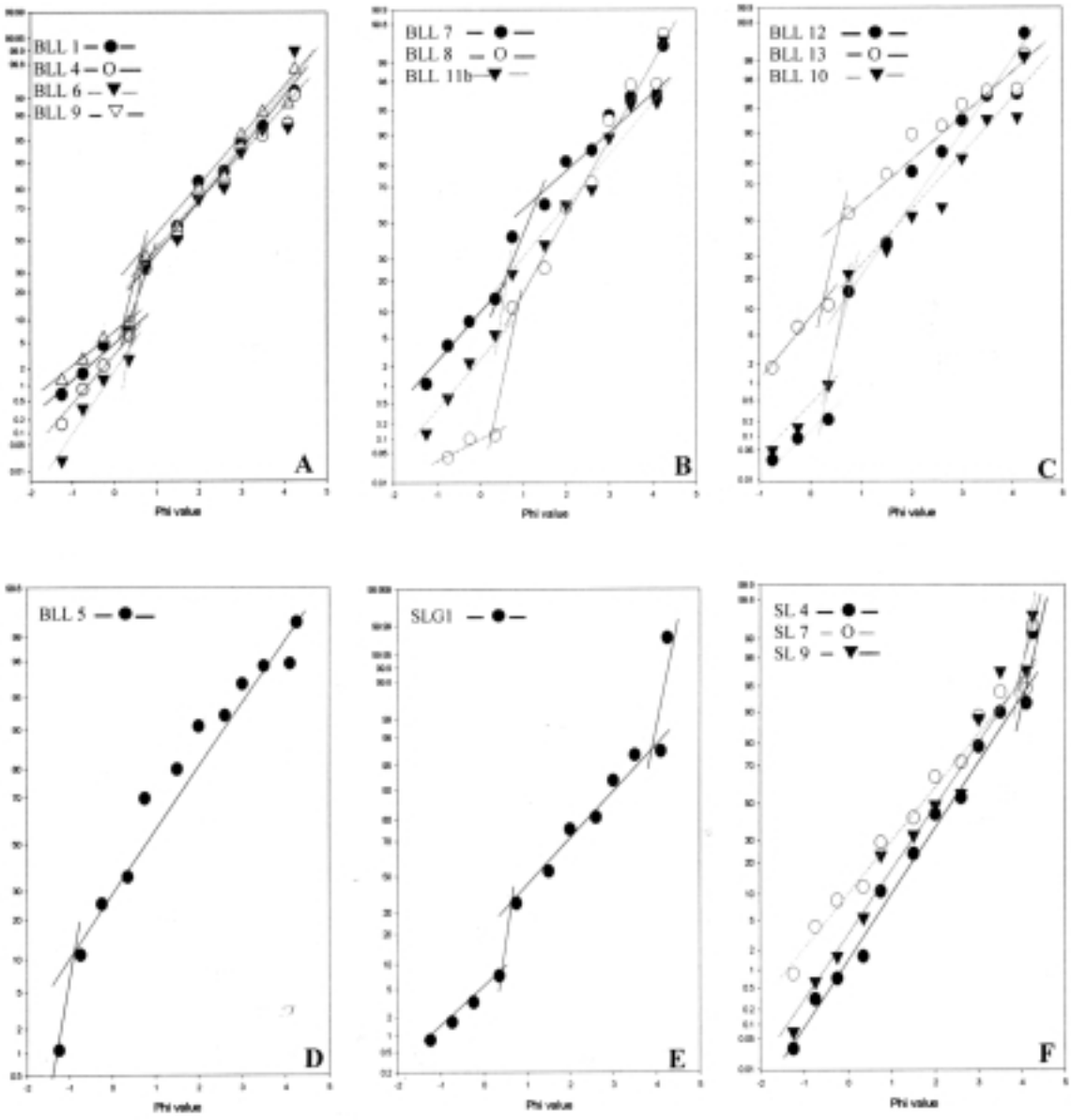

Fig. 10. Arithmetic probability curves (A to F) showing the trends of traction, saltation and suspension sub-populations of all samples.

size distribution and sediment transport. The plot is basically the representation of cumulatative grain-size distribution on the probability (ordinate) paper with a view to construct straight line sectors, known as sub-populations. The dimensions and inter-relationships of the sub-populations i.e., length, slope and intersection points provide an important information about mode of transporting i.e., traction, saltation and suspension. The log-probability plots of all the samples, in general, show that the major sub-population is of suspension followed by saltation, which is mainly due to the fine-grained nature of the sediments. The traction sub-population, though represented, but, constitutes a very less proportion (Figs. 10A, B, C, D & E). It is because of variable proportions of medium-grain sediments in a few samples. Most of the intersection points between traction and saltation sub-populations are close to 0.35ϕ value, whereas, it is closer to 1.0ϕ for saltation and suspension, wherever, the saltation is clearly demarcated by suspension. The general dominance of medium-grained sediments in a few samples are exhibited by a straight line graph which may show one traction point depending upon the content of fine-grained constituents in the admixture (Figs. 10F).

The dominance of suspension and saltation populations is comparable with established trend of modern and ancient fluvial deposits as proposed by Visher (1969).

CONCLUSIONS

Grain-size analysis of a total of sixteen sandstone samples belonging to calc-marl-arenaceous Lameta successions exposed at Belkher and Salbardi areas have been carried out. The sandstone units are restricted to the lower part of both the successions, however, thickness is comparatively more in Belkher area as compared to Salbardi area. The important conclusions drawn on the basis of granulometric analysis are as follows;

i. The frequency curves indicate a medium to fine-grained nature of the sediments, of which, medium-grained sand dominates. The same is also evident from the average mean-size value of the sediments.

ii. In general, the sediments are moderately sorted, near-symmetrically skewed and very leptokurtic in nature. However, skewness and kurtosis exhibits a wide range because of low to medium sorting of the sediments.

iii. The inter-relationship plots between mean, skewness, kurtosis and standard deviation as proposed by Folk and Ward (1957) indicate a unimodal to bimodal nature of the sediments. The principle mode is medium-sand which is mixed with coarse and fine-grained sands or silts.

iv. The plots between standard deviation vs. mean and standard deviation vs. skewness as proposed by Friedman (1967) and Moiola and Weiser (1968) indicate a fluvial environment of deposition. The same is also the outcome of SOS vs. SKS plot (Friedman, 1967).

v. The C-M pattern shows that the sediments are mostly rolled having little suspension, and deposited mainly by traction currents.

vi. The log-probability curves are also indicative of fluvial environment of deposition.

Acknowledgment: The authors are thankful to Sri. P. S. Parimal and Sri. P. S. Ingle, Department of Geology, SGB Amravati University, Amravati for their help and co-operation during field and laboratory studies.

References

Adyalkar, P.G. (1975). Palaeogeography, framework of sedimentation and groundwater potentialities of the upland alluvial valleys of India. Ph.D. thesis. Nag. Univ., Govt. of Maharashtra Publ., 261.

Bhusari, A.G. (1979). Mineral composition of the clay deposits near Achalpur, Amravati district, Maharashtra and Betul district of Madhya Pradesh. Min. Res., 5 (9), 8-10.

Deshpande, G.G. (1998). Geology of Maharashtra, Publ. Geol. Soc. India., Banglore, 221.

Folk R. L. and Ward, W. (1957). Brazos river bar: A study in the significance of grains size parameters. Jour. Sed. Pet., 27, 3-26.

Folk, R. L. (1980) Petrology of Sedimentary Rocks. Hemphill Austin, Texas, 159 p.

Friedman, G. M. (1961). Distinction between dune, beach and river sands from their textural characteristics. Jour. Sed. Pet., 31 (4), 514-529.

Friedman, G. M. (1967). Dynamic processes and statistical parameters compared for size frequency distribution of beach and river sands. Jour. Sed. Pet., 37 (2), 327-354.

Gawande, R.R. (2003). Facies analysis, palaeoecology and palaeoclimatology of Upper Gondwana succession (Early Cretaceous) of Bairam and adjoining area, districts Amravati, Maharashtra and Betul, Madhya Pradesh, Unpublished Ph.D. thesis, SGB Amravati University, Amravati, 157.

GSI. (2001) District Resource Map-Amravati district, Maharashtra, Govt. of India publ.

GSI. (2002). District Resource Map-Betul district, Madhya Pradesh, Govt. of India publ.

Ingram, R. L. (1971). Sieve analysis, In R. E. Carver (ed.) Procedures in Sedimentary Petrology. Wilson Interscience,49-68.

Kumar, S. and Tandon, K.K. (1978). *Thalassinoides* in the mottled nodular beds, Jabalpur area, M.P., Curr. Sci., 47, 52-53.

Kumar, S. and Tandon, K.K. (1979). Trace fossils and environment of deposition of the sedimentary succession of Jabalpur, M.P., Jour. Geol. Soc. India, 20, 103-106.

Kumar, S., Singh, M.P. and Mohabey, D.M. (1999). Lameta and Bagh beds, Central India. Field Guide., Pal. Soc. India Publ., Lucknow, 48.

Lindholmn, R. C. (1987). A Practical Approach to Sedimentology. Allen & Unwin Publ, 270.

Mohabey, D.M. and Samant, B. (2005). Lacustrine facies association of a Maastrichtian Lake (Lameta Formation) from Deccan volcanic terrain, Central India: Implication to deposition history, sediment cyclicity and climates. Gond. Geol. Mag. Spec. 8, 37-52.

Moiola, R. J. and Weiser, D. (1968). Textural parameters: An evaluation. Jour. Sed. Pet., 38 (1), 45-53.

Pascoe, E.H. (1959). Manual of Geology of India and Burma, 2, 3rd edition, Govt. of India Publ., New Delhi, 485-1344.

Passega, R. (1964). Grain size representation by C-M pattern as a geological tool. Jour. Sed. Pet., 34, 830-847.

Passega, R. and Byramjee, R. (1969). Grain size image of clastic deposits, Sedimentology, 13, 180-190.

Passega, R., (1957). Texture and characteristics of clastic deposition. Am. Assoc. Petrol. Geol., 41, 1952-1984.

Pettijohn, F.J. (1984). Sedimentary Rocks. 3rd edition, CBS Publ., New Delhi, 628.

Raiverman, V. (1995). Facies transition among Nimar, Bagh and Lameta beds. In Verma, V.K. (eds.), Researches in Geology, 2, 123-139.

Ravi Shankar, Gupta, S.K., Seth, N.N., Muthuraman, K., Pitale, U.L., Jangi, B.L., Gyan Prakash, Bandyopadhyaay, A.K. and Sinha, R.K. (1991). Geothermal Atlas of India, GSI. Spl. Publ. 19, 144.

Rawale, P.S. (2004). Detailed petrology and geochemistry of the Gondwana succession of Salbardi area, district Amravati, Maharashtra and district Betul, Madhya Pradesh with special reference to the environment of deposition. Unpublished Ph.D. thesis, SGB Amravati University, Amravati, 250.

Reineck, H.E. and Singh, I.B. (1980). Depositional Sedimentary Environments, 2nd edition., Springer-Verlag-Berlin, Heidelberg, New York, 543.

Saxena, R.K. (1987). Geothermal potential of Salbardi warm spring, districts Betul, Madhya Pradesh and Amravati, Maharashtra. Rec. Geol. Sur. India, 115, pt. 6, 175-183.

Sengupta, S. M. (1996). Introduction to Sedimentology. Oxford & IBH publishing Co-Pvt. Ltd., New Delhi, 305.

Srivastava A.K., Banubakode P.D., Kale V.M. and Patil G.V. (1996). Record of the trace fossils from Upper Gondwana succession of Bairam and adjoining area, district Amravati, Maharashtra. Gond. Geol. Mag. 11 (1), 33-44.

Srivastava, A.K. and Mankar, R.S. (2008) Lithofacies, depositional environment and age of upper Gondwana succession of Salbardi area, Amravati district, Maharashtra and Betul, Madhya Pradesh. Jour. Geol. Soc. India., 72, 190-198

Srivastava, A.K., Banubakode, P.D., Kale, V.M. and Patil, G.V. (1995). Record of Upper Gondwana flora from Bairam-Belkher area of district Amravati, Maharashtra and district Betul, Madhya Pradesh. Curr. Sci., 69 (5), 397-400.

Srivastava, A.K., Banubakode, P.D., Kale, V.M., Patil, G.V. and Manik, S.R. (1999). Lower Cretaceous plant fossil from Bairam-Belkher area, districts Amravati, Maharashtra and district Betul, Madhya Pradesh and their significance in stratigraphy. Palaeobotanist, 48, 39-48.

Srivastava, A.K., Manik, S.R., and Gawande, R.R. (2001). Record of genus *Hausmannia* dunkar from the Upper Gondwana succession of Bairam-Belkher area, Amravati district, Maharashtra and Betul district, Madhya Pradesh. Curr. Sci., 81(7), 756-757.

Srivastava, A.K., Manik, S.R., Patil, G.V. and Gawande, R.R. (2003). The genus *Araucarites* from Upper Gondwana succession (Early Cretaceous) of Bairam-Belkher area, district Amravati, Maharashtra and district Betul, Madhya Pradesh. Palaeobotanist, 53, 91-95.

Tandon, S.K. and Andrews, J.E. (2001). Lithofacies associations and stable isotopes of palustrine and calcrete carbonates: Examples from an India Maastrichtian regolith; Sedimentol., 48, 339-355.

Visher, G. S., (1969) Grain size distributions and depositional processes. Jour. Sed. Pet., 39, 1074-1106.

Jour. Indian Association of Sedimentologists, Vol. 28, No. 1 (2009), pp. 85-93

Hydrodynamic Processes and Heavy Mineral Distribution along Ekakula Beach, Gahirmatha Coast, NE Bay of Bengal

VEERANARAYANA, B[1], SIRISH CHANDRA, T[2]., SRIDHAR, P.N[1]., SATYANARAYANA REDDY, K[3]., LINDA, P. B.[2] and DHANANJAYA RAO, E. N[3]
[1]National Remote Sensing Agency, Hyderabad
[2]Dept. of Geology, Osmania University, Hyderabad
[3]Dept. of Geology, Andhra University, Visakhapatnam
E-mail: sirishct@yahoo.com

Abstract: The controlling factors for the formation of heavy minerals along the Ekakula beach of Gahirmatha coast, Orissa are complex. Erosion of beach and dunes by tide and tidal currents, wave induced currents, inducing inner shelf sediment transportation and alongshore currents cause frequent geomorphologic changes, sediment sorting and bathymetry variations. The shallow bathymetry of the shore regions and intertidal flats act as a sink for the sediments. The satellite data reveals the shape of the present study area to be circular causing nearshore circulation of sediments. This coast is under the influence of NE monsoon with considerable rainfall and river discharge resulting in the influx of heavies. All these hydrodynamic processes point out that the heavy minerals have been worked and reworked and concentrated along the coast. The textural analysis of sediments in three environments like Foreshore, Backshore and Frontal dune sands also affirms that the concentrations of heavies are controlled by various hydrodynamic processes.

Key words: Heavy minerals, Foreshore, Backshore, Frontal dune sands, Textures, Sink, Hydrodynamic processes.

INTRODUCTION

In general, the heavy mineral placer deposits that formed by mechanical concentration of detrital mineral particles were deposited mainly in the environment of rivers, beaches and offshore regions (Sherman 1996). The textural behavior of sediment may indicate the exact relevant physical and bio-geo chemical processes that acted upon them. Hydrodynamic processes like waves, tidal currents, wave-induced currents, longshore processes, sea level fluctuations, bathymetric changes, sediment circulation pattern and wind action have played their role in concentration of heavies in different environments. Acharya et al. (1998) have studied the grain size distribution and chemistry of Ekakula beach sands up to mid tide watermark, a small stretch along the Gahirmatha coast. This study is based on textural behavior and heavies' distribution that responds to changing environments and caused by relative hydrodynamic processes. High-resolution temporal satellite data can be useful for this tidally dynamic coast.

STUDY AREA

Gahirmatha coast in Orissa, NE Bay of Bengal is well known as the world's largest mass nesting ground of Olive Ridely turtles. It is a stretch about 35 km sandy beach with elongated sand spit in the NE extremity named as Ekakula. The present study area of interest extends from Satabya to NE extremity named as Ekakula spit about 16 km long and is located at 86°55' to 87°05' E longitude and 20°35' to 20°45' N latitude (Fig.1).

Morphologically the present coast is dynamic and an elongated barrier beach is separated from the main land by creeks of Maipura with mangroves up to southern Hansua River. The morphological features mainly in and around the study area are paleo- beach ridges, sand spit, sand bars, islands, channel bars, tidal flats and ebb tidal beaches, mangrove swamps and creeks, dune sands and, runnels and ripples on ebb beaches, which are highly influenced by all nearshore coastal processes (Fig.2). The majority of the river borne sediment is delivered by Brahmani River which is formed by the confluence of Koel and Sankh rivers, which divides into as Hansua in the southern direction and Maipura to the northeastern direction. The Brahmani river is joined by Baitarani to form Dhamra before it enters the Bay of Bengal. This meso-tidal coast, ranges between 0.4-3.8 m, giving rise to the shallow bathymetry directly in front of the river mouth. The presence of several islands at northeastern extremity acts as sink.

The catchment area of the Baitarani and Brahamani is dominantly Granitic terrain along with Eastern Ghat Granulites (i.e. khondalite, charnokite, leptynite, migmatite, pegmatite and gneisses) which contain heavy minerals like Ilmenite, Monazite, Zircon, Garnet, Magnetite, Hematite, Rutile, Sillimanite, Epidote,

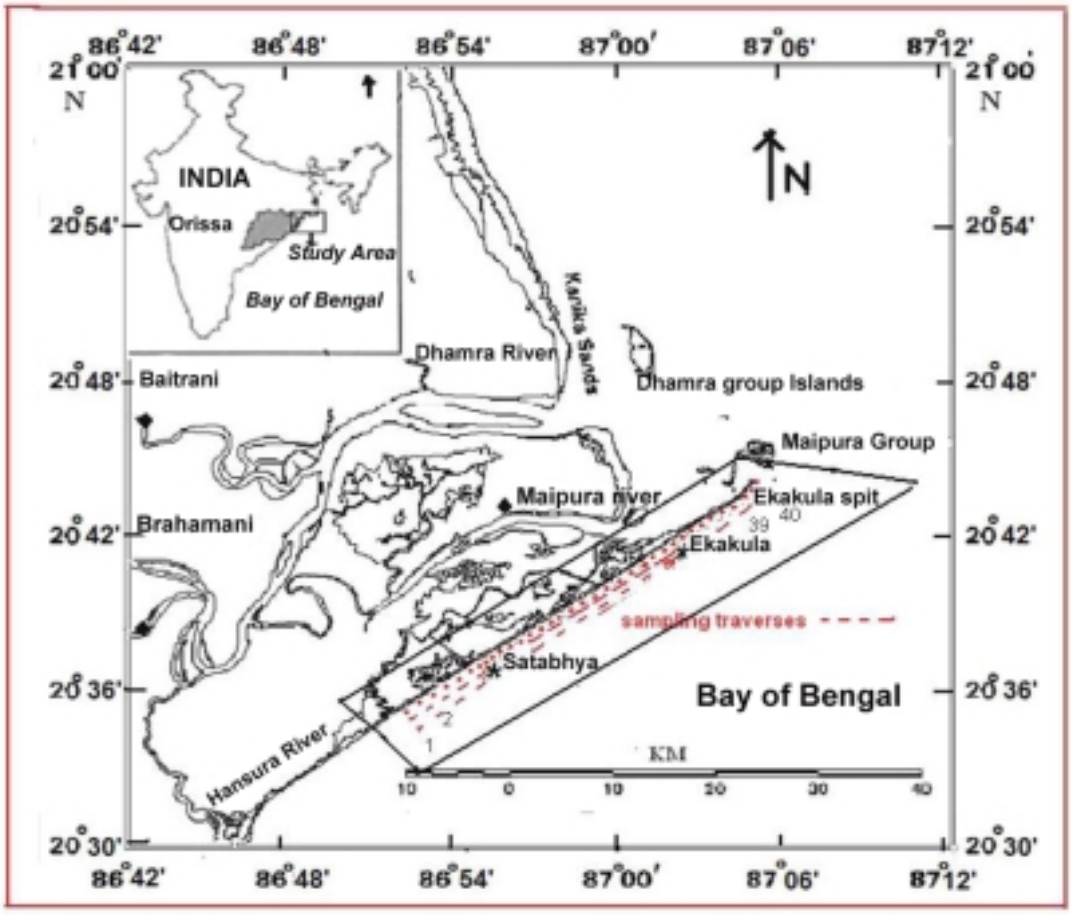

Fig. 1. Location map of the study area.

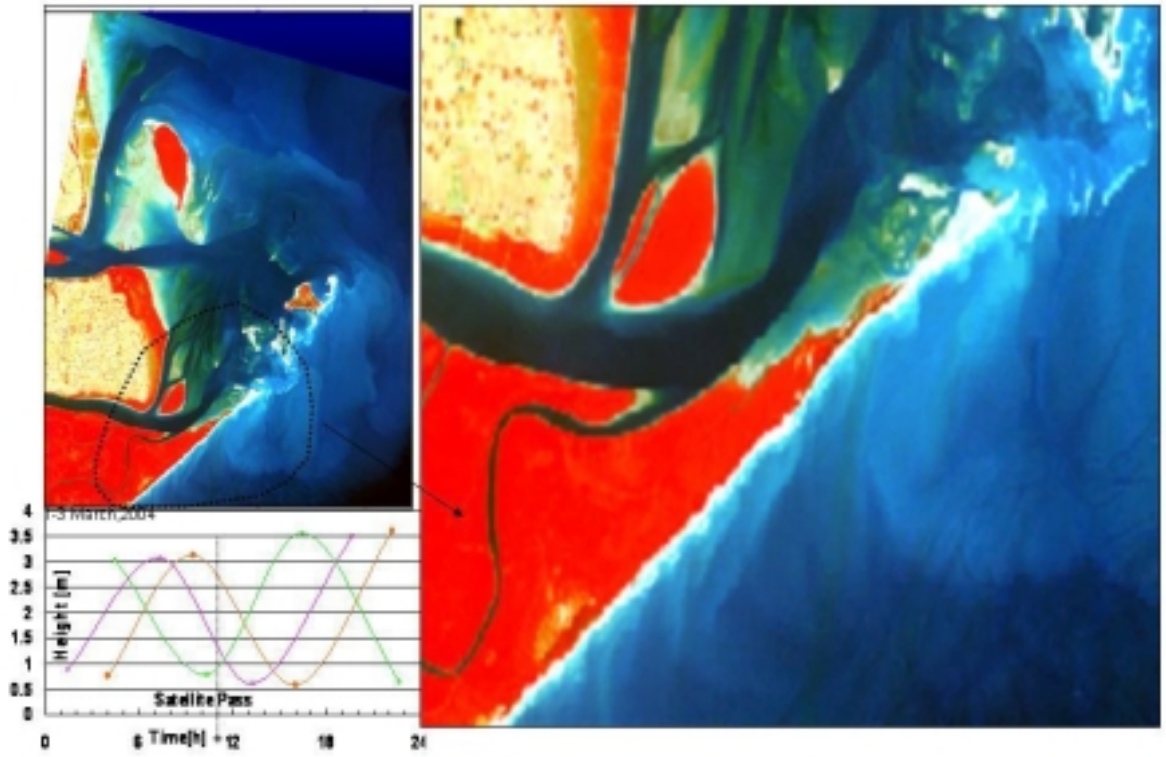

Fig. 2. Satellite data for the study area at low tide water level during 2004, March. (IRSP6-LISS IV).

Pyrobole together with lighter mineral grains like Quartz, Orthoclase and microcline etc., (Rao, 1998).

METHODS OF STUDY

Forty traverses were laid perpendicular to the coast with an interval of 400 m from Satabhya to NE extremity of Ekakula spit at the end of the post-monsoon period. Total 120 samples (40x3=120) were collected at three domains of interest along each traverse like, foreshore (especially ebb region) where the low tide water level starts up and backshore beach to the end of frontal dunes, which followed by the particular tidal datum i.e. low tide level from Indian tide tables. The representative samples were taken by cone and quartering after mixing uniformly for textural and mineralogical studies. About 50 gms of the dried bulk samples were sieved for textural studies at ¼ Ö interval in ASTM sieve sets.The weight percentage of each fraction was calculated and the cumulative curves were drawn on logarithmic graphs with respect to Ö (phi) values corresponding to the cumulative weight %. Folk and Ward (1957) method was used to measure the statistical textural characters viz.Mean (M_z), Standard deviation (ó), Skewness (S_k) and Kurtosis (K_G) of the samples and data was given in the Table1. Representative portion of the bulk samples were treated with 10% of HCl, 6% of H_2SO_4 and Stan's chloride for removing the carbonates, organic matter and ferrous oxide coating respectively. The treated samples were fractionized into +60 (>250µ), +120 (<250 to >125µ) and +230(<125 to >63 µ). Bromoform liquid was used to separate the heavies of the above sample fractions. Bar magnet was used to separate these heavies into magnetic and nonmagnetic fractions (Milner, 1967). Non-magnetic heavies were studied under Petrological microscope and number counted, and number percentages were calculated, which was multiplied by particular mineral specific gravity for calculating the individual heavy mineral weight percentages and result are given in the Tables 2. a & b.

IRS P6 - LISS IV, Resource-sat satellite Data (on 4th march, 2004) has been used for the present study (Pre-monsoon). The radiometric and atmospheric corrections for the above satellite data were made by using NRSC (National Remote sensing Centre) software's. Geometrically corrected and image enhancement of the above satellite data was done by using ERDAS Imagine software 9.0 (Fig.2). Tide data taken from the Indian Tide Tables and NHO (Naval Hydrography) charts were used to retrieve Bathymetry.

RESULTS AND DISCUSSION

The textures of foreshore (FS), backshore (BS) and frontal dune (FD) sands in the three environments of Ekakula beach, Gahirmatha coast are given in Table1.

The foreshore sediments are fine grained with Mean size (Mz) values varies from 1.91-3.21Ö (avg.2.72Ö). The backshore sediments are fine grained to very fine nature with Mz values varies from 2.3-3.5Ö (avg. 2.88Ö), while in frontal dunes are fine grained with Mz values varies from 2.2-3.15Ö (avg.2.52Ö). General, the sediments are fine grained in nature from Satabhya to Ekakula and are in coarse grained at the extreme end which is oriented in the NE direction. The foreshore and backshore sediments are well sorted with Standard deviation (ó) values varies from 0.30-0.59Ö (avg.0.48 Ö), and 0.31-0.61Ö (avg.0.42Ö), while in Frontal dunes are moderately well sorted with ó value varies from 0.45-0.62Ö (avg.0.59 Ö). The foreshore sediments and Frontal dune sands are coarse (-ve) skewed with S_k value varies from -0.32 to 0.12Ö (avg.-0.15Ö), and -0.27 to 0.01 Ö (avg.-0.14 Ö) respectively, while in Backshore sediments are near-symmetrical with S_k value varies from -0.31 to 0.51Ö (avg.-0.001Ö).The Backshore and Frontal dune sands are mesokurtic with Kurtosis (K_G) values varies from 0.81-1.42Ö (avg.1.00 Ö), and 0.80-1.38Ö (avg.1.02Ö), while in Foreshore sediments are leptokurtic with K_G value varies from 0.68-1.08Ö (avg.1.28).

The heavy mineral concentration in different fractions (+ 60, +120, +230) of Foreshore, Backshore and Frontal dune sands are given in Table 2.a. The total heavies are varying from 80.10-97.34% (avg.85.02%) in Foreshore region, 78.21-97.42% (avg.90.8%) in Backshore and 61.76-89.92% (avg.75.02%) in Frontal dune sands (Fig.5a). The heavy mineral concentration were more in finer fractions (+120, +230) than Coarse fraction (+60) at all the environments. The Magnetic mineral concentrations were varying from 8.64-24.97% in Foreshore, 8.92-25.56% in Backshore and 9.15-16.96% in Frontal dune sediments. The non-magnetic principal heavies are ilmenite (25.10 -58.44%), zircon (3.79 -5.38%), monazite (2.15%-4.98%), garnet (4.73-9.41%), rutile (2.60-5.29%), sillimanite (2.86%-3.81%), and pyroboles (3.63-6.39%) (Table2.b).The ilmenites are occurring as sub rounded to rounded shape, with exsolved, streaks and irregular laths present between the intergrowths. The ilmenite concentrations are more in Backshore than Foreshore and Frontal dune environments and its concentration is slightly decreasing towards NE end. The ilmenite concentrations are more in finer fractions (+120, +230) than coarse fraction (+60). Zircons are fine-grained with elliptical to subhedral form and also occurs as well-developed crystals with zoning and its concentration are more in finer fractions. The Monazites are yellowish colored, rounded to sub-rounded grains and its concentration are quite less in coarse fraction. The Garnets are angular to sub angular in shape with conchoidal to sub conchoidal fractures with sharp edges and the concentration is ranges from 5.12 – 12.1%. The Garnets concentration are decreasing from coarse fraction (+60) to the finer

Table 1. Textures of heavies in different environments of the Gahirmatha coast.

Traverse	Fore shore region				Back shore Region				Frontal Dunes		
	Mean	Standard Deviation	Skewness	Kurtosis	Mean	Standard Deviation	Skewness	Kurtosis	Mean	Standard Deviation	Skewness
1	2.32	0.35	0.09	1.38	2.60	0.35	-0.210	1.21	2.89	0.59	-0.15
2	2.41	0.48	-0.24	0.99	3.20	0.48	-0.020	1.42	3.15	0.55	-0.24
3	2.65	0.56	-0.18	1.20	2.90	0.44	-0.280	1.23	2.51	0.56	-0.22
4	2.97	0.39	-0.29	1.56	2.30	0.39	-0.130	1.11	2.40	0.60	-0.16
5	2.98	0.54	-0.22	1.48	2.90	0.51	-0.230	1.10	2.56	0.49	-0.11
6	2.78	0.48	-0.24	1.34	2.65	0.45	-0.120	0.81	3.12	0.56	0.01
7	3.10	0.44	0.03	1.45	3.20	0.48	-0.300	0.99	2.55	0.55	-0.13
8	2.80	0.49	-0.29	1.34	2.50	0.31	-0.060	0.86	2.32	0.59	-0.15
9	2.25	0.51	-0.12	0.90	3.51	0.39	0.480	1.21	2.56	0.61	-0.14
10	2.21	0.53	-0.18	1.38	3.20	0.45	0.230	1.34	2.80	0.59	-0.19
11	2.80	0.37	-0.12	1.45	2.80	0.35	-0.280	1.41	2.45	0.62	-0.26
12	2.60	0.46	-0.22	1.44	2.40	0.45	0.490	1.22	2.56	0.56	-0.27
13	2.21	0.58	-0.12	0.70	2.80	0.34	-0.230	1.10	2.50	0.61	-0.23
14	3.21	0.43	-0.10	1.40	2.70	0.61	-0.310	0.84	2.34	0.59	-0.22
15	2.52	0.44	-0.23	1.45	2.90	0.45	-0.100	0.98	2.45	0.60	-0.26
16	2.50	0.48	0.07	1.38	3.20	0.38	-0.180	0.91	2.55	0.57	-0.14
17	2.76	0.53	-0.14	1.58	3.11	0.36	-0.040	0.98	2.82	0.59	-0.09
18	3.07	0.49	-0.24	1.49	3.09	0.45	-0.010	1.21	2.32	0.55	-0.03
19	2.57	0.55	0.12	1.22	2.45	0.36	0.510	1.10	2.54	0.61	-0.02
20	2.69	0.59	-0.11	1.33	2.47	0.49	-0.300	1.34	2.20	0.58	-0.01
21	2.46	0.43	-0.14	1.34	2.67	0.41	-0.100	0.90	2.60	0.58	-0.09
22	2.78	0.30	-0.23	1.56	2.89	0.47	-0.270	0.88	2.58	0.62	-0.04
23	2.88	0.45	-0.29	0.68	3.21	0.43	-0.300	0.91	2.81	0.58	-0.09
24	2.96	0.39	-0.32	1.34	3.41	0.52	0.020	0.87	2.54	0.55	-0.14
25	3.16	0.49	-0.23	1.28	2.40	0.34	-0.300	1.20	2.65	0.61	-0.11
26	2.87	0.38	-0.27	1.22	2.56	0.48	0.450	1.10	2.47	0.57	-0.16
27	2.75	0.53	-0.12	1.34	3.12	0.34	-0.040	1.33	2.50	0.54	-0.14
28	2.89	0.43	-0.16	1.46	3.45	0.39	-0.250	1.05	2.64	0.61	-0.11
29	2.21	0.45	-0.10	0.92	2.80	0.48	0.490	1.18	2.69	0.58	-0.22
30	2.67	0.48	-0.12	1.23	2.45	0.46	-0.040	0.87	3.05	0.59	-0.15
31	2.89	0.49	0.01	1.34	2.67	0.33	-0.300	0.94	2.56	0.55	-0.18
32	2.66	0.57	-0.17	1.45	2.56	0.43	-0.240	0.99	2.34	0.60	-0.12
33	2.74	0.54	-0.23	1.39	2.45	0.39	-0.020	1.10	2.45	0.56	-0.18
34	2.98	0.44	-0.29	0.70	2.98	0.44	0.500	0.86	2.59	0.59	-0.13
35	2.88	0.54	0.08	1.22	2.76	0.48	-0.020	0.88	2.45	0.59	-0.10
36	2.67	0.56	-0.24	1.32	3.32	0.40	-0.110	0.85	2.59	0.58	-0.09
37	2.65	0.47	-0.08	0.87	3.43	0.36	-0.280	1.01	2.88	0.52	-0.17
38	2.98	0.49	0.02	1.44	3.48	0.32	-0.010	1.23	2.32	0.57	-0.13
39	1.91	0.52	-0.18	1.23	2.87	0.45	-0.230	1.10	2.43	0.53	-0.11
40	2.89	0.38	-0.24	1.21	3.20	0.39	-0.290	1.32	2.32	0.59	-0.18
	Avg:2.72 Min-max: 1.91-3.21	Avg:0.48 Min-max: 0.30-0.59	Avg:-0.15; Min-max: -0.32 0.12	Avg:1.28; Min-max: 0.68-1.58	Avg:2.88 Min-max: 2.30-3.51	Avg:0.42; Min-max: 0.31-0.61	Avg:-0.001; Min-max: -0.31 to 0.51	Avg:1.00; Min-max: 0.81-1.42	Avg:2.52 Min-max: 2.2-3.15	Avg:0.59; Min-max: 0.45-0.62	Avg:-0.14; Min-max: -0.27 to 0.01

Table 2a. Total Heavies weight percentage in different fractions of the Gahirmatha coast.

Traverse	Foreshore (FS)					Backshore (BS)					Frontal dune (FD)				
	Heavies Wt%			Total Heavies Wt%	Magnetic Wt%	Heavies Wt%			Total Heavies Wt%	Magnetic Wt%	Heavies Wt%			Total Heavies Wt%	Magnetic Wt%
	.+60	.+120	.+230			.+60	.+120	.+230			.+60	.+120	.+230		
1	0.52	81.07	10.62	92.21	8.64	2.04	79.41	12.97	94.42	8.91	1.26	70.80	14.86	86.92	11.10
2	2.20	83.61	9.40	95.21	11.89	3.72	81.95	11.75	97.42	11.98	2.94	73.34	13.64	89.92	9.15
3	3.10	78.53	12.00	93.63	10.81	4.62	76.87	14.35	95.84	16.02	3.84	58.26	16.24	78.34	16.03
4	1.20	77.02	14.12	92.34	14.9	2.72	75.36	16.47	94.55	19.25	1.94	56.75	18.36	77.05	12.25
5	0.60	84.13	9.50	94.23	19.51	2.12	82.47	11.85	96.44	15.90	1.34	63.86	13.74	78.94	12.71
6	0.79	80.60	6.81	88.20	14.74	2.31	78.94	9.16	90.41	17.54	1.53	60.33	11.05	72.91	12.97
7	1.20	75.50	15.30	92.00	11.89	2.72	73.84	17.65	94.21	15.34	1.94	54.78	19.99	76.71	11.53
8	2.10	80.04	12.20	94.34	13.88	3.62	78.38	14.55	96.55	14.28	2.41	59.75	16.89	79.05	12.89
9	2.50	70.03	16.70	89.23	18.23	4.02	68.37	19.05	91.44	24.02	2.81	49.74	21.39	73.94	12.66
10	4.50	65.53	21.20	91.23	21.37	3.25	66.00	19.64	88.89	22.59	2.04	53.64	21.98	77.66	11.79
11	3.90	68.03	16.30	88.23	21.69	2.65	68.50	14.74	85.89	21.89	1.44	56.14	17.08	74.66	12.77
12	4.70	61.42	25.00	91.12	18.42	3.45	61.89	23.44	88.78	19.61	2.24	49.53	25.78	77.55	16.00
13	5.10	54.13	28.00	87.23	23.33	3.85	54.60	26.44	84.89	19.01	2.64	42.24	28.78	73.66	12.38
14	0.40	71.49	22.34	94.23	19.65	1.65	69.46	20.78	91.89	16.52	0.44	57.10	23.12	80.66	16.96
15	0.51	53.29	35.20	89.00	24.97	1.76	51.26	33.64	86.66	14.62	0.55	38.90	35.98	75.43	16.09
16	2.40	79.62	13.21	95.23	21.76	1.15	80.09	11.65	92.89	16.03	0.35	67.32	13.99	81.66	11.46
17	1.80	71.53	15.00	88.33	16.65	0.55	72.00	13.44	85.99	13.90	0.12	58.87	11.77	70.76	11.13
18	3.20	80.01	13.00	96.21	16.86	1.95	76.64	15.28	93.87	14.29	1.15	63.88	13.61	78.64	9.65
19	2.30	74.70	17.00	94.00	11.89	4.45	67.93	19.28	91.66	20.27	3.65	55.17	17.61	76.43	14.13
20	2.40	70.92	19.00	92.32	14.45	4.55	64.15	21.28	89.98	21.39	3.75	51.39	19.61	74.75	14.13
21	3.20	73.03	15.00	91.23	20.46	5.35	66.26	17.28	88.89	24.02	4.55	53.50	15.61	73.66	15.05
22	4.20	79.14	14.00	97.34	16.6	6.35	72.82	16.28	95.45	25.56	5.55	60.06	14.61	80.22	15.88
23	3.12	78.50	6.66	88.28	13.87	5.27	72.18	8.94	86.39	23.51	4.47	59.42	7.27	71.16	12.99
24	2.80	78.20	14.23	95.23	18.62	4.95	71.88	16.51	93.34	20.16	3.72	55.32	19.07	78.11	14.91
25	3.10	69.12	17.10	89.32	21.74	5.25	62.80	19.38	87.43	21.23	4.02	45.02	21.94	70.98	12.68
26	3.30	65.70	23.00	92.00	20.22	5.45	59.38	25.28	90.11	21.47	4.22	41.60	27.84	73.66	16.55
27	4.10	62.90	28.00	95.00	23.55	6.25	61.10	25.76	93.11	22.21	5.02	43.32	28.32	76.66	16.48
28	2.80	58.00	32.20	93.00	22.6	4.95	56.20	29.96	91.11	18.88	3.72	38.42	32.52	74.66	13.13
29	2.50	35.50	42.10	80.10	24.7	4.65	33.70	39.86	78.21	21.32	3.42	15.92	42.42	61.76	15.77
30	3.20	63.80	19.00	86.00	19.35	1.64	65.71	16.76	84.11	19.12	0.41	47.93	19.32	67.66	15.13
31	3.40	58.83	21.00	83.23	16.91	1.84	64.76	18.76	85.36	19.24	0.61	46.98	21.32	68.91	15.64
32	2.10	70.30	16.00	88.40	15.44	0.54	76.23	13.76	90.53	17.80	0.21	58.53	15.34	74.08	12.22
33	1.20	73.92	14.00	89.12	17.96	2.76	76.73	11.76	91.25	17.31	1.73	55.95	13.34	71.02	14.21
34	1.30	67.93	17.00	86.23	14.67	2.86	65.26	20.24	88.36	14.46	1.83	44.48	21.82	68.13	15.90
35	1.21	65.02	22.00	88.23	16.01	2.77	62.35	25.24	90.36	17.49	1.74	41.57	26.82	70.13	13.01
36	1.01	73.11	13.00	87.12	14.98	2.57	70.44	16.24	89.25	22.46	1.54	49.66	17.82	69.02	16.68
37	1.30	78.59	12.23	92.12	12.58	2.86	75.92	15.47	94.25	17.77	1.83	55.14	17.05	74.02	13.21
38	1.37	82.86	10.00	94.23	14.77	2.93	80.19	13.24	96.36	20.01	1.90	59.41	14.82	76.13	11.01
39	2.30	75.82	11.00	89.12	15.46	3.86	73.15	14.24	91.25	21.87	2.83	52.37	15.82	71.02	14.01
40	1.14	75.98	15.00	86.09	14.01	2.70	73.31	18.24	94.25	20.23	1.67	52.53	19.82	74.02	14.34
Avg	2.35	71.2	17.36	85.02	17.21	3.32	69.2	18.27	90.8	18.74	2.33	52.97	19.71	75.02	13.66

Table 2b. Average mineral Wt% in +60,+120 and +230 fractions of the three environments.

Mineral	Fore shore (FS)			Back shore (BS)			Frontal Dunes (FD)		
	.+60	.+120	.+230	.+60	.+120	.+230	.+60	.+120	.+230
Ilmanite	25.10	53.66	54.92	33.8	56.93	58.44	29.10	54.66	56.30
Zircon	4.07	3.99	4.48	5.07	5.27	3.79	4.59	5.02	4.33
Monazite	2.72	3.91	4.98	2.15	4.22	4.43	2.51	3.67	4.79
Garnet	7.59	8.10	6.19	9.41	6.71	4.73	8.35	7.59	5.93
Rutile	2.60	3.53	3.72	4.08	5.29	5.21	3.24	3.89	4.51
Sillimanite	2.86	3.51	3.77	3.19	3.26	3.82	3.07	3.38	3.81
Pyroboles	3.63	4.20	4.51	5.19	5.92	6.39	4.37	5.24	5.21
Unknown	51.3	19.21	17.51	37.11	12.41	13.19	44.87	16.56	14.96

Fig. 3a. Winnowing lighters from the foreshore (ebb) region, **b.** Wave wash and erode berm, **c.** Runnels and ripples on ebb region, and **d.** Frontal dune sands.

fractions (+120 and+230) in all environments (Figs.5.b, c, d). Rutiles are sub rounded and Sillimanites are in elongated shape. Except ilmenites and garnets, all other heavy mineral concentrations are more are less shows quite variation in all fractions (Fig.5.b-d).

Hydrodynamic processes relative to the heavies distribution

The understanding of the hydrodynamic processes along this coast helps us to infer the formation of heavies along the coast (Fig. 4). Wave and currents sort equally distributing grain size orientation and their shape with about 90% of the black sands in fine range (+120). The -ve skewness indicates that the dunes are eroded by storm waves and reworked fines are lost. Samples are drawn from area where heavies are concentrated due to winnowing of light minerals, enriched in fine for the –ve Skewness (Mislankar and Gujar, 1996). Predominantly beach placers dominated by coarser light minerals, further may be attributed to deflation effects on the windward dune slope or removal of fines by high waves associated with events like storms. Onshore winds are variable in strength along the coast and deflate the dunes in some pockets, the sands are –ve skewed in deflate dunes and +ve skewed in others (Fig. 3d). Platy to meso-kurtic reflects poor sorted nature, while lepto-kurtic indicates better sorting. Symmetrical Skewness

and decrease in sorting to certain extent is probably due to influx of coarse sands into fine beach sands from the river mouth of mobility from sorting of sands in response to high energy environment associated with strong out flow interacted with incoming waves and currents.

Sediments are subjected to high wave energy surf zone which is indicated by fractures in Garnet which were developed by wave induced collision (Acharya et al. 1998). Well-rounded, fine grained and well sorted nature of the black minerals is due to mechanical reworking by waves and tidal currents (Ramamohana Rao et al. 1982). In the ebb-tidal region the grains are arranged in a bed that affects the stability of the surface grain, and is harder for the fluid flow to move the grain out of a densely packed surface (Fig. 3.a). This activity exists subject to the wave and current interaction. The runnels are found on the surfaces (Fig. 3.c) which indicate the ebb flow current is more than that of flood (1 m - 1.5 m). The width of ebb tidal beach ranges from 200 – 600 m and tide level varies 0.5-3.8 m, which is compacted due to well sorted grains. The wind is responsible for the transport of lighter sediment grains over the ebb flat region and development of various landform morphological features or mixing in tidal flat region of estuarine delta, located just beyond the spit (Fig. 3a). From the NHO chart, the sub-aqua's slope (gentle to very steep) indicates the off shore wave dissipation which has a strong influence on the grain sorting (Shepard and Inman, 1950). Thus, the proximity to wave breaking further offshore results in these heavies, which are mechanically worked and reworked over a long period (Fig.4). The shallow waters lead to the sediment sorting shoreward. The velocity under crest which is higher, but shorter in lengths can move both heavies and lighter minerals. Nevertheless, the offshore velocity under trough, which is lower with longer duration, may transport only the lighter grains leading to the net shoreward moment of the heavies (Fig.3.c) (Chauhan,1992). Another important aspect is that there is no estuary between the river and sea, which can act as a sink for sediment. Therefore, whatever sediment is brought by the river is directly discharged into sea. Therefore, it is possible that the river has contributed to the enhancement of the heavies along the coast. The tidal derived coast currents are often and strongly asymmetrical resulting in dominant longshore transport of sediment away from the river mouth in high tidal ranges. The alternate stratified layers have undergone sorting before deposition on the shallow depths or shelf (Hughes, 1984). Repeatedly they are washed out by the currents carrying the lighter grains and leaving the heavies on the backshore regions (Fig.3.b). These shelf minerals contribute to the beach due to storm waves produced by strong winds. The occurrence of black sands in thin layers in the berm of dried up beds up to 3 m - 5 m depth, suggest that the source is from the fluid discharge, which is not flowing in to the beach but is

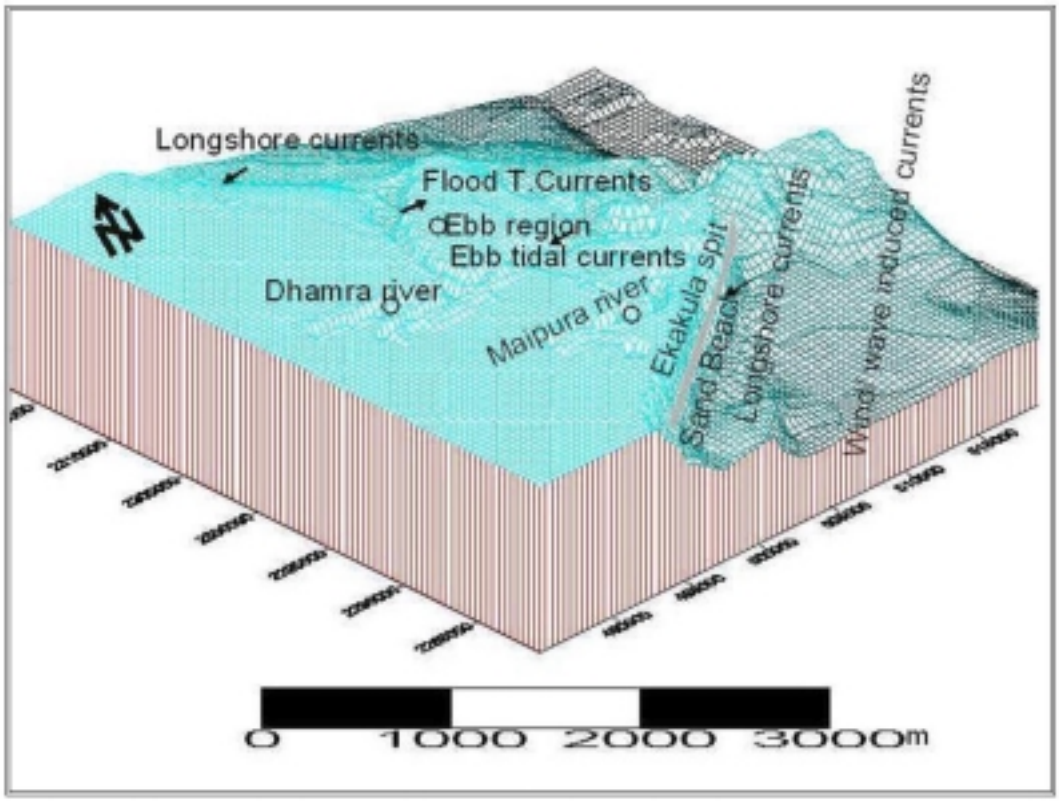

Fig. 4. Model showing the Hydrodynamics of Gahirmatha coast.

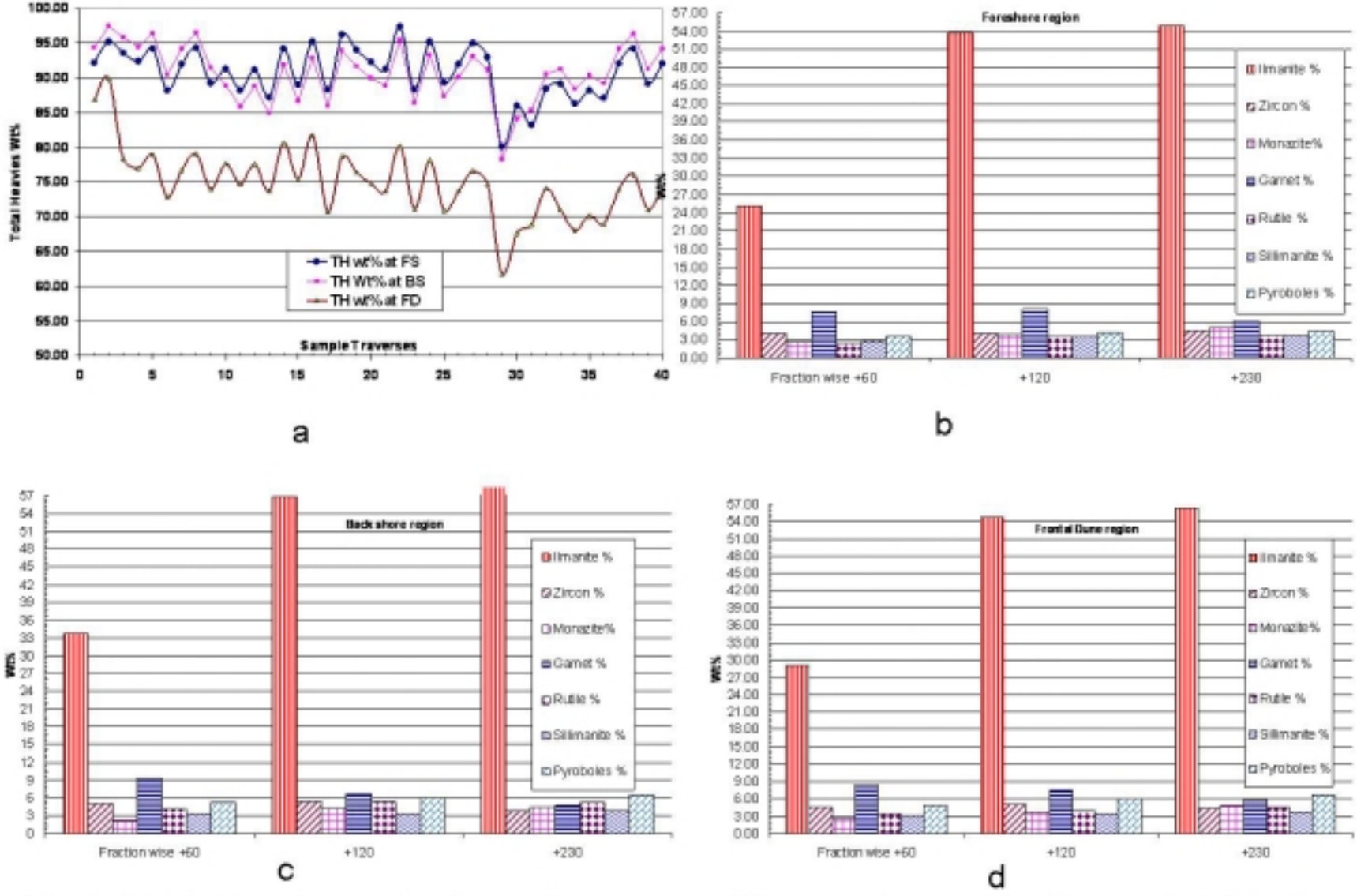

Fig.5a. Total heavies varies from all traverses of three environments, b. avg., individual heavy mineral wt% in different fractions of FS, **c.** BS and **d.** FD.

only a recycled mechanical work done by waves and currents including tidal currents. The fresh sediments deposited are not only from the rivers, floods but also from the storms and cyclones which can cause instability of the spit (Prusty et al. 2001). The shallow bathometry around the islands (2 m - 5 m) which shelters shoals, sand bars can cause wave-induced currents circulated around it by the sediments (Tarang Khangaonkar et al. 1998).

CONCLUSIONS

The hydrodynamic process along this coast is clearly understood and gives an inference of the formation of heavies along the coast. The dominance of particular size and sorting of sediments in any area reflects the composition and replicated by the near shore parameters. The coast is morphologically dynamic not only due to frequent cyclonic storms but is also due to shallow bathymetry, high tidal regime, wave induced currents, beach-dune erosion and sea level oscillation (Fig.4). As a result of, shallow depths and ebb/flood tidal influence, the sediments are mechanically reworked for a long time by counter and anti-counter circulations in nature.

Acknowledgements: The Authors are thankful to chief conservator (Forest Ranger) of Baitaranika mangrove wildlife forest, Govt. of Orissa for providing necessary facilities in the field and proper guided. Also are thankful to the Director, NRSC, Hyderabad, A.P. for providing the satellite data and required softwares. The authors are grateful to the Head, Department of Geology, Osmania University, Hyderabad and Andhra University, Waltair, A.P., India for the help rendered during the progress of the study.

References

Acharya, B.C., Panigrahy, P.K., Nayak B.B. and Ksahoo, R. (1998). Heavy mineral Placer deposits of Ekakula beach, Gahirmatha coast, Orissa coast. Resource Geology, 48 (2), 125-136.

Chauhan, O S. (1992). Sediment dynamics at Puri and konark beaches, along NE coast of India. Indian Jour. Mar. Sci., 21, 201-206.

Folk, R.I. and Ward, W.C. (1957). Brazos river bar study in the significance of grain size parameters. Jour. Sed. Petrology., 27, 3-27.

Hughes,S.A. (1984). The TMA Shallow-water Spectrum Description and Applications, Technical Report CERC-84-7, US Army Engineer Waterways Experiment Station, Vicksburg, MS. (December).

Mislankar, P. G. and Gujar, A. R. (1996). Heavy mineral distribution in the surfacial sediments from Eastern continental margin of India and their implication on paleo-environment, Indian Jour. Of Earth Science, 23 (3-4), 91-97.

Milner, I. (1967). Sedimentary Petrography, 643 (George Allen & Unwin Ltd –London).

Prusty, B. G., Sahoo, R. K. and Mehta ,S.D. (2001). Natural causes lead to mass exodus of Olive Ridely Turtles from Ekakulanasi, Orissa, India: A need alternate, Sea turtles,1-8.

Ramamohana Rao, T., Shanmukha Rao ,Ch. and SanyasiRao, K. (1982). Textural analysis and mineralogy of the black sand deposit of Visakhapatnam –Bhimunipatnam coast , A.P, India. Jour. Geol. Soc. India., 23, 284-289.

Rao, A.T. (1998). Geology and Tectonic evolution of the Indian Rivers. A Field Seminar on recent deltas, 25-30.

Shepard, F.P. and Inman,D.L. (1950). Nearshore water circulation due to bottom topography and wave refraction. Trans., American Geophy., Union, 31(2), 196-212.

Sherman. (1996). Over view of regional coastal process and controls. US Army corps of Engi., By Larson and Nicholas C.Kraus.

Tarang Khangaonkar., Felix Kristanovich., Mizan Rashid. and Bankim Mallick (1998). Tidal circulation and sediment transport modeling for port Dhamre-Chandbali expansion project. Technical papers, Port Dhamra documents.

Jour. Indian Association of Sedimentologists, Vol. 28, No. 1 (2009), pp. 95-99

Preliminary Studies of Grass Phytoliths in the Coastal areas around Navsari, South Gujarat : Micro-Environmental Implications

RINKU J. DESAI and VINAY M. RAOLE
Department of Botany, Faculty of Science,
The Maharaja Sayajirao University of Baroda, Vadodara-390002, Gujarat
E-mail: vinayraole@yahoomail.com

Abstract: The coastal areas in and around Navsari, forms an integral part of South Gujarat Alluvial plains; comprising silts, clays and sands of Holocene age occupying the newer and older alluvial and marshy areas which are mostly rich in grasses and shrubs. Grasses are present in varied climatic conditions and produce many types of phytoliths. Presence of grass phytoliths in sediments indicates local geomorphological variation and spatial heterogeneity associated with plant distribution. Phytoliths from the surface samples of the study area represents nine different grass species that depicts diverse phytolith assemblages and are grouped in five forms on the basis of their form and size.

Keywords: Grass phytoliths, Alluvial plain, South Gujarat.

INTRODUCTION

The name phytolith comes from the Greek words 'Phyto' (plant) and 'Lithos' (stones); its meaning refers to the particles of vegetal origin. Phytoliths are opaline microscopic silica bodies that occur in many plant families (Piperno 1988, 2001), but are especially abundant, diverse, and distinctive in the family Poaceae i. e. Grass family (Blackman 1971, Brown 1984, Piperno & Pearsall 1998). Other synonyms for phytoliths are opal phytolith, silica cells, grass opal, plant opal or biogenic opal. Phytoliths are released from plant tissues when they are decayed, burned, or digested and produce many types which are robust due to squat forms. Many taxa in Poaceae are characterized by their phytoliths assemblages with specific morphological characteristics and have taxonomic significance. Because of redundancy and multiplicity in phytolith shape (Rovner 1971, Mulholland 1989, Fredlund & Tieszen 1994), one phytolith type can rarely be related to one plant taxon and therefore in order to use phytoliths to discern taxonomic meaning a variety of phytolith forms must be considered. Hence, more generally they are identifiable at the plant family or tribe level and often plants can be identified at species level also.

Earlier, phytolith morphology, taxonomy and its applications have been the subjected to archaeological and paleo-environmental researches (Bowdery *et al*. 2001, Horrocks *et al*. 2000, Piperno 1988, Rovner 1988). Phytolith assemblages have recently been shown to be a promising tool to discriminate between the various grasslands (Fredlund & Tieszen 1994, Alexandre *et al*. 1997, Barboni *et al*. 1999). However, until recently very little attention has been paid to the use of phytoliths in the study of coastal environmental changes from different areas of the world (Fearn 1998, Horrocks *et al*. 2000, Lu & Liu 2005).

The coastal zones of the Navsari consist of different habitats such as fresh marshes, new and old alluvial plains with various vegetation types. These habitats are unique in nature, support a variety of genera and maintain the ecological health. The coastal environments create special challenges to Quaternary paleo-environmental reconstruction using conventional palaeo-ecological techniques such as pollen analysis (Bermond 2005a**).** Since the grass pollens cannot be identified below the family level however this constraint can be overcome by grass phytolith analysis (Bermond 2005b, Lu & Liu 2003).Grass phytoliths have been used to determine past ecological conditions (Rovner 1971), soil genesis (Twiss *et al.* 1969) and identify plants used by people in ancient and prehistoric periods (Rovner 1983). A classification of grass phytoliths is a prerequisite for effective use of silica bodies in palaeo-ecological studies and micro environmental changes (Krishanan *et al.* 2000).

The present report deals with the pioneer investigation of phytoliths in modern grasses growing in the coastal environments of Navsari district, which can be used as proxy for re-constructing the environmental changes occurring at micro-levels. Such indicators, when properly studied, help to predict locations and potential shifts of vegetation limits in response to past or future micro-environmental changes (Cramer 2002).

MATERIALS AND METHODS

Species Selection

Commonly known nine species of grasses belonging to Andropogoneae at flowering stage were collected from the Newer and older alluvial plain as well as from the marshy areas of Navsari, Gujarat (Fig. 1).

Phytolith Extraction

Two leaves below the flag leaf were sampled. Wash with distilled water and dried at 56ºC and charred at 600ºC for 2 hr. Ash were boiled in a 5 N HCl for 20 min. Washed with distilled water and filtered with Whatman filter paper No.1, until no more chloride ions were detected. Material was ignited at 760ºC for 2-5 hr. Final ashes mounted in Glycerin and observed by using a Leica Research microscope (Labouriau 1983, Parr *et al*. 2001, Honaine *et al*. 2006). Photomicrographs from all the studied plants are shown in fig 2. Observed phytoliths were classified following the schemes given by the ICPN (2005) & Madella *et al*. (2003) and summarized in Table 1.

RESULTS AND DISCUSSION

Phytolith from collected grasses showed a diverse phytolith assemblage, divided into 3 major groups on the basis of their form, size and wall ornamentation. Five morphotypes of the opaline phytoliths were extracted from 9 different grass species included in this study (Fig 2). The representative grasses have been segregated from prevailing varied micro environmental conditions, such as marshy area, newer alluvial plains and older alluvial plains (Table 1).

The dominant grasses from marshy area, such as *Ischaemum* spp., *Eremopogon* and *Iseilem*a produce primarily Dumbbell (A) as well as small short, Rondel/ Crenate shaped phytoliths (C), along with few Cross type (B) and elongated or broad Wavy Trapezoid morphophytes (E) (Fig 2: Group 1). The grasses from newer alluvial plains, such as *Vetiveria* and *Ischaemum* depict presence of more number of Dumbbell (A), Cross (B) phytoliths and shorter and broad Smooth Trapezoid forms (D) along with few broader and Wavy Trapezoid forms (E) (Fig 2: Group 2). While, the grasses from older alluvial plains, such as *Sorghum* and *Cymbopogon* produce more amount of Dumbbell (A) as well as small short Rondel/ Crenate shaped (C) phytoliths along with very small amount of Smooth Trapezoid morphophytes (D). (Fig 2: Group 3)

The phytolith types identified in the present investigation are characteristic of tribe Andropogoneae family Poaceae described by ICPN (2005). Previous reports on phytolith studies have focused mainly on broad vegetation types of temperate and tropical grasslands (Blinnikov 2005) and understanding the coastal environment. Within the study the predominance of Dumbbell, crenate/ rondel and wavy Trapezoid phytoliths in a sediment sample indicate salt marshy environment and further subdivided in to fresh water marshes and brackish

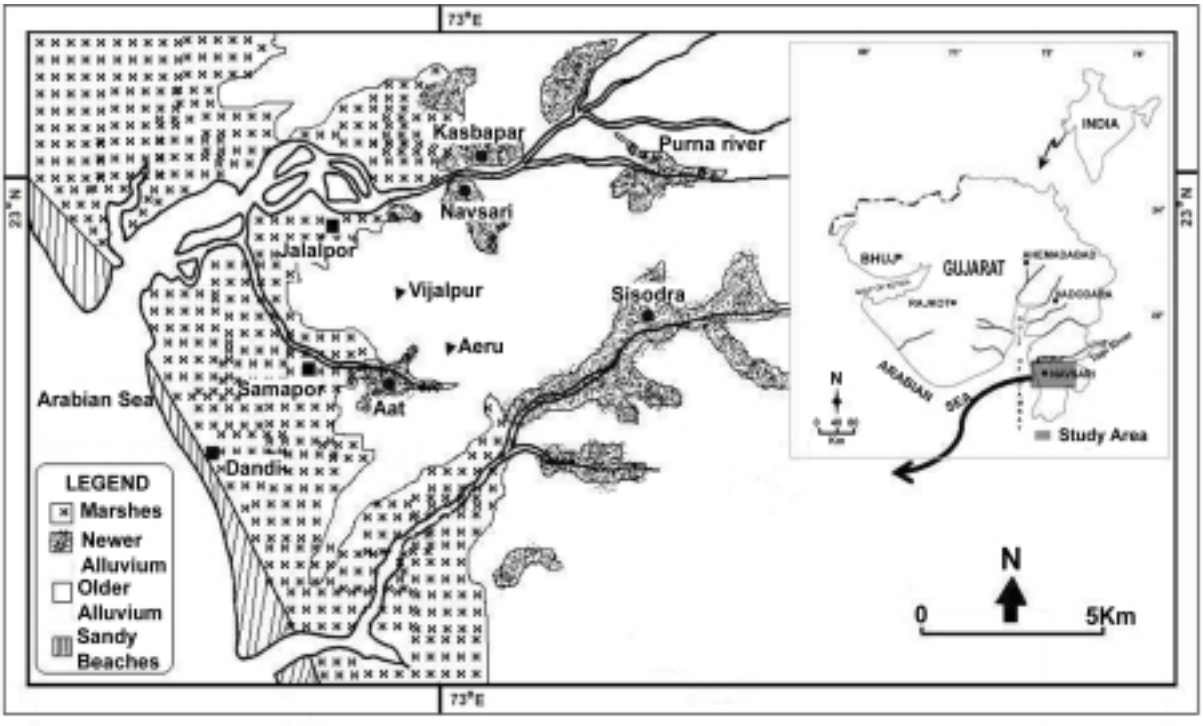

Fig.1. Location map of the study area.

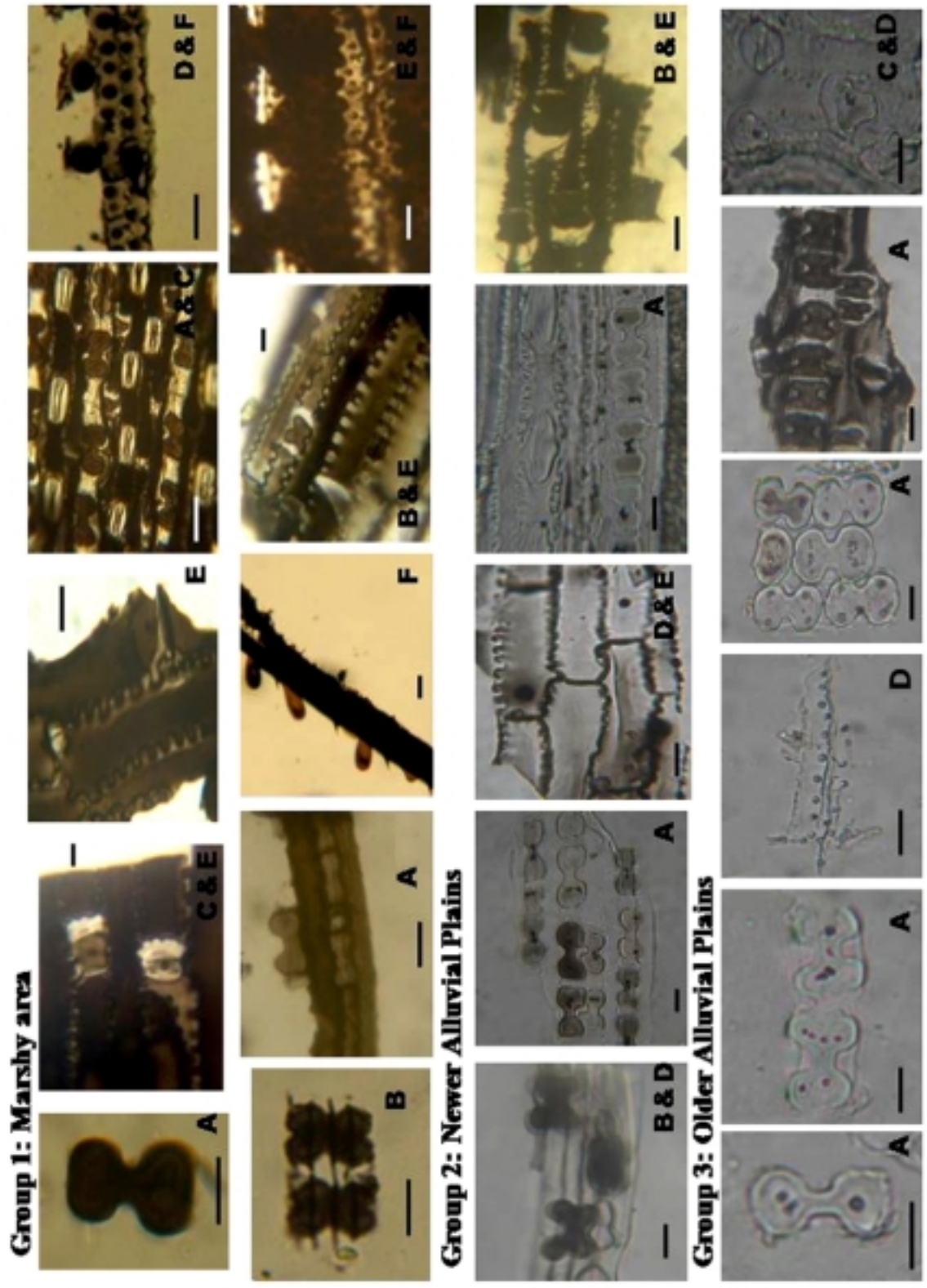

Fig.2. Photomicrographs of principle phytolith morpho-types in common grass species (Bar = 15µ).

A. Dumbbell shaped (Bilobate), B. Cross shaped (Quadrilobate), C. Rondel/ Crenate shaped, D. Smooth trapezoid forms, E. Wavy trapezoid forms, F. Silicified Papillae.

Table.1. Distribution of Phytolith types observed in grasses. (A: Abundant; C: Common; R: Rare)

Taxon Name	Morphotypes →	Dumbbell	Cross	Crenate/ Rondel	Smooth Trapezoid	Wavy Trapezoid
Marshy area						
Ischaemum rugosum Salisb.		R	A	R	R	A(Columellate)
Ischaemum impressum Hack.		A - C	R	-	R	A(Pilate)
Eremopogon foveolatus Stapf.		A	-	C – R	R	A(Granulate)
Iseilema wightii Andrs.		A	-	C	R	A(Columellate)
Newer Alluvial Plains						
Ophirus corymbosus Gaerth. f.		-	C	-	R	A(Granulate)
Ischaemum pilosum (Klein ex Willd.) Wt.		A	R	C	A(Papillate)	R
Vetiveria zizanioides (L.) Nash.		R	A	-	A(Echinate)	C
Older Alluvial Plains						
Sorghum halepense (L.) Pers.		A	-	C	A(Papillate)	R
Cymbopogon schoenanthus (L.) Spr.		A	-	C	R(Papillate)	-

water marshes on the basis of their occurrence. However, cross and dumbbell phytoliths along with few shorter and broad smooth and wavy trapezoid morphophytes represents newer or older alluvial plains as described by Lu and Liu (2005, 2003).

Based on the above studies a clear distinction is envisaged in terms of the distribution of different Phytolith assemblages representing varied environments. In the present investigation the observations on grasses have helped in the analysis of the soil phytoliths from the marshy (salt and brackish), alluvial, sand and sandy saline environments. Since phytoliths which are siliceous in nature which are preserved in the soils for millions of years even after the plant decay, they serve as an important indicator from the point of view of micro and palaeo-environmental studies. In terms of the present investigation, although the attempt was made to study the modern day grasses and their utility for micro-environmental zonation; however, the detail soil analysis is warranted to bring out an appreciable conclusion. Such studies can help to understand the palaeo-ecological conditions and demarcate the palaeo-strandline positions.

***Acknowledgements*:** Authors are thankful to Prof. Arun Arya, head, Department of Botany for providing the laboratory facilities. We are thankful to Dr. Atul Joshi, Reader, Department of Geology, for his suggestion for the preparation of manuscript.

References

Alexandre, C., Meunier, J. D., Colin, F. and Koud, M. (1997). Phytoliths: Indicators of grassland dynamics during the late Holocene in Intertropical Africa. *Palaeogeography, Palaeoclimatology, Palaeoecology*, 136, 213-229.

Barboni, D., Bonnefille, R., Alexandre, C. and Meunier, J. D. (1999). Phytoliths as a palaeo-environmental indicators, West side middle Awash valley, Ethopia. *Palaeogeography, Palaeoclimatology, Palaeoecology*, 152, 87-100.

Blackman, E. (1971). Opaline silica in the range grasses of southern Alberta. *Can J Bot*, 49, 769–781.

Blinnikov M. S. (2005) Phytolith in plants and soil

of interior Pacific Nothwest, USA. *Review of Palaeobotany and Palynology,* 135, 71-98

Bowdery, D., Hart, D. M., Lentfer, C., and Wallis, L. (2001). A universal phytolith key. In J. D. Meunier, & F.

Colin (Eds.*), Phytoliths: Applications in earth sciences and human history* (267–278). Amsterdam: Balkema.

Bremond, L., Alexandre, C., Hely, C. and Guiot, J. (2005a). A phytolith index as a proxy of tree cover density in tropical areas: Calibration with leaf area index along a forest-Savana transect in Southeastern Cameroon. *Global and Planetary change*, 45, 277-293.

Bremond, L., Alexandre, C., Peyron, O. and Guiot, J. (2005b). Grass water stress estimated from phytoliths in West Africa. *J Biogeo*, 32, 311-327.

Brown, DA. (1984). Prospects and limits of a phytolith key for grasses in the Central United States. *J Arch Sci,* 11, 345–368.

Cramer, W. (2002). Biome models. Encyclopedia of Global Environmental Change (ed. by T. Munn), 166–171. John Wiley & Sons, Chichester.

Fearn, M.L. (1998) .Phytolith in sediment as indicators of grass pollen source. *Review of Palaeobotany and Palynology,* 103, 75–81.

Fredlund, G. G. and Tieszen, L.T. (1994). Modern phytolith assamblages from the north American great plains. *J Biogeo*, 21, 321-335.

Gallego L. and Distel R. A. (2004). Phytolith assemblage in grasses native to central Argentina *Ann Bot,* 94, 865-874

Honaine, M. F., Zucol, A. F., and Osterrieth, M. L. (2006). Phytolith Assemblages and Systematic Associations in Grassland Species of the South-Eastern Pampean Plains, Argentina. *Ann Bot,* 98, 1155–1165.

Horrocks, M., Deng, Y., Ogden, J. and Sutton, D.G. (2000). A reconstruction of the history of a Holocene sand dune on Great Barrier Island, northern New Zealand, using pollen and phytolith analysis. *J Biogeo*, 27, 1269-1277.

ICPN. (2005). International code for phytoliths nomemclature1.0. *Ann Bot,* 96, 253-260.

Krishanan, S., Samson, N.P., Ravichandran, P., Narsimhan, D. and Dayanandan, P. (2000) Phytoliths of Indian Grasses and their potential use in identification. *Bot. J. Linn. Soc.*, 132, 241-252

Labouriau, L. G. (1983). Phytolith work in Brazil. A mini-review. *The Phytolitharien Newsletter,* 2, 6-11.

Lu, H. and Lui, K. (2005). Phytolith assemblages as indicators of coastal environmental changes and hurricane over wash deposition. *The Holocene,* 15(7), 965-972.

Lu, H. and Lui, K. (2003). Phytoliths of common grasses in the coastal environments of southeastern USA. *Estuarine, Coastal and Shelf Science,* 58, 587-/600.

Madella, M., Alexandre, A. & Ball, T. (2003). International Code for Phytolith Nomenclature 1.0. *The Phytolitharien,* 15(1), 7-16.

Mulholland, S. C. (1989). Phytolith shape frequencies in north Dakota grasses: a comparison to general patterns. *J Archae Sci,* 16, 489–511.

Parr, J. F., Letfer, C. J. and Boyd, W. E. (2001). A comparative analysis of wet and dry ashing techniques for the extraction of phytoliths from plant material. *J Archae Sci,* 28, 875-886.

Piperno, D.R. (1988). *Phytolith Analysis: an archaeological and geological perspective*. Academic Press: San Diego.

Piperno, D.R. (2001). Phytoliths. In J. P. Smol, H. J. B. Birks, & W. M. Last (Eds.), *Tracking environmental change using lake sediments, Terrestrial, algal, and siliceous indicators* 3 (235–251). Dordrecht: Kluwer Academic.

Piperno, D. R., and Pearsall, D. M. (1998). The silica bodies of tropical American grasses: morphology, taxonomy, and implications for grass systematics and fossil phytolith identification. *Annals of Smithsonian Institute,* 85, 1–40.

Rovner, I. (1988). Macro- and micro-ecological reconstruction using plant opal phytolith data from archaeological sediments. *Geoarchaeology,* 3, 155–163.

Rovner, I. (1983). Plant opal phytolith analysis: major advances in archaeobotanical research. In: Schiffer, M., ed. *Advances in archaeological methods and theory*. Academic press, New york. 225-260.

Rovner, I. (1971). Potential of opal phytoliths for use in Paleoecological Reconstruction. *Quaternary Research*, 1, 343-359.

Twiss, P.C., Suess, C.E. and Smith, R.N. (1969) Morphological classification of grass Phytoliths. *Soil Science Society of America Proceedings*, 33, 109-115.